NO_x Control Options and Integration for US Coal Fired Boilers

Quarterly Progress Report

Reporting Period Start Date October 1, 2003
Reporting Period End Date: December 31, 2003

Mike Bockelie, REI
Kevin Davis, REI
Temi Linjewile, REI
Connie Senior, REI
Eric Eddings, University of Utah
Kevin Whitty, University of Utah
Larry Baxter, Brigham Young University
Calvin Bartholomew, Brigham Young University
William Hecker, Brigham Young University
Stan Harding, N.S. Harding & Associates
Robert Hurt, Brown University

January 31, 2004

DOE Cooperative Agreement No: DE-FC26-00NT40753

Reaction Engineering International
77 West 200 South, Suite 210
Salt Lake City, UT 84101

Disclaimer

Abstract

This is the fourteenth Quarterly Technical Report for DOE Cooperative Agreement No: DE-FC26-00NT40753. The goal of the project is to develop cost effective analysis tools and techniques for demonstrating and evaluating low NO_x control strategies and their possible impact on boiler performance for boilers firing US coals. The Electric Power Research Institute (EPRI) is providing co-funding for this program. Using the initial CFD baseline modeling of the Gavin Station and the plant corrosion maps, six boiler locations for the corrosion probes were identified and access ports have been installed. Preliminary corrosion data obtained appear consistent and believable. *In situ*, spectroscopic experiments at BYU reported in part last quarter were completed. New reactor tubes have been made for BYU's CCR that allow for testing smaller amounts of catalyst and thus increasing space velocity; monolith catalysts have been cut and a small reactor that can accommodate these pieces for testing is in its final stages of construction. A poisoning study on Ca-poisoned catalysts was begun this quarter. A possible site for a biomass co-firing test of the slipstream reactor was visited this quarter. The slipstream reactor at Rockport required repair and refurbishment, and will be re-started in the next quarter. This report describes the final results of an experimental project at Brown University on the fundamentals of ammonia / fly ash interactions with relevance to the operation of advanced NO_x control technologies such as selective catalytic reduction. The Brown task focused on the measurement of ammonia adsorption isotherms on commercial fly ash samples subjected to a variety of treatments and on the chemistry of dry and semi-dry ammonia removal processes.

Table of Contents

1

Executive Summary

The work to be conducted in this project received funding from the Department of Energy under Cooperative Agreement No: DE-FC26-00NT40753. This project has a period of performance that started February 14, 2000 and continues through December 30, 2004.

Our program contains five major technical tasks:

- evaluation of Rich Reagent Injection (RRI) for in-furnace NO_x control;
- demonstration of RRI technologies in full-scale field tests at utility boilers;
- impacts of combustion modifications (including corrosion and soot);
- ammonia adsorption / removal from fly ash; and
- SCR catalyst testing.

To date, good progress is being made on the overall program. We have seen considerable interest from industry in the program due to our successful initial field tests of the RRI technology and the corrosion monitor.

During the last three months, our accomplishments include the following:

- Using the initial CFD baseline modeling of the Gavin Station and the plant corrosion maps, six boiler locations for the corrosion probes were identified and access ports have been installed.
- One probe has been collecting data for more than three months and two others have been in service for more than two months; preliminary corrosion data obtained appear consistent and believable.
- *In situ*, spectroscopic experiments at BYU reported in part last quarter were completed; the most significant finding of these investigations was a consistent indication that vanadium does not sulfate during SCR reaction in the presence of gas-phase SO_2 while both the substrate (anatase) and modifiers (molybdenum) do.
- New reactor tubes have been made for BYU's CCR that allow for testing smaller amounts of catalyst and thus increasing space velocity; monolith catalysts have been cut and a small reactor that can accommodate these pieces for testing is in its final stages of construction.
- A preliminary poisoning study on Ca-poisoned catalysts at 380°C indicates that Ca actually increases SCR catalyst activity at a Ca:V ratio of 0.5:1 (as compared to unpoisoned catalyst), although further investigation is necessary to validate this result.
- Further analysis of the catalyst activity data based on measurements in the slipstream reactor suggests that catalysts C2, C3 and C4 showed a loss of activity from March to August, while catalyst C5 had about the same activity in August relative to March. It was difficult to make the comparison for catalyst C6 because of lack of data at similar process conditions.
- REI visited Alabama Power's Plant Gadsden and discussed the possibility of conducting biomass co-firing tests at the plant with the slipstream reactor.
- After a visit to Rockport, it was determined that the slipstream reactor there required repair and refurbishment; the reactor will be re-started in the next quarter.
- The final results of an experimental project at Brown University on the fundamentals of ammonia / fly ash interactions with relevance to the operation of advanced NOx control

technologies such as selective catalytic reduction is included. The Brown task focused on the measurement of ammonia adsorption isotherms on commercial fly ash samples subjected to a variety of treatments and on the chemistry of dry and semi-dry ammonia removal processes.

3

Experimental Methods

Within this section we present in order, brief discussions on the different tasks that are contained within this program. For simplicity, the discussion items are presented in the order of the tasks as outlined in our original proposal.

Task 1 - Program Management

During the last performance period,

- Corrosion Probe:
  - Initial CFD baseline modeling of the Gavin Station has been completed; as a result of this modeling and the use of the plant corrosion maps, six boiler locations for the corrosion probes were identified and access ports have been installed.
  - One probe has been collecting data for more than three months and two others have been in service for more than two months; preliminary corrosion data obtained appear consistent and believable.
- SCR:
  - *In situ*, spectroscopic experiments at BYU reported in part last quarter were completed.
  - New reactor tubes have been made for BYU's CCR that allow for testing smaller amounts of catalyst and thus increasing space velocity; monolith catalysts have been cut and a small reactor that can accommodate these pieces for testing is in its final stages of construction.
  - A poisoning study on Ca-poisoned catalysts was begun this quarter.
  - The slipstream reactor at Rockport required repair and refurbishment, and will be re-started in the next quarter.
  - A visit was made to Alabama Power's Gadsden Plant to discuss the possibility of hosting a biomass co-firing test.
- Fly Ash Management/Disposal:
  - The subcontract with Brown University (Professor Robert Hurt, Principal Investigator) to support Task 5 "Fly Ash Management/Disposal" for their research on ammonia adsorption onto flyash was completed this quarter. Included in this report is an extensive write-up that constitutes their contribution to the project Final Report.

Industry Involvement

Results from portions of this research program have been reported to industry through technical presentations at conferences. One paper will be presented in the next quarter at the Electric Power Conference, Baltimore, Maryland, March 30-April 1, 2004:

- Constance Senior and Temi Linjewile, "Understanding Oxidation of Mercury Across SCR Catalysts in Power Plants Burning Low Rank Coals."

Two papers have been accepted for presentation at the Coal Utilization & Fuel Systems Conference in Clearwater, Florida, April 18-22, 2004:

- Kevin Davis, Temi Linjewile, David Swensen, Darrin Shino, J.J. Letcavits, William Cox and Richard Carr, "A Multi-point Corrosion Monitoring System Applied in a 1300 MW Coal-fired Boiler."

- Constance Senior and Temi Linjewile, “Oxidation Of Mercury Across SCR Catalysts In Coal-Fired Power Plants.”

Task 3 Minimization of Impacts

Using the initial CFD baseline modeling of the Gavin Station and the plant corrosion maps, six boiler locations for the corrosion probes were identified and access ports have been installed.

Six corrosion probes operating based on electrochemical noise have been inserted into the unit. Alongside each of the electrochemical noise corrosion probes, three EPRI/KEMA screw-in type corrosion coupons (KEMCOP) have been installed. Shakedown tests have been completed; a power surge caused three of the probes to malfunction. The replacement parts have been received and additional surge protection installed on all probe electronics. The wireless data transfer between probes has been successfully demonstrated as has the software needed to perform data collection on all six probes. Further, remote monitoring of the electrochemical noise probes from REI's office in Salt Lake City, Utah, has been established.

One probe has been collecting data for more than three months and two others have been in service for more than two months.

Probe Installation at AEP Gavin Plant and Preliminary Data

Preparations for Installation of the Corrosion Monitoring System

REI, Corrosion Management engineers, and plant engineers were involved in the setup of the corrosion system at different stages during the installation period. Personnel from Brown Electric were involved in the installation of power outlets, compressed air outlets and mounting of the corrosion probe boxes. Further, KEMA personnel installed the KEMA screw-in type corrosion coupons.

An advance party was sent to the plant on Thursday, October 16 to install a host site PC and oversee the corrosion box installation process. The advance party had the responsibility of ensuring that the wireless communication system between the North wall probe box and the host PC was established.

The focus of activities between Monday, October 20 and Thursday, October 23, 2003 was to install six probe control boxes fitted with cabinet coolers. All remaining preparations for installation of power outlets and compressed air outlets were completed during this time period.

Figure 1 shows the control layout for the multi-probe installation. There are six control boxes, five of which are located on the south wall and one is located on the north wall. The south wall holds the central probe (designated as the Main probe for convenience) and probe numbers 1 to 4. The probe located on the north wall is designated as probe #5. Each one of the six control boxes has its own Fieldpoint embedded controller for probe data acquisition and control. In addition, due to its remote location relative to the location of the host PC, the control box for probe #5 has a wireless communication kit installed. This allows direct communication between control box #5 and the host PC.

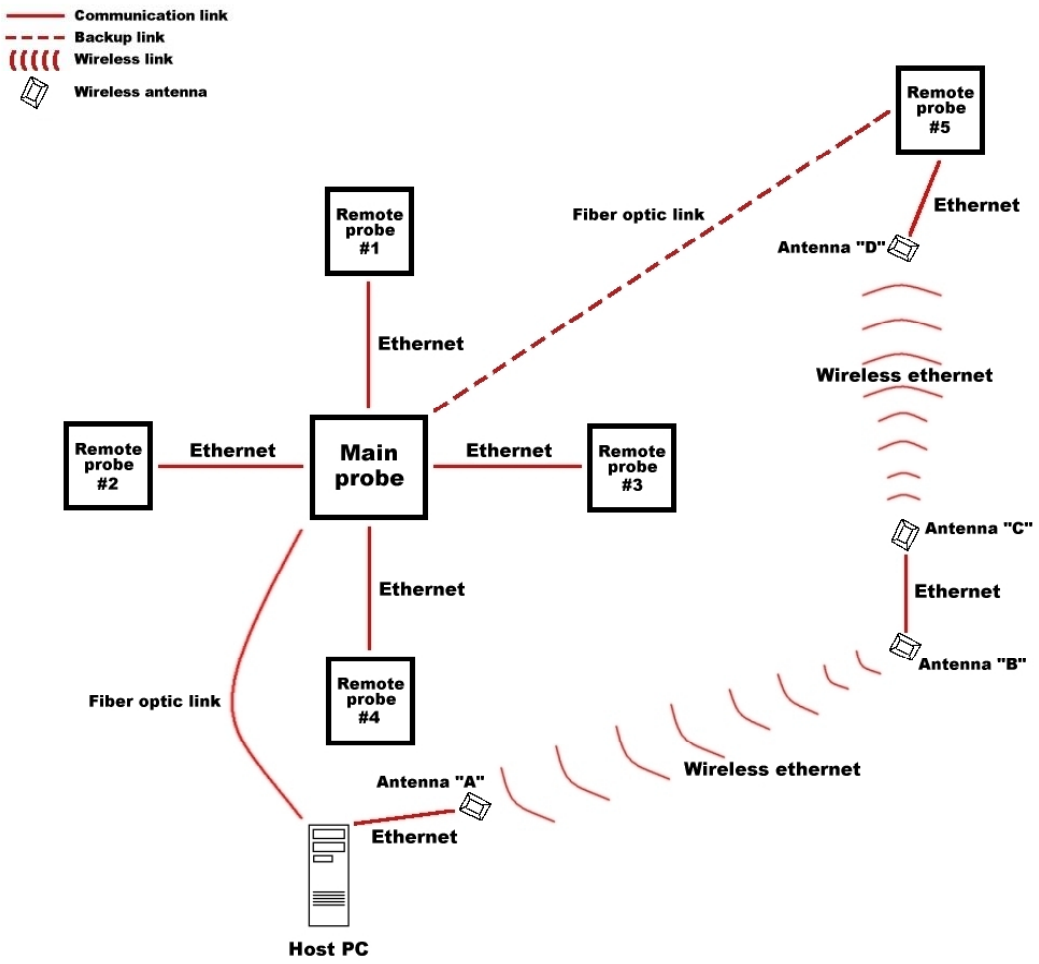

Figure 1. Schematic diagram of the multi-probe communication and control layout.

In order to ensure uninterruptible communication between probe #5 and the host PC, a backup fiber optic link via the main probe control box is provided should the wireless set fail. A special feature of the main probe control box is that it contains network connectivity modules that facilitate communication between the individual Fieldpoint embedded controllers and the host PC via a fiber optic link. Figure 2 shows the external appearance of the main control box along with the interior view revealing the location of the Fieldpoint modules (top row) and network connectivity modules (middle row). Figure 3 shows the interior of the control box for probe #5 located on the north wall. The figure also shows a wireless antenna C that relays information between the control box and the host PC as illustrated in detail in Figure 1.

Figure 2. Outside (left) and inside views (right) of the main probe control box installed on the boiler south wall.

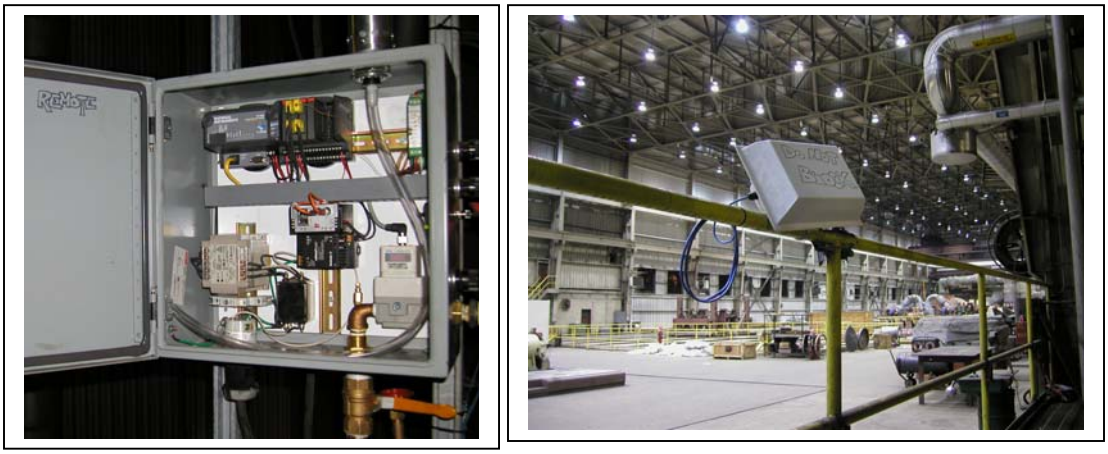

Figure 3. Inside view (left) of the control box for probe #5 installed on the boiler north wall and wireless antenna C (right).

Installation of the Corrosion Sensors

Installation of the corrosion probes started with cleaning of the probe ports. After remaining idle for approximately six months since installation, the probe ports were filled with unburned carbon, ash, solidified slag and semi-molten slag and liquid slag on the waterwall fireside. The ports had to be cleaned and the solidified slag crushed out. Figure 4 shows a picture of a probe port before and after cleaning. Only after cleaning out a port could a probe be installed. The procedure for installation of the probes involved gradual advancing of the probe into the furnace to allow for thermal equilibration. The probes were finally advanced into the furnace such that the probe face was halfway between the membrane and the crown of the tubes. Figure 5 shows two fully installed probes.

Figure 4. Appearance of a probe port before (left) and after cleaning (right).

Figure 5. Probe #2 (left) and the main probe (right) installed on the south wall.

Installation of the KEMCOP Screw-in type Corrosion Coupons

During the week of October 19th –24th, twenty three passive corrosion probes were installed at AEP's Plant Gavin Station in Cheshire, Ohio. The corrosion probes were mounted at the webbing at the locations near the wall boxes placed for the REI monitor probes. An array of four holes were drilled and cleaned during the last outage, where a dummy probes was installed in each hole as seen in Figure 6.

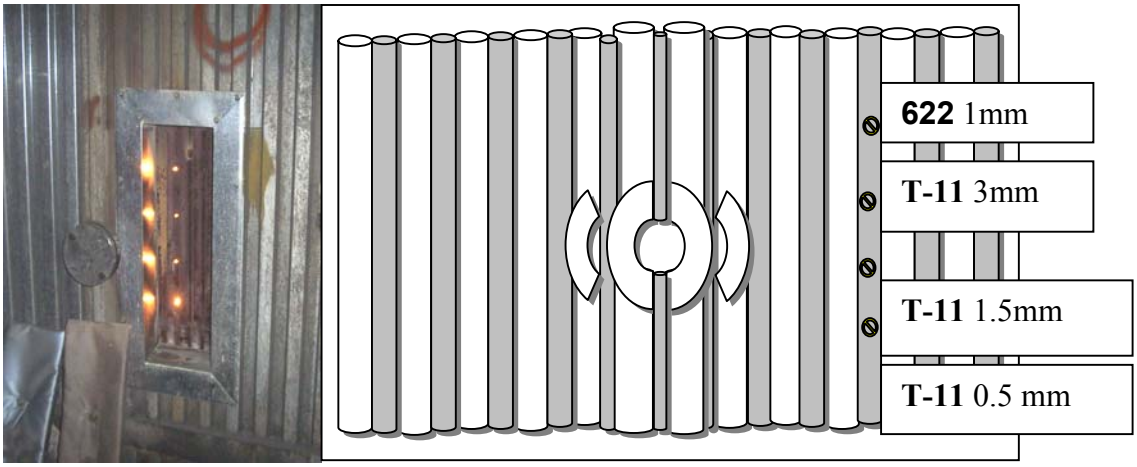

Figure 6. Probe Installation in the drilled and tapped webbing as seen in the left, Three T-11 material and one of Inconel 622 probe were installed at different incremental lengths.

Dummy corrosion probes were removed from the North Wall and five locations of the South Wall. Elevations 214' and 155' had the most difficult access and required extra caution and time during removal. After removal, each of the probe holes was cleaned. During the cleaning process a broken tap occurred at one of the locations on elevation 155'. Following removal, new measurements of web thickness were performed and manual temperature measurements were carried out at each location to gather data on probe exposure temperatures as seen in Figure 7. Load cycling temperature data was also taken at two different incremental insertion lengths in the NW location as seen in Figure 8.

Figure 7. Temperature Readings at Elevation 214'

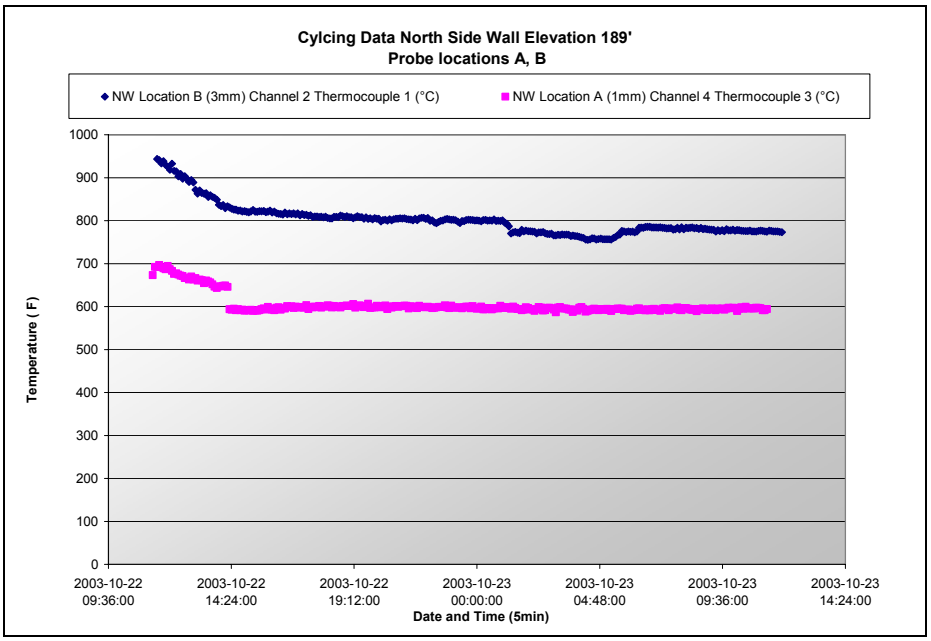

Figure 8. Cycling load temperature data at the North Side Wall Elevation 189' at two different incremental lengths.

Upon completion of temperature readings, the web thickness data was used to adjust and install the twenty-three corrosion probes at the location described in Figure 9.

North Wall 189’ South Wall 214’ South Wall 155’

South Wall 189’ (t220-221) South Wall 189’ (t152-153) South Wall 189’ (t84-85)

Figure 9. Location of installed passive probes near the six REI active probes.

Task 4 - SCR Catalyst Testing

The cost and effectiveness of NO_x control strategies for coal-fired boilers have received considerable attention over the last two decades and a number of successful approaches have been applied. Utilities weigh a number of issues when determining the best strategy for their specific units. Comparisons routinely include cost and the amount of NO_x reduction, with selective catalytic reduction (SCR) often used as a standard for comparison. However, to make this comparison meaningful, the total cost of combustion modifications must be considered (carbon-in ash levels, waterwall wastage, etc.). Industry is developing experience evaluating many of these costs and it is one of the tasks of this program to better understand two such areas – waterwall corrosion and soot formation. For SCR, the "real" cost for coal-fired boilers using US coals and coal/biomass blends is uncertain.

The economics of SCR are closely tied to catalyst costs, including initial investment cost and the cost of regeneration or replacement. The need for data and models that enable assessment of such costs is emphasized.

The purpose of this task is to develop databases and a model for assessing catalyst deactivation and its effects on SCR catalyst life and cost.

Within this task there are for principal sub-tasks:

1. technology assessment and fundamental analysis of chemical poisoning of SCR catalysts by alkali and alkaline earth materials;
2. evaluation of commercial catalysts in a continuous flow system that simulates commercial operation;
3. evaluation of the effectiveness of catalyst regeneration; and
4. development of a model of deactivation of SCR catalysts suitable for use in a CFD code.

Items 1 and 3 are principally performed at Brigham Young University (BYU) under the direction of Profs. Larry Baxter, Calvin Bartholomew, and William Hecker. The work effort for items 2 and 4 is being performed by REI, with assistance from the University of Utah and BYU. Progress during the last performance period on this task is described below.

Task 4.1 Technology Assessment/Fundamental Analysis

The objectives of this subtask are (1) to supplement the SCR-catalyst-deactivation literature with results from new laboratory-scale, experimental investigations conducted under well-controlled and commercially relevant conditions in the presence of SO_2, and (2) to provide a laboratory catalyst test reactor suitable for testing catalyst activity and deactivation of samples from commercial facilities, slipstream reactors, and laboratory experiments. Two catalysts flow reactors and several additional characterization systems provide the analytical tools required to achieve these objectives. The flow reactors include the *in situ* surface spectroscopy reactor (ISSR) and the catalyst characterization system (CCS), both of which are described in more detail in previous reports. Additional characterization systems include a temperature-programmable surface area and pore size distribution analyzer, scanning electron microscopes and microprobes.

The sample test matrix includes two classes of catalysts: commercial, vendor-supplied SCR catalysts and research catalysts synthesized at BYU. The commercial catalysts provide

immediate relevance to practical application while the research catalysts provide unfettered ability to publish details of catalyst properties. The five commercial catalysts selected for use come from most commercially significant catalyst manufacturers (Cormetech, Haldor-Topsoe, Hitachi, and Siemens) and provide a wide range of catalyst designs and compositions. The in-house catalysts will be subjected to detailed analysis, activity testing, and characterization, thus providing a comprehensive test and analysis platform from which to determine rates and mechanisms of catalyst deactivation. The result of this task will be a mathematical model capable of describing rates and mechanisms of deactivation.

Within the last performance period, *in situ*, spectroscopic experiments partially reported last quarter were completed. The most significant finding of these investigations is a consistent indication that vanadium does not sulfate during SCR reaction in the presence of gas-phase SO_2 while both the substrate (anatase) and modifiers (molybdenum) do. In addition, mass-spectroscopy-based analyses of product gases from this reactor system help elucidate fundamental kinetics and deactivation mechanisms.

ISSR Overview

The purpose of the FTIR-ISSR is to provide definitive indication of surface-active species through *in situ* monitoring of infrared spectra from catalytic surfaces exposed to a variety of laboratory and field conditions. The ISSR provides *in situ* transmission FTIR spectra of SO_2, NH_3, and NO_x, among other species. Adsorption and desorption behaviors of these and other species are monitored. Quantitative indications of critical parameters, including Brønsted and Lewis acidities on fresh and exposed catalysts, are included. Indications of coadsorption of NH_3 and NO_x help elucidate mechanisms and rates of both reactions and deactivation.

FTIR Transient ISSR Experiments

During previous sulfation tests, the reactant gas flow rate had not been consistent for each test because settings of two of the mass flow controllers were gradually drifting during the tests, despite efforts to keep gas composition and flow rate the same for each sample. Therefore, during this quarter sulfation was repeated at constant gas flow rate and gas composition for better comparison among 2, 5% V_2O_5/TiO_2, and pure TiO_2. Sulfation conditions are summarized in Table 1.

Table 1. Sulfation test conditions.

Sample Name	Sample Details	Notes	Gas Stream Composition, %				Flow (sccm)	Temp (°C)
			He	O_2	SO_2	H_2O		
VTOD	5% V_2O_5/TiO_2	Preoxidation	88.2	11.8		0	56.7	380
		24 Hours Sulfation	89.01	10.72	0.27	0	62.3	380
VTOF	2% V_2O_5/TiO_2	Preoxidation	88.2	11.8		0	56.7	380
		24 Hours Sulfation	89.01	10.72	0.27	0	62.3	380
TiO8	TiO_2	Preoxidation	88.2	11.8		0	56.7	380
		24 Hours Sulfation	89.01	10.72	0.27	0	62.3	380
VTHF	5% V_2O_5/TiO_2	Preoxidation	88.2	11.8		0	56.7	380
		24 Hours Sulfation	87.33	10.51	0.267	1.88	63.54	380
VTHG	2% V_2O_5/TiO_2	Preoxidation	88.2	11.8		0	56.7	380
		24 Hours Sulfation	87.33	10.51	0.267	1.88	63.54	380
TiO9	TiO_2	Preoxidation	88.2	11.8		0	56.7	380
		24 Hours Sulfation	87.33	10.51	0.267	1.88	63.54	380

We have observed plugging in the FTIR reactor cell outlet tube during the sulfation process. To deal with this problem, the FTIR reactor cell was cleaned carefully before each sulfation. The plugging happens mostly during wet sulfation of the vanadia catalyst, although some powder did deposit on the inside wall of the outlet tubing from the cell during dry sulfation. Plugging was not a problem for sulfation of pure titania under both dry and wet sulfation conditions.

The light green color of the substance plugging the cell is very close to the color of the catalyst before calcination. ICP-MS analysis of the substances responsible for plugging during both 5 and 2% vanadium catalyst sulfation processes was conducted, while XPS analysis was conducted only on the plugged substance resulting from the 2% vanadium catalyst sulfation process because not enough plugging substance from the 5% vanadium catalyst sulfation process remained for XPS analysis. ICP results from both samples show high amounts of Fe, Mn, Cr and smaller amounts of V and Ti, and XPS results show high content of S and Mn. These findings suggest that sulfur oxides plus water react with metal surfaces in the reactor or connecting metal tubes, forming metal sulfates. This is probably more likely to happen at welded joints, since stainless steel surfaces are likely to be passive to SO_2 or sulfuric acid attack. Catalyst powder could also have become dislodged from the wafer surface and deposited on the outlet tubing wall, resulting in metal sulfates depositing on the catalyst powder, and together plugging the cell outlet.

In situ FTIR spectra were collected during sulfation reaction, and XPS analysis was applied to determine the surface composition of each of the sulfated samples. Results are shown below (See Figures 10 through 15.)

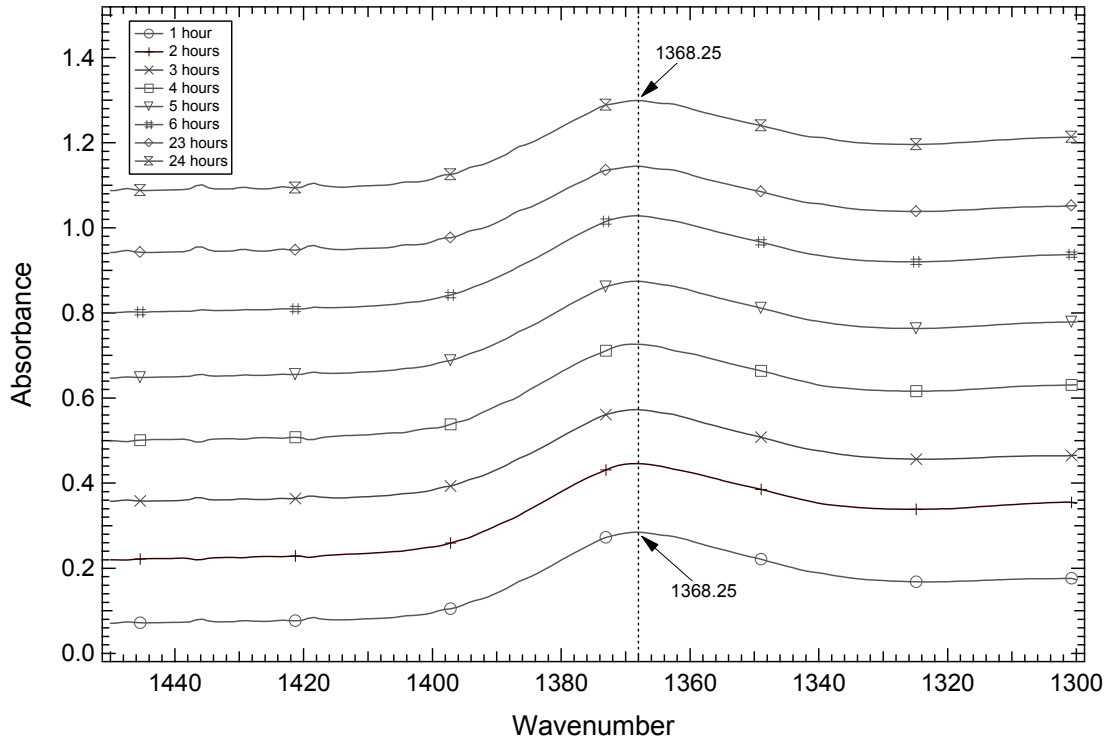

Figure 10. ***In situ*** **IR spectra of dry sulfation on 5% V_2O_5/TiO_2.**

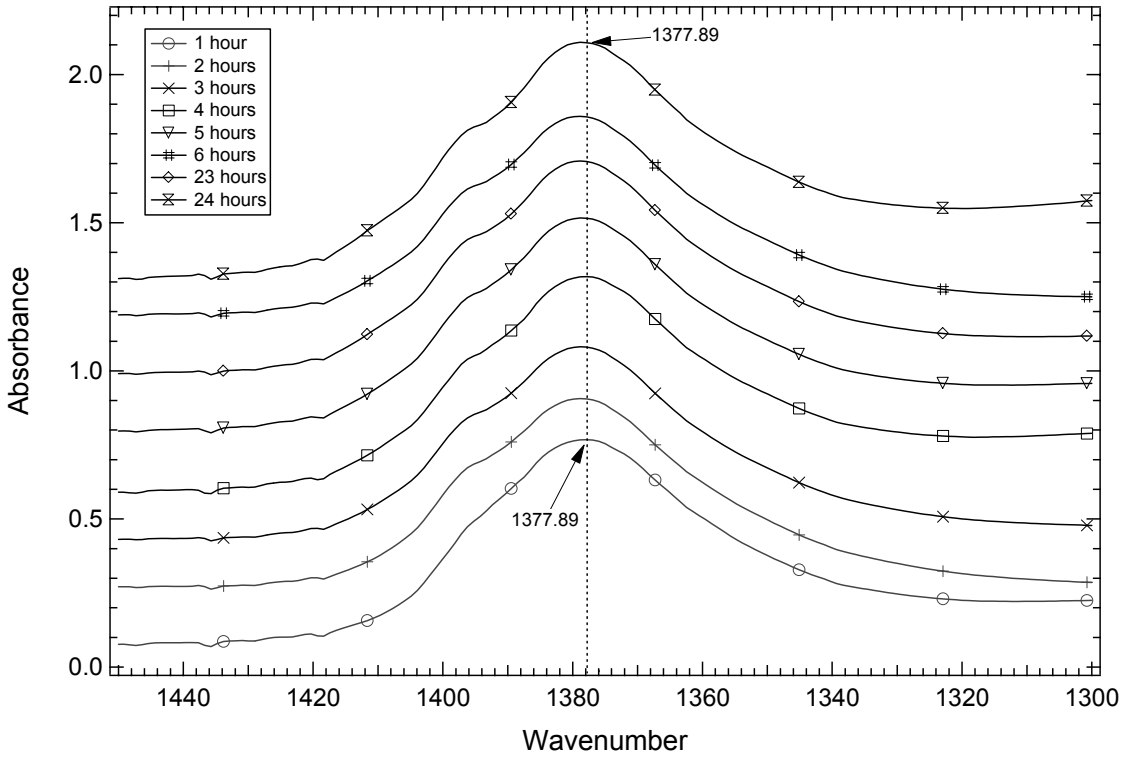

Figure 11. ***In situ*** **IR spectra of dry sulfation on 2% V_2O_5/TiO_2.**

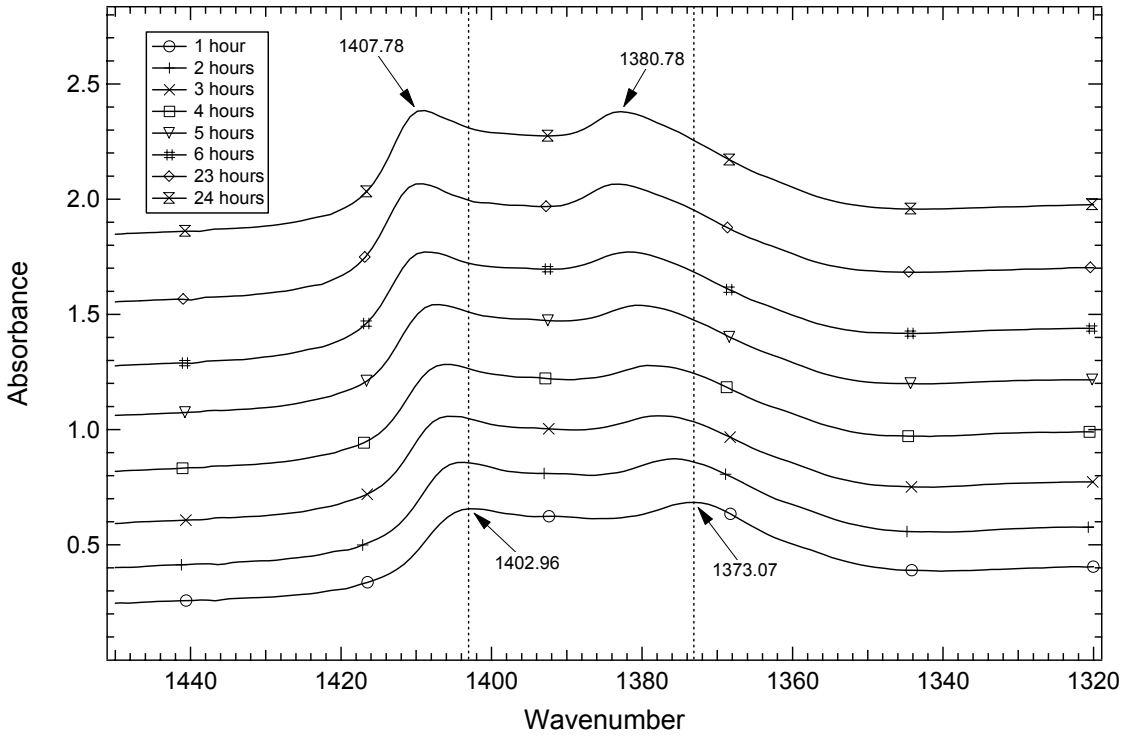

Figure 12. ***In situ*** **IR spectra of dry sulfation on TiO_2.**

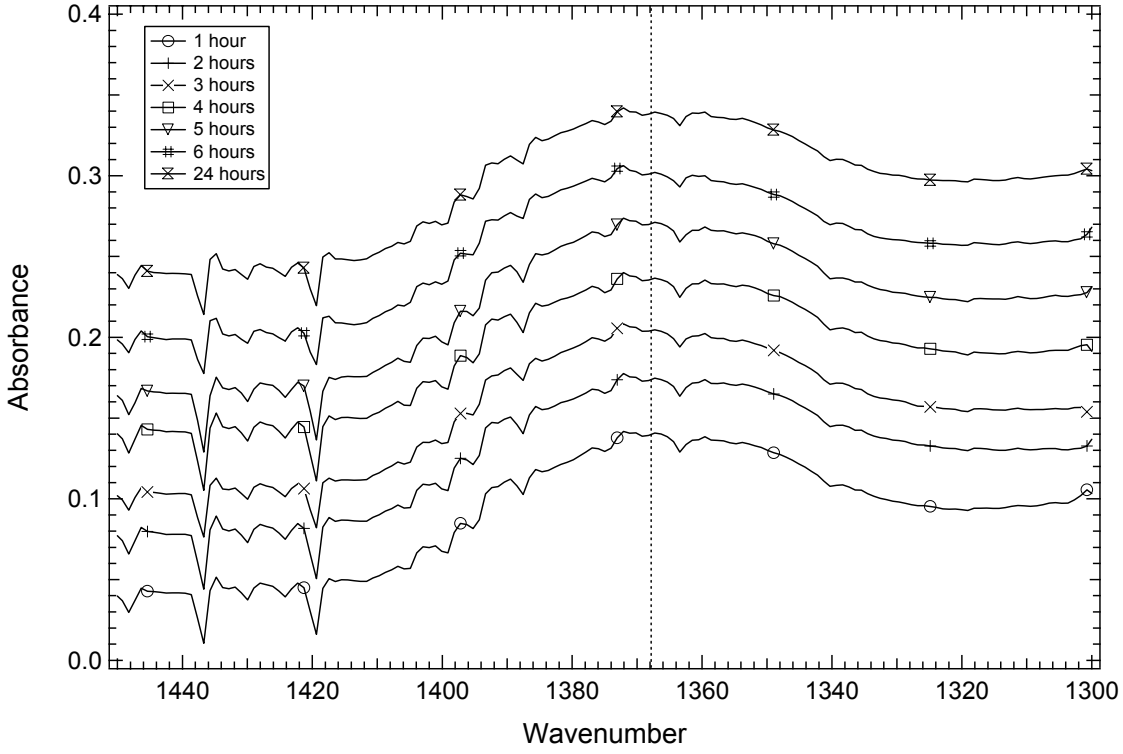

Figure 13. ***In situ*** **IR spectra of wet sulfation on 5% V_2O_5/TiO_2.**

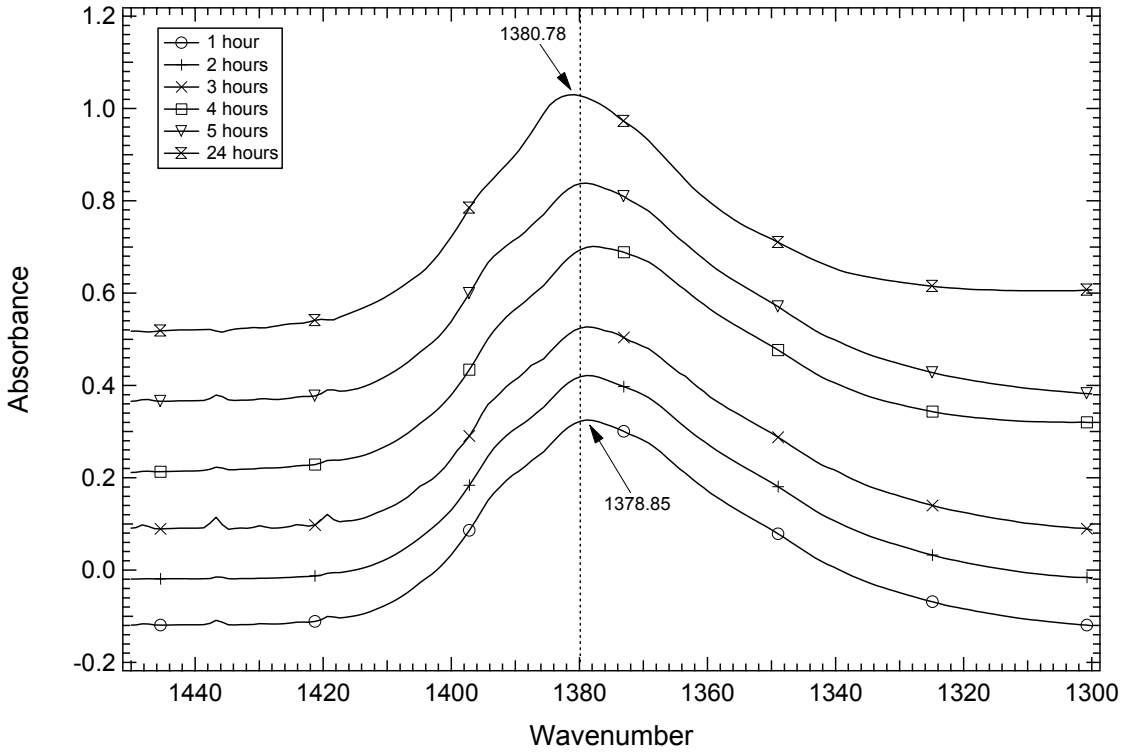

Figure 14. ***In situ*** **IR spectra of wet sulfation on 2% V_2O_5/TiO_2.**

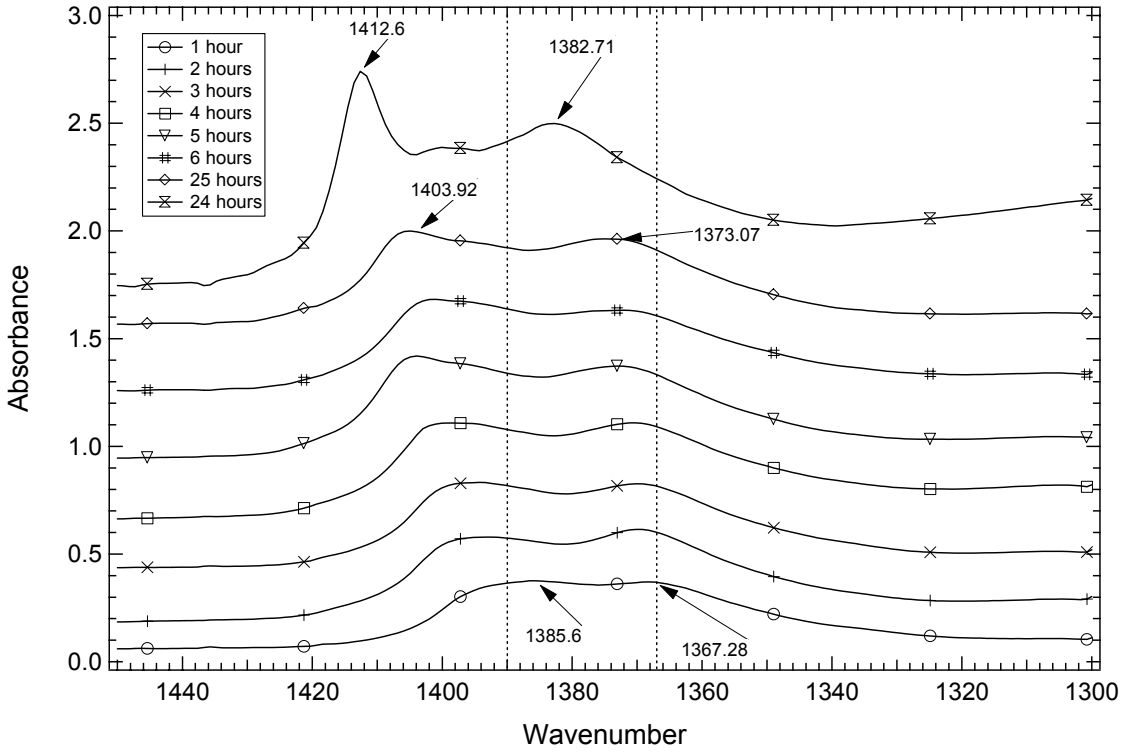

Figure 15. ***In situ*** **IR spectra of wet sulfation on TiO_2.**

The same trend in sulfate IR peak intensity as reported previously is seen in this study, i.e., the intensity of the peak at ~1375 cm^{-1} decreases with increasing vanadia content on the catalyst surface. Doublet sulfate IR peak signals appear on sulfated titania samples under both dry and wet sulfation conditions, while corresponding sulfate IR peaks for catalysts containing 2% vanadia show only minor evidence of peaks at the same wave numbers.

Doublet sulfate IR peaks of TiO_2 were further analyzed with curve fitting software (Figure 16 and Figure 17).

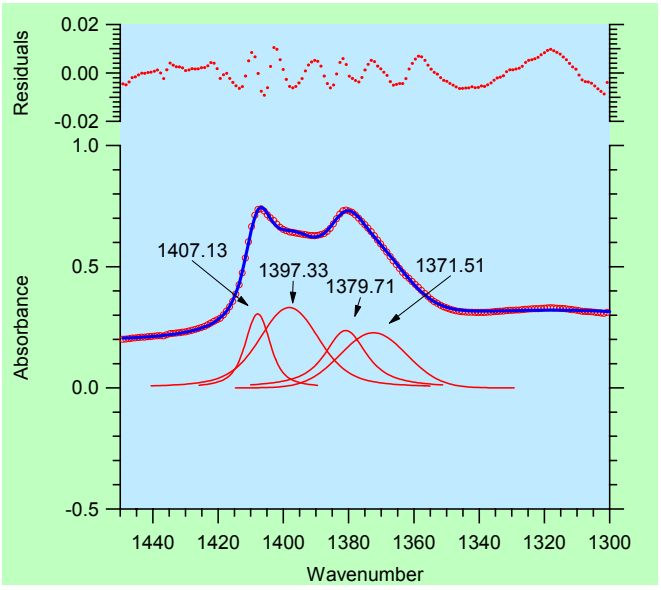

Figure 16. Curve fitting of FTIR spectrum for TiO_2 sample 1.

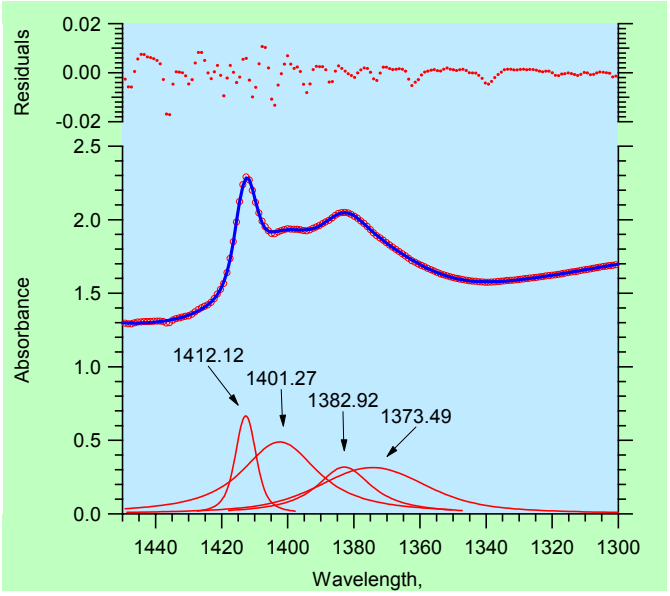

Figure 17. Curve fitting of FTIR spectrum for TiO_5-sample 2.

A doublet peak can also be seen in Yang et al.'s work (Chen and Yang, 1993), although their IR peak around 1380 cm^{-1} is more intense than the one around 1401 cm^{-1}. Our results, on the other hand, show the IR peak around 1401 cm^{-1} to be more intense. The four deconvoluted peaks from the fits of the IR sulfate spectra for both samples can be classified as being either above or below 1390 cm^{-1}. The IR peak around 1390–1375 cm^{-1} is assigned to an S=O stretching mode. No assignment for the peak centered around 1401 cm^{-1} has been found yet. Further study is needed for explanation.

ISSR Transient MS Experiments

The SCR reaction of ammonia and nitric oxide in the presence of oxygen was conducted at 380 ˚C first on pure titania (Figure 18), second on dry sulfated titania (Figure 19), and finally on an empty cell (Figure 20) in order to identify possible catalytic effects of materials other than vanadia. The inlet gas composition was 88% He, 10.75% O_2, 6400 ppm NH_3, and 5100 ppm NO. Total flowrate was 62 sccm.

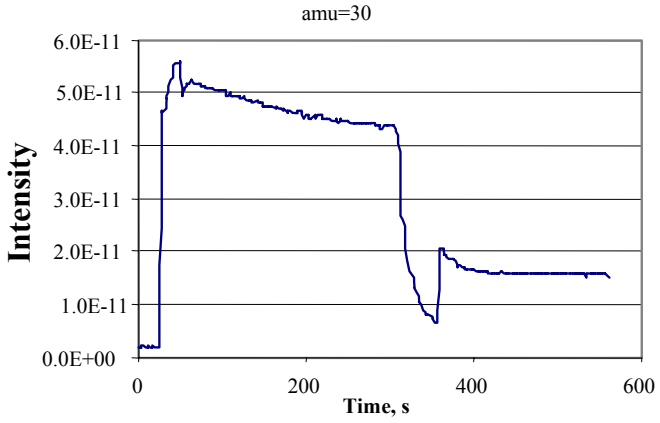

Figure 18. SCR reaction (NH_3+NO+O_2) on pure TiO_2

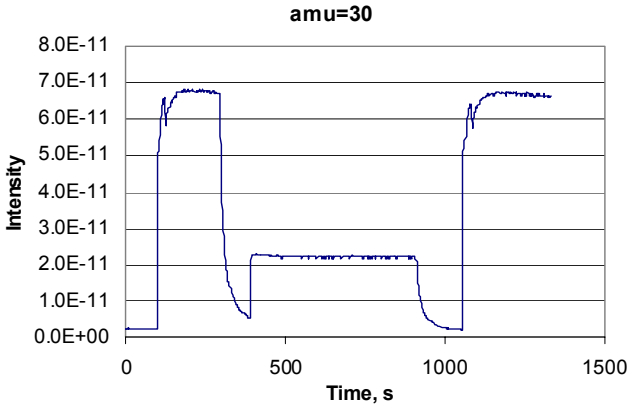

Figure 19. SCR reaction (NH_3+NO+O_2) on sulfated TiO_2 at 380 ˚C.

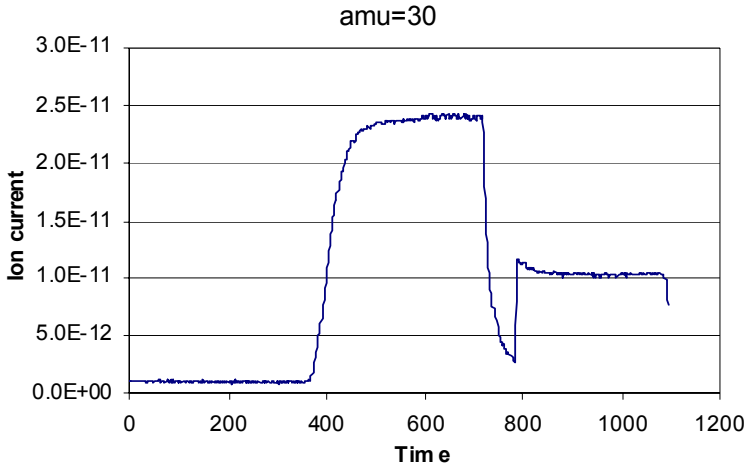

Figure 20. SCR reaction (NH_3+NO+O_2) in empty cell at 380 °C.

The MS signals for NO (30 amu) corresponding to the IR cell inlet (lower signals) and outlet (higher signals) are shown above in Figures 18 through 20. The intensity change of the NO signal before and after the reactor cell normalized to outlet concentration (see Table 2) is proportional to the change in concentration through the reactor; conversion is proportional to the difference normalized by inlet concentration.

Table 2. NO MS intensity ratios and NO conversions.

	Empty cell	on pure TiO_2	on sulfated TiO_2
NO-a intensity before reactor	2.4E-11	4.34E-11	6.74E-11
NO-b intensity after reactor	1.04E-11	1.64E-11	2.24E-11
ratio = [(NO-a) - (NO-b)] / (NO-b)	1.3	1.8	2.1
conv = [(NO-a) - (NO-b)] / (NO-a)	0.57	0.62	0.67

Although the filament intensities are only approximate due to fouling of the filament, information about differences are still qualitatively useful. The changes in the NO intensity ratio and conversion of NO increase in this order: empty cell, pure TiO_2, and sulfated TiO_2. Conversion in the empty cell is largely a consequence of deposits in the reactor outlet tube, as described previously. Accounting for the conversion due to that material, NO conversions occurring on pure and sulfated TiO_2 are on the order of 5 and 10% respectively.

Internal standard methods will be utilized in future tests for more accurate conversion calculations.

XPS Analyses

Table 3 summarizes XPS analyses conducted on the six sulfated samples listed in Table 1. Previous XPS results are presented in Table 4. Sulfate contents are plotted in Figure 21.

Table 3. XPS analysis results for repeat sulfation tests.

Sample		Elements	B.E.	Atom %	Sample		Element	B.E.	Atom %
VTOD	5% V	C 1s	285	14.99	VTHF	5% V	C 1s	285.00	20.32
	Sulfation	O 1s	530.417	61.72		Sulfation	O 1s	530.03	58.55
	without	S 2p	168.738	0.83		with	S 2p	168.88	2.17
	water	Ti 2p	459.143	18.79		water	Ti 2p	458.77	16.42
		V 2p3/2	517.767	3.67			V 2p3/2	516.76	2.53
VTOF	2% V	C 1s	285.00	14.34	VTHG	2% V	C 1s	285.00	13.94
	Sulfation	O 1s	529.98	62.29		Sulfation	O 1s	529.96	62.04
	without	S 2p	169.03	1.66		with	S 2p	168.80	1.50
	water	Ti 2p	460.32	19.63		water	Ti 2p	460.20	20.45
		V 2p3/2	516.88	2.06			V 2p3/2	516.92	2.07
TiO8	Titanium dioxide	C 1s	285	8.7	TiO9	Titanium dioxide	C 1s	285.00	16.10
	Sulfation	O 1s	529.48	66.4		Sulfation	O 1s	530.85	60.76
	without	S 2p	168.47	2.8		with	S 2p	168.76	2.71
	water	Ti 2p	458.42	23.2		water	Ti 2p	460.39	20.42

Table 4. Previous XPS analysis results.

Sample		Elements	B.E.	Atom %	Sample		Element	B.E.	Atom %
V8TO	5% V	C1s	285	24.2	V8TH	5% V	C 1s	285	5.3
	Sulfation	O1s	533.99	56		Sulfation	O 1s	533.39	65.8
	without	S2p	168.46	1.5		with	S 2p	168.55	2.8
	water	Ti2p	458.19	16.5		water	Ti 2p	458.14	20.2
		V 2p3/2	516.72	3.3			V 2p3/2	516.68	3.3
V9TO	2% V	C 1s	285	8.3	V9TH	2% V	C 1s	285	10.1
	Sulfation	O 1s	533.74	67.7		Sulfation	O 1s	530.63	65.2
	without	S 2p	168.97	2.1		with	S 2p	169.25	2.4
	water	Ti 2p	458.16	20.9		water	Ti 2p	458.72	20.2
		V 2p3/2	516.36	1.9			V 2p3/2	517.24	2.1
TiO_2-O	Titanium dioxide	C 1s	285	8.7	TiO_2-H	Titanium dioxide	C 1s	285	10.2
	Sulfation	O 1s	529.48	66.4		Sulfation	O 1s	530.48	70.7
	without	S 2p	168.47	2.8		with	S 2p	169.5	3.4
	water	Ti 2p	458.42	23.2		water	Ti 2p	459.5	15.6

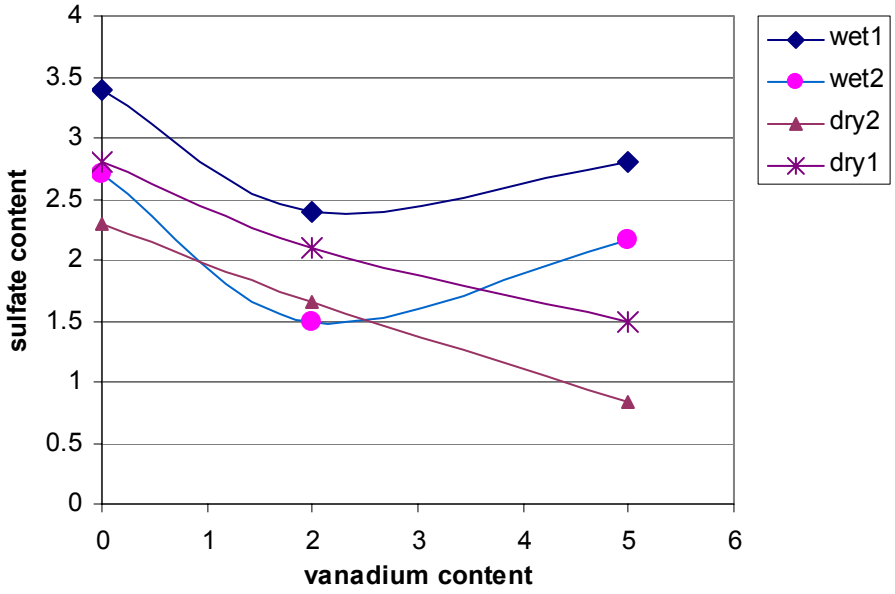

Figure 21. Comparison of XPS results of previous and repeat sulfation tests

Wet1 and dry1 represent data from the previous tests, and wet2 and dry2 represent data for the repeat tests.

The two sets of experiments are in good qualitative agreement. For both dry sulfate samples, sulfate content is directly inversely proportional to vanadium content; however, for both wet sulfate samples, sulfate content decreases and then increases with increasing vanadium content.

One way to explain the later observation is that water may facilitate vanadia species migration and redistribution on the catalyst surface. At the highest vanadia content (5%), water may facilitate the aggregation of vanadia species on the catalyst surface; thus more titania species are exposed, and more titania sulfates are formed (since previous results indicate sulfates are formed on titania sites instead of vanadia sites).

CCS Overview

The catalyst characterization system (CCS) provides capabilities for long-term catalyst exposure tests required for ascertaining deactivation rates and mechanisms and a characterization facility for samples from the slipstream reactor to determine changes in reactivity and responses to well-controlled environments. This system simulates industrial flows by providing a test gas with the following nominal composition: NO, 0.1%; NH_3, 0.1%; SO_2, 0.1%; O_2, 2%; H_2O, 10%; and He, 87.7%. Both custom and commercial catalysts are tested as fresh samples and after a variety of laboratory and field exposures under steady conditions.

Deactivation rates are quantitatively determined by measuring specific, intrinsic catalyst reactivity of custom (laboratory) and commercial catalysts under a variety of conditions. Laboratory catalysts are impregnated with a variety of contaminants, including Ca, Na, and K. Samples of catalyst from slipstream field tests are tested to determine changes in activity with exposure. Advanced surface and composition analyses are used to determine composition, pore size distribution, surface area, and surface properties (acidity, extent of sulfation, etc.).

CCS Reactor Fabrication and Activity Tests

New powder reactors fabricated

In the previous quarterly progress report, the effects of temperature and gas flow rate over ~200 mg of powdered V_2O_5 catalyst packed inside a 0.30" ID reactor tube were reported (See "Preliminary Data on Powdered BYU Catalyst" section in that report). It was concluded that the best option to operate the reactor in a differential manner would be to reduce the amount of catalyst. Since reducing the amount of catalyst results in a shallow packed bed that is susceptible to channeling, new reactor tubes were constructed according to the design shown in the last QPR. A cutaway of the AutoCAD drawing is displayed in Figure 22. This new reactor tube was built by machining a hollowed, funneled piece for the reduced diameter section. Two stainless steel tubes were then welded to the machined piece, as shown in the figure below. The reduced section has a length of 1" and an ID of 0.18".

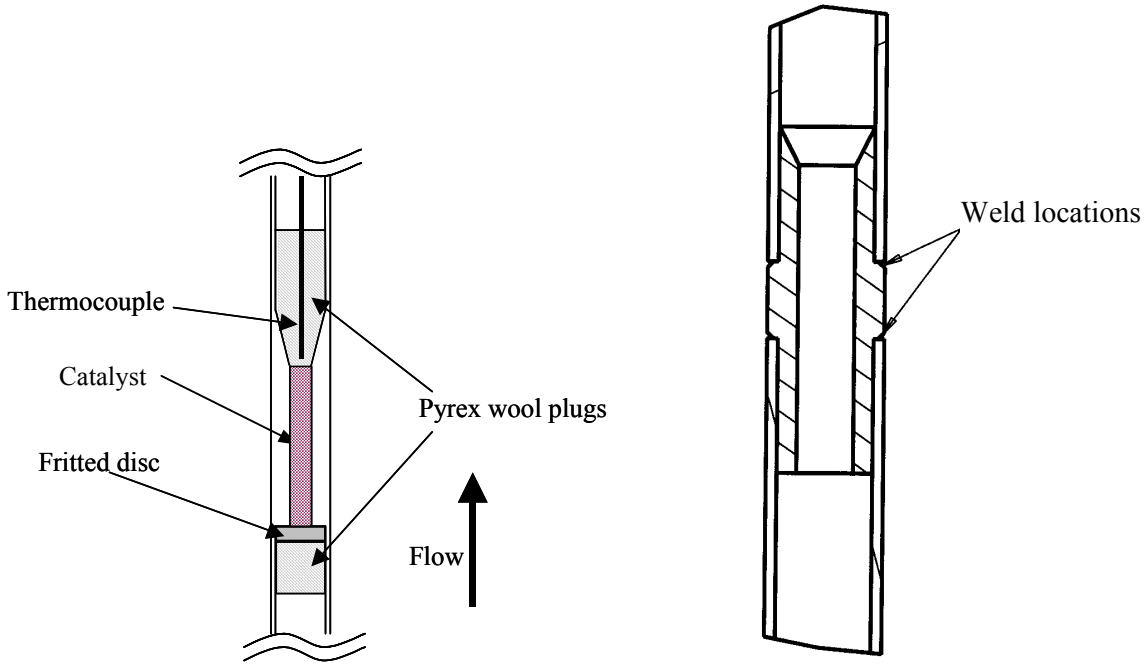

Figure 22. Schematic of new reactor tube design for testing smaller amounts of catalyst.

Optimizing powdered catalyst test runs

A preliminary set of runs was conducted with 100 and 200 mg of crushed catalyst (1%V_2O_5, 9%WO_3 on TiO_2). The catalysts were conditioned in He and O_2 for ~2 hours at 380 °C, after which the temperature was reduced to 350 °C and reactant gas was introduced (2% O_2, ~1000 ppm NO, and ~1000 ppm NH_3). Flow rate was increased through the catalyst until a drop in NO conversion was observed. Even with the smaller catalyst amount (100 mg), the conversion did not drop below 90% even at space velocities in excess of 300,000 hr^{-1} (based on catalyst bed volume at STP), the point at which our mass flow controllers had maxed out. Furthermore, the pressure drop across the catalyst bed was high, i.e., around 12 psi. To ameliorate this problem of high conversion and large pressure drop, all subsequent tests have been performed with 50 mg of catalyst.

Figure 23 shows NO conversion at very high space velocities across 50 mg of catalyst at 350°C. These high gas flow rates were attainable only by running one reactor at a time (rather than 4 simultaneously, which is what the system was designed for). At a SV of 700,000 h^{-1} (about 540 cm^3/min gas flow at STP), NO conversion was around 0.45 and pressure drop across the reactor about 2.9 psi. The pressure drop and conversion were much more acceptable with 50 mg of catalyst as compared to 100 mg, although conversion is still not in the desirable 10-20% range.

Because conversion in this range is apparently difficult to obtain, several options are being considered: (1) using less catalyst (provided that reproducibility does not suffer due to uneven catalyst packing at low catalyst volumes); (2) applying integral reactor equations to calculate rate; (3) distributing a thin coating of catalyst on 0.5 to 1.0 mm solid ceramic spheres or small monolith channels to lower pressure drop while avoiding channeling; or (4) reducing initial catalytic activity to correspond to that of steady-state operation in a commercial reactor after many hours at high reaction temperature (350-400°C) in the presence of water vapor by exposing freshly prepared catalysts to 420-450°C in an air/water vapor mixture.

The last alternative involving treatments in steam at 20-100°C above the normal reaction temperature appears to be necessary to ensure that comparisons of activity for unpoisoned, pre-poisoned and field-tested catalysts reflect only the effects of poisoning, fouling or masking while excluding effects of hydrothermal conditioning that are observed to cause relatively rapid reduction in activity at the beginning of laboratory or commercial operation. Indeed, design requirements for a commercial plant are based on steady-state activity (after a few hundred hours of operation) rather than on the activity of the fresh catalyst.

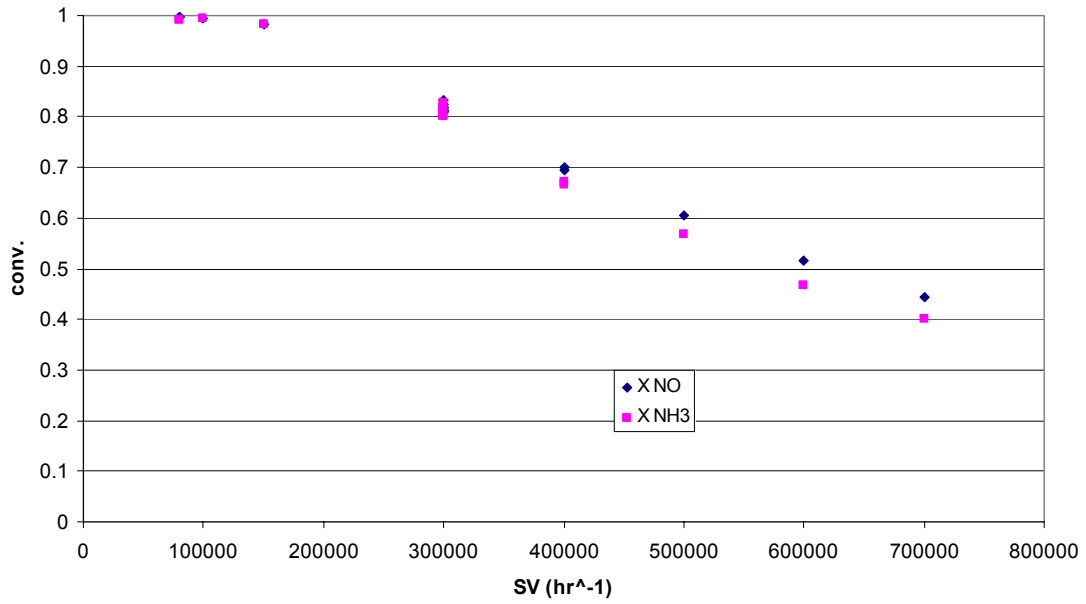

Figure 23. Conversion vs. Space Velocity for 50 mg of crushed BYU catalyst.

Preliminary poisoning study

A simple study was conducted to determine effects of (1) the calcium to vanadium ratio and (2) the effects of SO_2 pretreatment on catalyst activity (i.e. conversion). It should be noted that this was done as a *preliminary* exploratory study in order to gain some experience with the reactors and to fulfill the requirements of a statistics class.

Experimental design

Given the short amount of time available for this study and relatively long run times (each run required in excess of 10 hours), only two factors could be selected: SO_2 effect in pretreatment and Ca/V ratio in the catalyst content. These factors have been reported to significantly influence catalyst activity and lifetime.

A full factorial experiment was designed, as shown in Table 5. Conversion of NO, representative of catalyst activity, was the response variable. X1 represents the catalyst pretreatment procedure: with SO_2 (-1) and without SO_2 (1). X2 denotes the atomic ratio of calcium to vanadia, and which has three levels: 0, 0.5, 1. These levels were selected because catalysts of these Ca/V ratios had already been prepared. The experiment was run in random order and two replicates were conducted of each run.

Table 5. Experimental design table.

	Run Order		Coded factors		Pretreatment	Ca/V ratio
Runs	Rep. 1	Rep. 2	X1	X2	X1	X2
1	6	4	-1	0	with SO_2	0
2	10	3	-1	0.5	with SO_2	0.5
3	1	11	-1	1	with SO_2	1
4	7	8	1	0	without SO_2	0
5	5	2	1	0.5	without SO_2	0.5
6	12	9	1	1	without SO_2	1

Procedure

The procedure for preparation of fresh catalyst is as follows:

1. Mix P25 Degussa titania with water in a 1:1.75 titania to water ratio by weight.
2. Dry resulting paste at 120 °C for 24 hrs.
3. Crush dried titania with mortar and pestle and calcine at 600 °C for 4 hrs.
4. Dissolve ammonium metavanadate and oxalic acid in warm water.
5. Dissolve appropriate amount of ammonium metatungstate in the solution.
6. Mix calcined titania into solution.
7. Dry resulting slurry at 120 °C for 15 hrs.
8. Crush catalyst solid with mortar and pestle and calcine at 550 °C for 5 hrs.

Some of the catalyst samples thus prepared were doped with alkali or alkaline earth elements as follows:

1. Measure appropriate amount of fresh catalyst
2. Dissolve appropriate amount of $CaNO_3$, $NaNO_3$, or KNO_3 (for CaO-, Na_2O-, or K_2O-poisoned samples, respectively) in water
3. Mix fresh catalyst with solution to incipient wetness

4. Dry in furnace (at 120 °C? at least overnight) and crush

50 mg of finely crushed catalyst was placed in one of four reactor tubes according to the run schedule shown in Table 5 (corresponding run and reactor numbers are shown in Table 6 below). Four catalysts were tested simultaneously in four identical reactors mounted in two different furnaces. The reactors were heated to 380°C in He/O_2 (O_2 ~6%), after which "pretreatment" was carried out. Pretreatment consisted of running about 150 sccm of gas over the catalyst at 380°C for two hours. The pretreatment gas composition was the same as the purge gas composition for runs 1–3 ("without SO_2 pretreatment"), while for runs 4–6 it contained ~2000 ppm SO_2 ("with SO_2 pretreatment"). After two hours of pretreatment time, the reactor temperature was reduced to 350 °C and the reactant species were introduced (~1000 ppm each NO and NH_3). Here, the rate of flow was increased to 390 sccm in order to keep conversion as low as possible. SO_2 was not introduced during reaction. Conversion data were obtained and averaged for the first four hours of catalyst operation for each catalyst, as reported below.

Results and Analysis

Results are shown in Table 6.

Table 6. Experiment results.

Runs	Pretreament X1	Ca/V X2	Y Rep1	Rep2	Yave	Yvar	DF	Reactor	
1	with SO_2	0	62.000	73.000	67.50	60.5	1	R4	R2
2	with SO_2	0.5	92.200	91.500	91.85	0.245	1	R3	R2
3	with SO_2	1	72.000	63.500	67.75	36.125	1	R1	R3
4	without SO_2	0	61.000	38.000	49.50	264.5	1	R3	R4
5	without SO_2	0.5	70.000	88.700	79.35	174.845	1	R2	R1
6	without SO_2	1	65.100	50.900	58.00	100.82	1	R1	R4

Figure 24 shows all data points (conversions) plotted versus run number, while Figure 25 shows the data plotted versus calcium content. Note that catalysts in runs 1–3 were not pretreated in SO_2, while pretreatment of catalysts in runs 4–6 included SO_2. It appears from the data set that Ca/V ratio has an effect on conversion, going through a maximum at Ca/V = 0.5 for all cases.

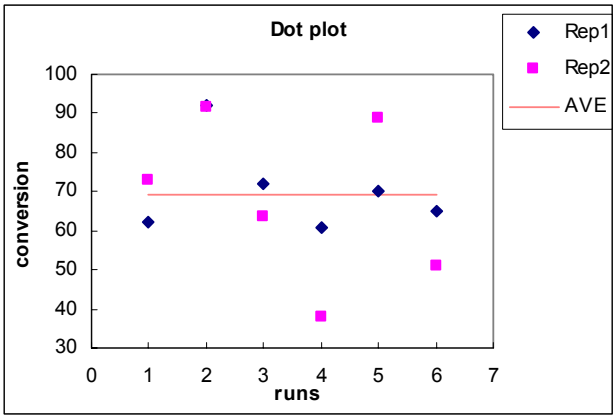

Figure 24. Dot plot of experimental results

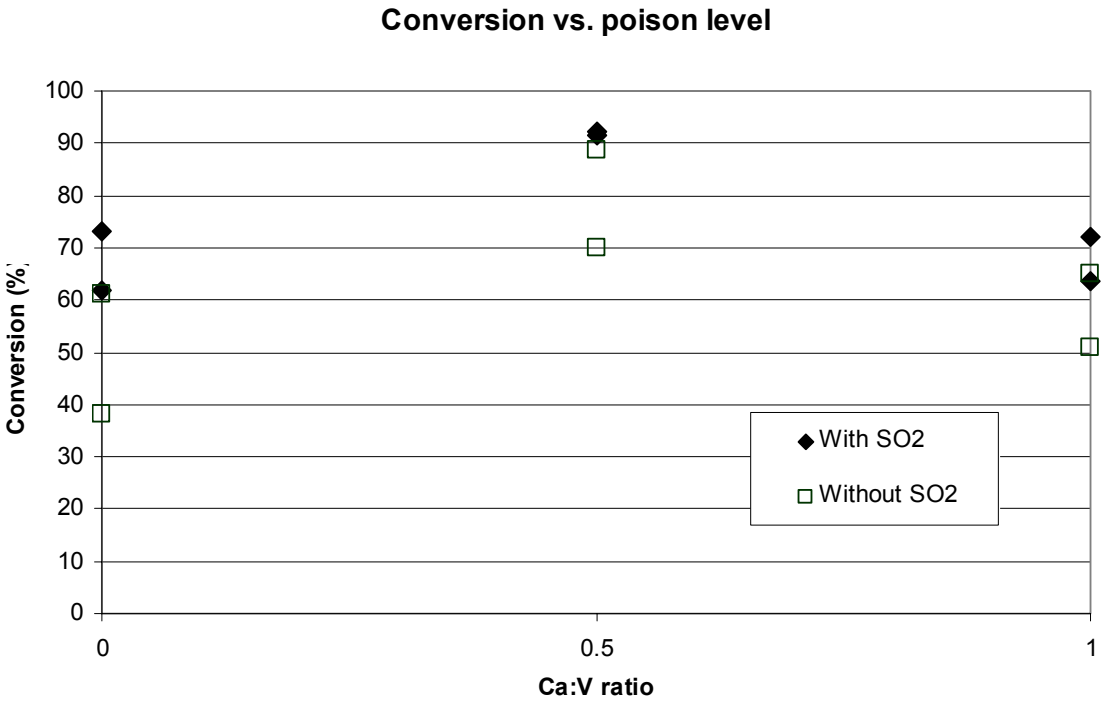

Figure 25. Conversion vs. Ca:V ratio.

Pooled variance, standard deviation, effect and t-value were calculated, and sample size and curvature were checked, as described in detail in Appendix A. At 95% confidence as a cutoff, only poisoning level is significant (although SO_2 pretreatment is close). Activity (conversion) goes through a maximum as the Ca/V ratio is increased from zero to one.

Complementing the curvature test, an ANOVA contrast analysis was performed on the Ca/V ratio to identify the most appropriate model (linear or quadratic) for the effect of Ca/V. The results are discussed in more detail in Appendix A. ANOVA analyses were conducted for two reasons: first, to find out whether there was a significant difference between the effects of the

two factors, SO_2 pretreatment and Ca/V, and second, to see if the reactors had any observable effect on conversion since four separate reactors were used to collect data. The ANOVA results (Table A.4) show that X2 (Ca/V) is significant (p-value < 0.05), in accord with the t-test analysis.

A regression model was set up based on the above analysis (Eq. (1)) and contrast tests, i.e., a linear relationship for pretreatment (X1) and a quadratic relationship for Ca/V (X2). X1 was kept in the model because it is one of the studied objects, although the above results indicate X1 does not have a significant effect on NO conversion. Thus,

$$Y = b0 + b1*X1 + b2*X2 + b3*X2^2 + b4*X1X2 \quad (1)$$

Based on the model (Eqn. 1) a regression analysis was carried out (see Table 7).

The residuals are randomly distributed as shown in the residual plots below, indicating the model is adequate. The results show that most p values are smaller than 0.05 except the p value of the interaction parameter, X1X2. Therefore a new model was established with X1X2 removed (Eq. (2) and Table 8):

$$Y = b0 + b1*X1 + b2*X2 + b3*X2^2 \quad (2)$$

The residual plots in Table 8 indicate the residual is distributed randomly, and thus the model is adequate.

Table 7. Regression analysis of Eq. (1).

I	X1	X2	$X2^2$	X1X2	Y
1	-1	0	0	0	67.5
1	-1	0.5	0.25	-0.5	91.85
1	-1	1	1	-1	67.75
1	1	0	0	0	49.50
1	1	0.5	0.25	0.5	79.35
1	1	1	1	1	58.00

SUMMARY OUTPUT

Regression Statistics	
Multiple R	1.000
R Square	0.999
Adjusted R Square	0.997
Standard Error	0.794
Observations	6

ANOVA

	Df	*SS*	*MS*	*F*	*Significance F*
Regression	4	1133.677	283.419	449.723	0.035
Residual	1	0.630	0.630		
Total	5	1134.307			

	Coefficients	*Standard Error*	*t Stat*	*P-value*	*Lower 95%*	*Upper 95.0%*
Intercept	58.500	0.561	104.215	0.006	51.368	65.632
X1	-8.771	0.512	-17.116	0.037	-15.282	-2.260
X2	104.025	2.862	36.343	0.018	67.656	140.394
$X2^2$	-99.650	2.750	-36.236	0.018	-134.592	-64.708
X1X2	4.125	0.794	5.196	0.121	-5.962	14.212

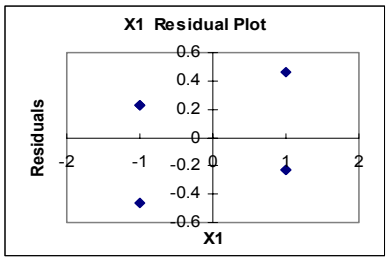

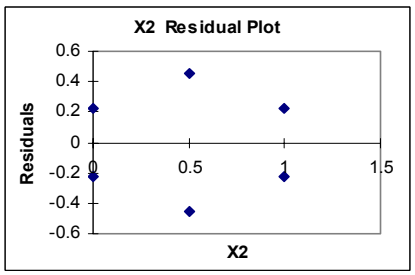

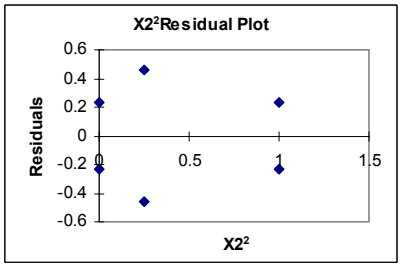

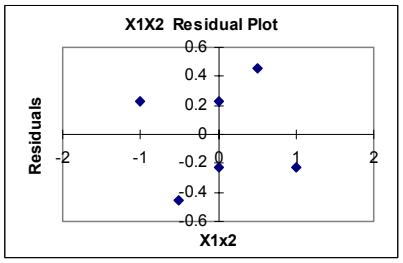

Table 8. Regression analysis of Eq. (2).

I	X1	X2	$X2^2$	Y
1	0	0	0	67.5
1	0	0.5	0.25	91.85
1	0	1	1	67.75
1	1	0	0	49.5
1	1	0.5	0.25	79.35
1	1	1	1	58

SUMMARY OUTPUT

Regression Statistics	
Multiple R	0.992
R Square	0.984
Adjusted R Square	0.961
Standard Error	2.970
Observations	6

ANOVA

	Df	*SS*	*MS*	*F*	*Significance F*
Regression	3	1116.661	372.220	42.188	0.023
Residual	2	17.646	8.823		
Total	5	1134.307			

	Coefficients	*Standard Error*	*t Stat*	*P-value*	*Lower 95%*	*Upper 95%*
Intercept	65.208	2.425	26.887	0.001	54.773	75.643
X Variable 1	-13.417	2.425	-5.532	0.031	-23.852	-2.982
X Variable 2	104.025	10.710	9.713	0.010	57.945	150.105
X Variable 3	-99.650	10.290	-9.685	0.010	-143.922	-55.378

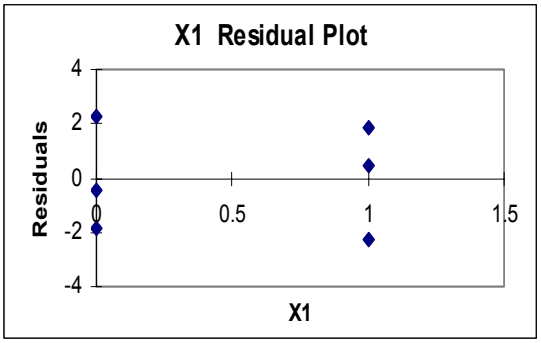

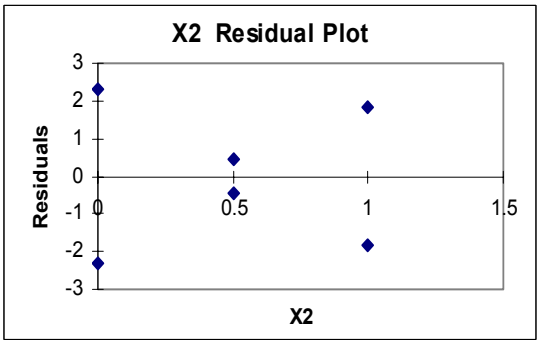

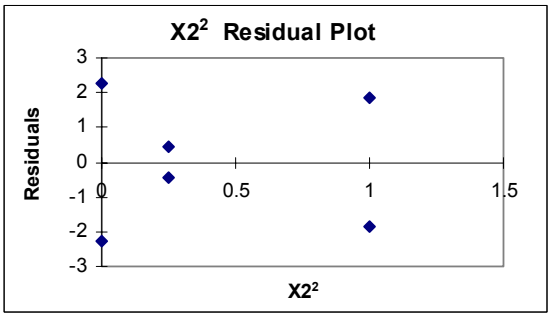

Monolith catalysts cut

A simple method for cutting the fresh and exposed commercial monolith catalysts has been devised. A common scroll saw is used with a fine-toothed blade to cut out square sections of the monolith. Figure 26 shows an example of a cut made on exposed M1. At this time, M4 (BYU) cannot be cut by the scroll saw because it consists of a very hard cordierite material. The plan is to purchase a diamond-impregnated wire to use in the scroll saw in order to cut this material.

Figure 26. Photo showing a cut in M1.

Monolith test reactor design

An economical reactor that will accommodate small cutouts from both monoliths and plates has been designed as shown in Figure 27. This monolith test reactor (MTR) consists of an 8"x 1"x 1" hollow square tube that has flanges on either end. Machined aluminum inserts that hold pieces of monolith or plate catalysts are inserted in this square tube and are placed near the center (See Figure 28). The tube is heated with four plate-type heaters on the outside. The feed gas is routed through a ¼" tube that is placed lengthwise against the outside of one of the heaters in order to preheat the gas (top of Figure 27). Product gases will exit on the opposite end and will be sent to gas analyzer equipment. The whole device will be insulated on the outside and placed on a welded stand, which will stand on a lab bench top.

The aluminum inserts will accommodate up to four channels of commercially representative honeycomb monoliths. This design is advantageous because it allows for minimal changes to the existing reactor system, does not require a bulky and high-energy-consuming furnace, allows for economical gas usage, and provides versatility for this and future applications since various shapes of aluminum inserts may be used for different monolithic catalysts.

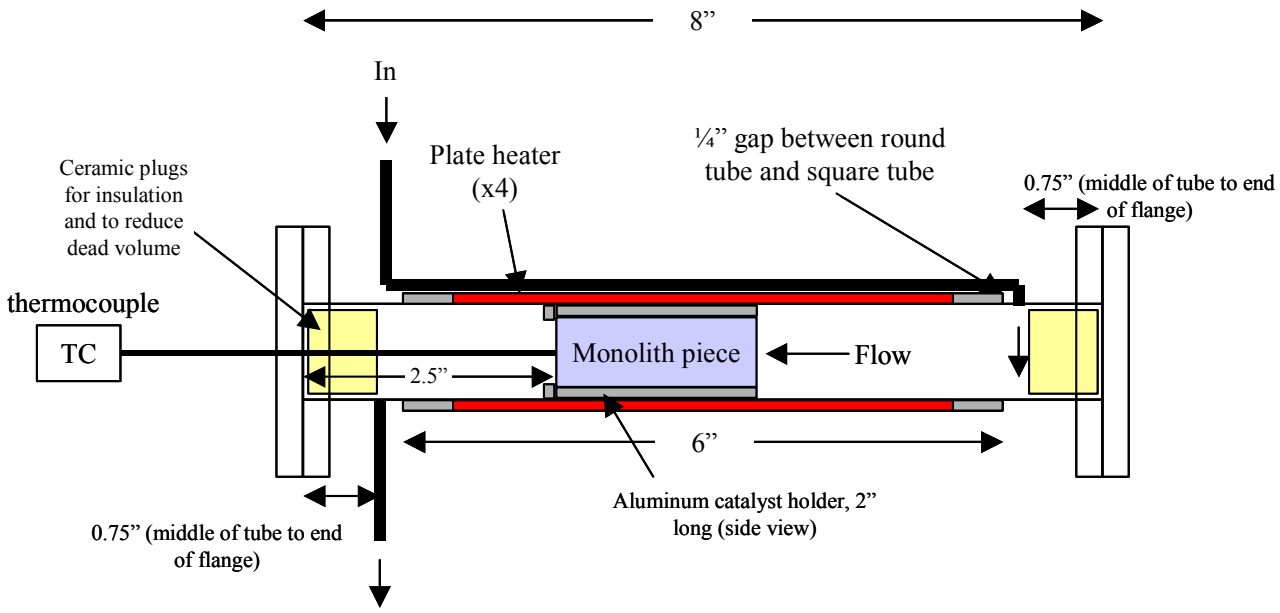

Figure 27. Schematic of monolith test reactor.

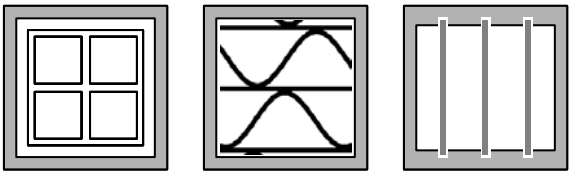

Figure 28. Front view of aluminum catalyst holders displaying (left to right) square honeycomb monoliths (M1, M2, M4), corrugated monolith (M3) and plate catalysts (P1 and P2).

Task 4.2 Evaluation of Commercial SCR Catalysts for Power Plant Conditions

Slipstream Reactor at Rockport

In the last quarter, the slip-stream reactor was not operated due to a major outage at the plant. Also in this quarter the contract to continue testing at the plant was renewed. Following the outage, REI visited the plant to prepare the reactor for restarting the tests after a long period of inactivity. Due to the large number of activities during the outage in the vicinity of the SCR slip-stream reactor, air to the eductors was inadvertently disconnected. This caused the eductors to plug. Further, connections between two control boxes were lost. It was also found that the SMC air control valves behaved incorrectly. These problems are currently being addressed and the reactor is expected to be back in operation in the next quarter.

NO_x Activity from Slipstream Testing

Problems with the sampling system, as documented in previous quarterly reports, have made it difficult to obtain NO_x reduction data continuously from the slipstream reactor. The problems were chiefly plugging in the sample lines and in the heated switching valve. We have addressed these problems by increasing the frequency of purge in the sample lines, by changing the start-up and shut-down procedures for the reactor and by increasing the temperature in the heated switching valve.

NO_x data were obtained in late March and early April (approximately 750 hours of operating time on flue gas) and in late August (approximately 2200 hours of operating time on flue gas). These data will be analyzed to look at the effects of operating conditions and catalyst age on NO_x reduction.

Appendix B contains the NO_x data from the blank catalyst as well as catalysts C2 through C6. The NO_x concentration at the inlet is calculated at 5% O_2. The inlet concentration has been interpolated based on measurements of the inlet concentration made before and after the measurement of the NO_x concentration at the outlet of each chamber. The ammonia concentration was calculated at 5% O_2, based on the total flow measured in the slipstream reactor and the set point to the ammonia mass flow controller. The NH_3/NO ratio is calculated from the ammonia concentration divided by the estimated inlet NO_x concentration. The average catalyst chamber temperature is calculated from the average of the temperature before the catalyst and at the exit of the catalyst chamber. The space velocity is calculated at 32 F (0 C).

There were differences in the temperatures, space velocities and ratios of NH_3/NO between the March/April data and the August data. In order to compare the NO_x reduction, the effects of these parameters must first be characterized.

The March/April data were taken at excess ammonia (NH_3/NO ~ 1.2-1.6) in order to remove any effects of ammonia concentration. The temperatures were in the range of 620-650 F. The main factor that affected the NO_x reduction was the space velocity. Figure 29 shows the NO_x reduction as a function of space velocity for all five catalysts. The NO_x reduction for catalysts C2, C3 and C4 appeared to follow a single curve with space velocity. Catalysts C5 and C6 had different levels of NO_x reduction from the other three; the slopes were about the same, but the intercepts were different.

Some of the August NO_x data were taken during the mercury testing; at this time the ammonia to NO ratios were varied. As the NH_3/NO ratio dropped below 0.95, the NO_x conversion began to fall off. This is seen in Figure 30, which shows the NO_x reduction as a function of NH_3/NO ratio at fixed temperatures and space velocities.

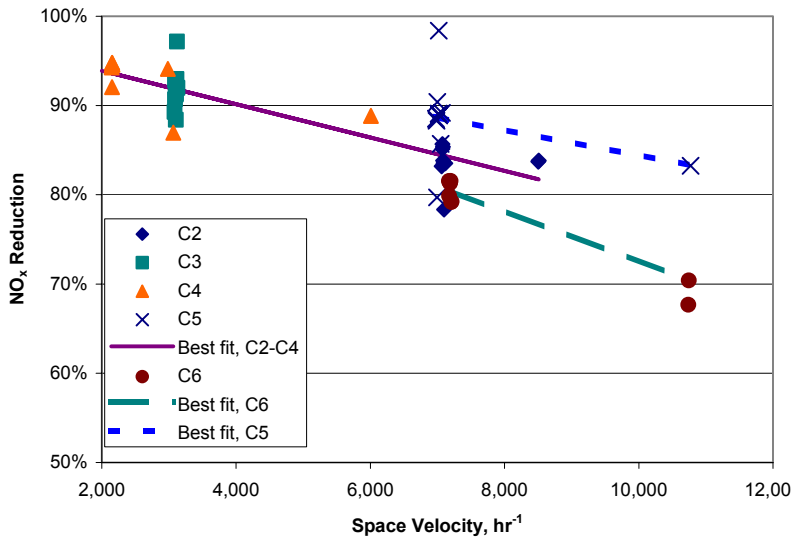

Figure 29. NO_x reduction as a function of space velocity for commercial catalysts from March/April for excess ammonia and catalyst temperatures in the range of 620-650 F.

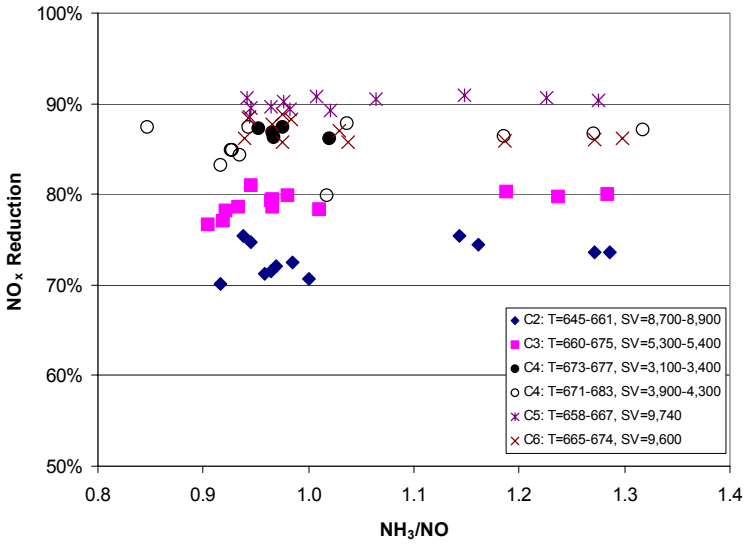

Figure 30. NO_x reduction as a function of NH_3/NO ratio for commercial catalysts from August; temperatures (in degrees F) and space velocities (in hr^{-1}) as indicated on legend.

The effect of temperature on NO_x reduction can also be seen in the August data. Figure 31 shows the NO_x reduction as a function of temperature at a fixed space velocity, all for NH_3/NO > 0.95. Since the March/April data were obtained at different temperatures and space velocities than the August data, the August data were corrected for temperature by using the curvefits shown in Figure 31 and Table 9. Such curvefits should not be used for large temperature corrections; however, the upper end of the range of temperatures in March/April data is generally close (0 to 8 F) to the lower end of the August temperature range for catalysts C2 through C5. There is a 20 F gap in temperature ranges for C6; therefore extrapolation of the C6 data is suspect.

Figure 32 compares the March/April NO_x data with the August NO_x data. The August data show the range of NO_x reductions that correspond to the temperature range of the data of the March/April data. Catalysts C2, C3 and C4 appear to have lower NOx reduction in August as compared to March/April. Catalyst C5 has about the same NOx reduction. Catalyst C6 appears to have higher NOx reduction in August as compared to March/April; however, extrapolating the C6 NO_x reduction to the range of temperatures of the March/April tests may produce larger errors than for the other catalysts, as discussed previously.

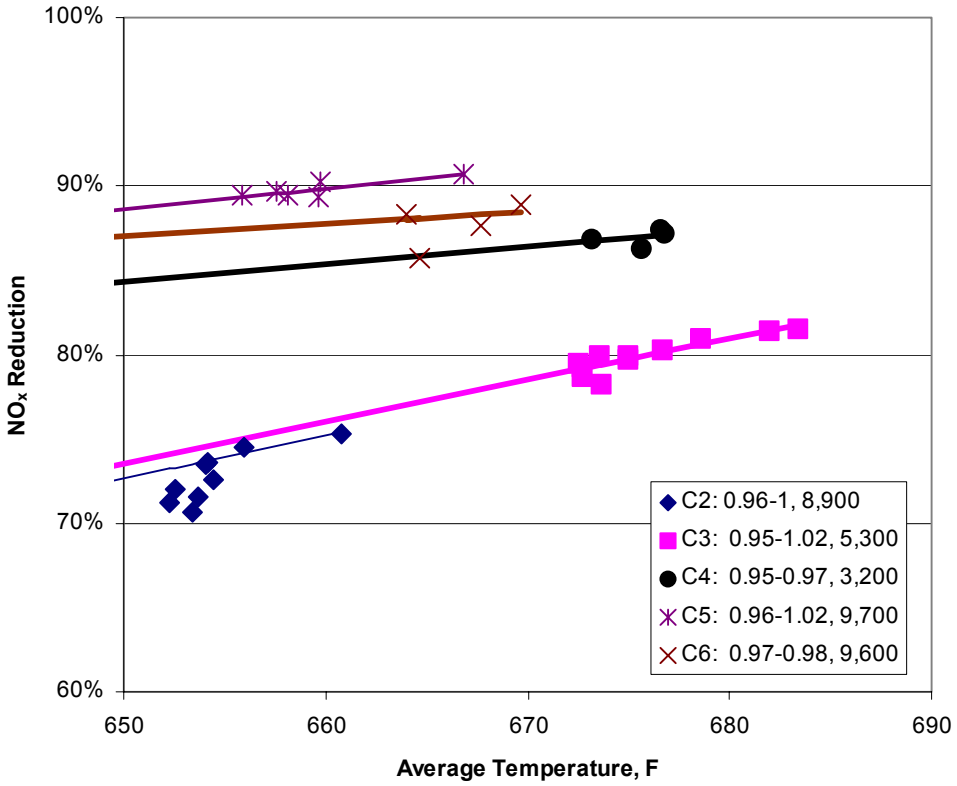

Figure 31. NO_x reduction as a function of temperature for commercial catalysts from August; NH_3/NO ratios and space velocities (in hr^{-1}) as

Table 9. Relationship between NO_x reduction and temperature from August test data.

Catalyst	C2	C3	C4	C5	C6
Space velocity, hr^{-1}	8,900	5,300	3,200	9,700	9,600
NH_3/NO	1.14-1.29	0.95-1.02	0.97-0.97	0.96-1.02	0.97-0.98
Temperature range, F	653-661	674-683	676-685	660-669	670-675
r^2	0.95	0.80	0.38	0.68	0.12
Intercept	-97.2	-87.1	16.7	9.2	39.4
Slope	0.261	0.247	0.104	0.122	0.073

For catalysts C2 and C3, the activity in August (relative to the March/April data) was 85%. For catalyst C4, the activity was 93%. Catalyst C5 had an activity of about 100%. The difficulty in interpreting the NO_x reduction data highlight the importance of obtaining NO_x data over a range of temperatures and space velocities in the slipstream reactor, in order to be able to make meaningful comparisons.

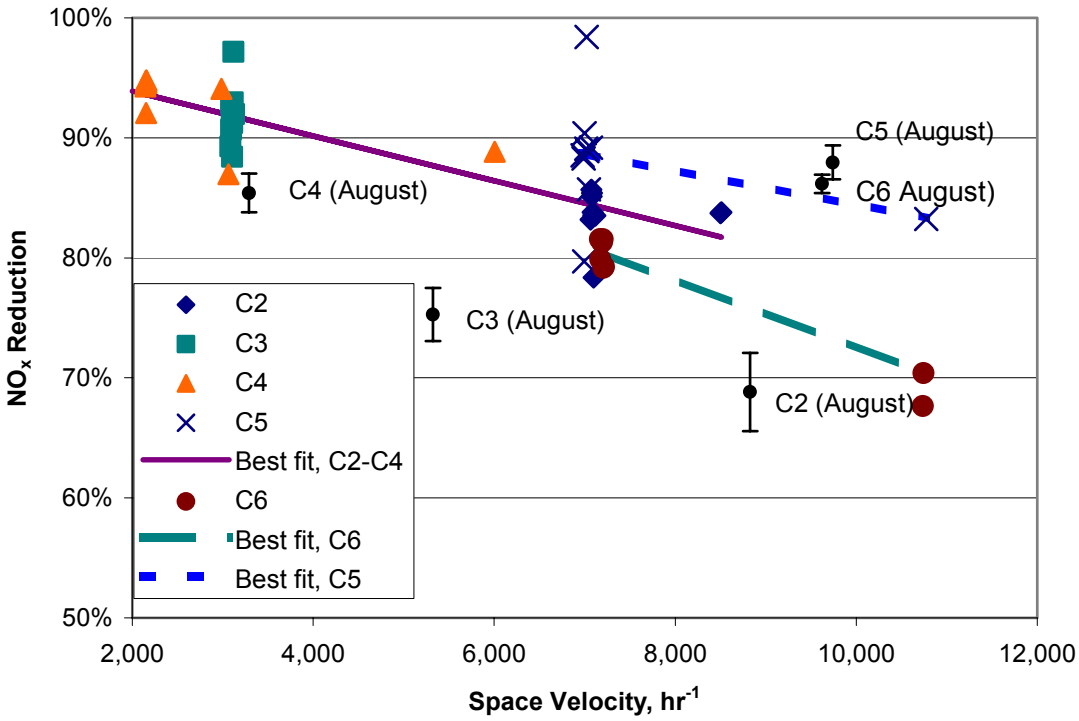

Figure 32. NO_x reduction as a function of space velocity for commercial catalysts from March/April for excess ammonia and catalyst temperatures in the range of 620-650 F compared with August data (extrapolated to the appropriate temperature range.

Biomass Co-firing Tests

REI personnel visited Alabama Power's Plant Gadsden on 19 November 2003 and met with personnel from Southern Company and Plant Gadsden. Plant Gadsden has two 70 MW tangential-fired boilers. The plant is due to be retired in 2008. It has been burning biomass as part of a three-year DOE program. It will probably continue to burn biomass after this year, when the program is over. They are currently burning switchgrass 7-8 hours/day, five days a week in Unit 2. The switchgrass is ground and fed pneumatically into two corners of the boiler, just below the topmost coal port. The switchgrass is fired at 2.5 tons per hour, or about 5% on an energy input basis. The plant has tried co-milling different biomass fuels at Gadsden; this was generally unsuccessful. Co-milling sawdust did seem to be successful.

Southern Company has built two slipstream reactors that are currently installed on Unit 2. Each reactor has one meter of monolith catalyst, two cells by two cells wide. The flow through each reactor is 25 scfm. One reactor runs when biomass is being co-fired. The other runs when coal alone is being fired in order to provide a control. Flow through the slipstream reactor is down through the catalyst, which is mounted vertically. The inlet probes are about seven feet long. Extensive traverse measurements of ash loading were made to decide how to place the probes. Because the switchgrass is injected in two corners of the boiler, there is stratification of the biomass ash in the duct.

Data collection from the existing slipstream reactors will finish in May 2004, at which time they hope to have 1000 hours of operation on switchgrass; in November they had about 250 hours. Weekly coal, switchgrass, and ash samples are taken. The data acquisition system monitors the auger feed rate to calculate the biomass feed rate. They plan to periodically pull samples for analysis and add fresh catalyst; this will give a range of exposure times. Analyses include:

- Activity
- Bulk chemical analysis
- Porosimetry
- SEM
- XES analysis
- Chemical analysis of ash, biomass, coal
- BET surface analysis

Southern Company and Alabama Power personnel were very interested in the REI's slipstream reactor being deployed at Gadsden for testing. They suggested two different ways to go for long-term testing:

- Switchgrass firing on Unit 2 for 7-8 hours per day as with the existing slipstream reactor.
- Continuous sawdust firing on Unit 1 by co-milling sawdust at about 5% weight basis.

Plant personnel believe that they could co-mill 5% sawdust twenty-four hours per day. This would have the advantage of longer exposure times for the catalysts to biomass and a fairly steady fuel source. The disadvantage is that the amount of biomass would be small (2-3% of the fuel on an energy basis). There will be an outage on Unit 2 some time in the spring. Unit 1 will have an outage in the spring. While nothing has yet been finalized, there was genuine interest from Southern Company and the plant in hosting a test. Discussions will continue in the next quarter.

Task 5 - Fly Ash Management/Disposal

This task deals with the undesirable adsorption of ammonia on fly ash associated with the operation of advanced NOx control technologies such as selective catalytic reduction. The task examines the fundamentals of the adsorption process as well as the fundamental process underlying potential techniques for post-combustion removal of adsorbed ammonia.

The work effort for this task has been completed. The work was performed at Brown University under the leadership of Prof. Bob Hurt. The subcontract with Brown University ended September 30, 2003. Included in Appendix C of this report is an extensive write-up that constitutes a final report for this Task.

This work presents the first fundamental ammonia isotherms on carbon-containing fly ash samples obtained after a custom retrofit of a commercial vapor adsorption apparatus for compatibility with ammonia. Ammonia adsorption near room temperature is shown to be dominated by adsorption on carbon with only of order 20 ppm adsorbed on the mineral component. The adsorption on carbon is a combination of physisorption and chemisorption on acidic surface sites. Introduction of additional oxygen functional groups on carbon increases ammonia adsorption by increasing the number of these acidic sites. The absolute amounts of ammonia adsorbed on fly ash in this study are much less than those of concern in the utility sector and much less than those found by Muzio in a study using simulated flue gas. Secondary components of the flue gas, either water, SO_2, or SO_3 are likely responsible for most of the ammonia observed associated with ash in utility practice, with a lesser component attributed to true adsorption on carbon surfaces.

This work also demonstrates that ammonia species can be removed from fly ash at or near room temperature by a variety of dry and semi-dry techniques. The work confirms industrial reports that aqueous solution chemistry takes place upon the introduction of even very small amounts of water, while the ash remains in a semi-dry state for handling. Rapid ammonia removal occurs from a microscopic water film on surfaces, in fine pores, and in ash particle interstitial regions whenever the film pH is high — achieved either by dissolution of the natural basic components of the ash or by the separate introduction of soluble basic additives. Flowing humid air and flowing water aerosol (fog) are promising methods for the uniform addition of small amounts of water to fly ash for semi-dry ammonia removal. Ozone is capable of destroying ammonia on ash in the dry state, but is less effective under semi-dry conditions due to kinetic limitations on the aqueous phase reaction at the lower pH values needed to keep ammonia in solution.

Results and Discussion

Preliminary Results for the Electrochemical Noise Corrosion Monitors

To aid a quick assessment of how the probes are performing, the data from the Main (central) probe was plotted. Initially as the system was being commissioned the data appeared unstable, but thereafter looked perfectly sensible. The corrosion data was replotted from the point where consistent monitoring commenced. The result was the screenshot of the corrosion rate shown in Figure 33.

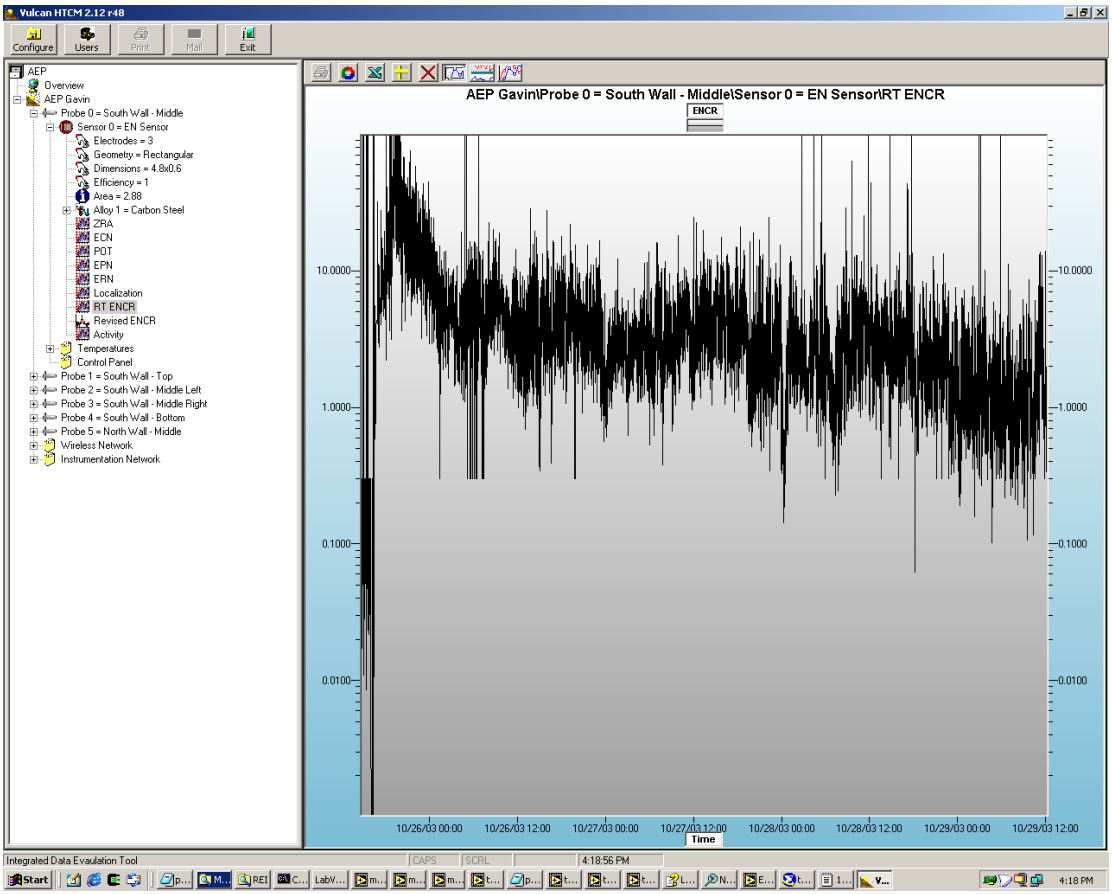

Figure 33. Gavin Main Probe Corrosion Rate (first ~3 days of monitoring).

It can be seen that the rate was very low as the probe went in, but rose quite rapidly to around 50 mmpy. Over the course of the next 12 hours or so it fell quite quickly to around 4 mmpy, but from around midnight on the 24th to around mid-day on the 26th it remained reasonably steady at around 3 mmpy. Thereafter it declined over the next 20 hours or so to around 1 mmpy, but it kicked up again during the last ~4 hrs of monitoring shown in the screenshot.

The trend shown by the data appears consistent and quite representative of what we might expect during the immediate post-installation conditioning period. From this point forward, however,

the EN response looks very much more typical of what we might hope to see from the instrumentation. Fluctuations are responsive but consistent and the general trend of activity appears to be very stable.

It is very early to start drawing conclusions as to what exactly each little bump in the response means. Nevertheless, during the first thirty-six hours of monitoring, when the system was still shaking down, the corrosion data we have obtained appear consistent and believable. There are restrictions, however, on the absolute accuracy of the indicated corrosion rates, and of the precise sensor temperature, but these issues will be investigated, clarified and resolved in due course. In addition, Figure 29 was plotted without the plant data, as these are not yet available.

Discussion of the Catalyst Sulfation Study

Study of VO_x/TiO_2 sulfation is important to the understanding of poisoning and deactivation in SCR since: (1) SO_2, typically present in the stack gas, apparently reacts in the presence of water to form surface vanadium and/or titanium sulfate during SCR (previous works in the literature suggest vanadium sulfate but evidence is not definitive --hence basic research is needed to resolve this issue); (2) formation of sulfates may impact activity, since SO_2 may adsorb on or near Brønsted acid sites, which are active sites for the reaction, and previous studies are not in agreement regarding the effect on activity--hence more work of a fundamental nature is needed to resolve these issues; (3) acidic surface sulfates probably influence, maybe even mitigate, poisoning by basic compounds such as CaO, Na_2O, K_2O, etc.; and (4) formation of surface vanadium or titanium sulfates may play a role in pore plugging or masking by calcium sulfate (e.g. one hypothesis is that calcium oxide may adsorb first and then react with SO_3 or with the other sulfates already present on the surface to form Ca sulfate).

Discussion of the Catalyst Poisoning Study

This preliminary study has allowed us to assess the performance of the reactor system, perform initial catalyst characterization, and gain some experience with an appropriate statistical design. Several important points are in order.

The most interesting result is that calcium appears to *increase* catalyst activity, something that contradicts the results of previous research (Chen, Buzanowski et al. 1990; Chen and Yang 1990). At the present time we have no logical explanation for this phenomenon. Differences between our study and those of Chen et al., including reaction temperature, vanadia loading, and catalyst poisoning technique, need to be explored.

Reaction temperature can substantially affect adsorption strengths and hence extents of poisoning; for example, it is generally observed that poisoning becomes more reversible at high reaction temperatures. The temperature in this study (350°C) is somewhat higher than that of Chen and Yang (300°C); accordingly, effects of poisoning on activity might be much less important at the higher temperature—a temperature representative of commercial operation. They used considerably larger pellets @ 20-32 mesh (841-500 micron), while we used fine powder (average particle size on order of 100 microns). We are currently investigating external mass transfer and pore diffusion effects with our catalyst in order to increase size without entering in the mass-transfer and pore-diffusion limiting regimes. Preliminary calculations indicate that pore diffusion is important in particles larger than 300 microns, and we wonder if such pore diffusion limits may have gone undetected by Chen and Yang, even with the

experiments that they did to confirm there was no mass transfer limits. Our preparation procedure was essentially the same as theirs except for the following: (1) our catalyst composition was 1% vanadia, 9% tungsta, and balance titania, while their composition was 5% vanadia on titania, and no tungsta; (2) they calcined the catalyst after poisoning before running it in the reactor, while we did not.

Although this study provides a statistically meaningful prediction of the effect of Ca/V ratio, the data were quite scattered within the replications (where identical catalysts under identical conditions were run). It is thought that this is principally due to the catalyst packing and its resultant effects on flow through the packed bed. The packing procedure consists of inserting 2 parts of glass wool, 1 frit, and the catalyst powder. The amount of glass wool and catalyst is specified, and packing sequence is standardized. However, how the glass wool and catalyst powder reside inside the reactor can only be kept approximately consistent. Indeed, pressure drop through the bed varied greatly between runs (anywhere from ~0.5 to 5.6 psig). High reactor inlet pressure changes the concentration of reactants and thus may alter the observed kinetics. Furthermore, lower pressure at the catalyst inlet may be indicative of channeling where reactants may bypass the catalyst bed. The effects of inlet pressure were not analyzed in the present study, but are currently being evaluated.

In this study, the catalyst powder was not sieved prior to loading in the reactor as it was assumed the powder would be small enough to prevent pore diffusion effects (subsequent sieving indicates that average particle size was at most 100 microns). The principal reason for such high pressure drops is due to this small powder, as lower pressure drops are encountered in runs conducted with an equivalent mass of catalyst consisting of larger pellets (diameter between 250 and 297 microns).

Mass transfer and pore diffusion effects are currently being investigated in addition to the pressure drop issues. Once these issues are resolved, and we are satisfied that we are operating in the intrinsic regime, reaction rate constants will be calculated and reported.

A number of experimental issues need to be resolved: (1) the uniformity of V and Ca in the catalysts; (2) whether a measurable activity loss occurs during the first few hours of reaction due to restructuring of the catalyst in the presence of reactants, including steam; and (3) how to eliminate effects of pressure drop, channeling and other non ideal reactor effects. Resolution of these issues could lead to significant improvements in experimental design and measurement of more statistically significant data. Activity measurements for unpoisoned and poisoned catalysts as a function of temperature between 250 and 400°C appear to be key to an understanding of the deactivation mechanism.

Conclusions

Good progress has been made on several fronts during the last three months. In particular:

- Using the initial CFD baseline modeling of the Gavin Station and the plant corrosion maps, six boiler locations for the corrosion probes were identified and access ports have been installed.
- One probe has been collecting data for more than three months and two others have been in service for more than two months; preliminary corrosion data obtained appear consistent and believable.
- *In situ*, spectroscopic experiments at BYU reported in part last quarter were completed; the most significant finding of these investigations was a consistent indication that vanadium does not sulfate during SCR reaction in the presence of gas-phase SO_2 while both the substrate (anatase) and modifiers (molybdenum) do.
- New reactor tubes have been made for BYU's CCR that allow for testing smaller amounts of catalyst and thus increasing space velocity; monolith catalysts have been cut and a small reactor that can accommodate these pieces for testing is in its final stages of construction.
- A preliminary poisoning study on Ca-poisoned catalysts at 380°C indicates that Ca actually increases SCR catalyst activity at a Ca:V ratio of 0.5:1 (as compared to unpoisoned catalyst), although further investigation is necessary to validate this result.
- Further analysis of the catalyst activity data based on measurements in the slipstream reactor suggests that for catalysts C2 and C3, the activity in August (relative to the March/April data) was 85%. For catalyst C4, the activity was 93%. Catalyst C5 had about the same activity in August relative to March/April, while it was difficult to make the comparison for catalyst C6 because of lack of data at similar process conditions.
- REI visited Alabama Power's Plant Gadsden and discussed the possibility of conducting biomass co-firing tests at the plant with the slipstream reactor.
- After a visit to Rockport, it was determined that the slipstream reactor there required repair and refurbishment; the reactor will be re-started in the next quarter.
- The final results of an experimental project at Brown University on the fundamentals of ammonia / fly ash interactions with relevance to the operation of advanced NOx control technologies such as selective catalytic reduction is included. The Brown task focused on the measurement of ammonia adsorption isotherms on commercial fly ash samples subjected to a variety of treatments and on the chemistry of dry and semi-dry ammonia removal processes.

Plans for Next Quarter

Corrosion probe activity for the next quarter will focus on the following:

- Replace and install the remaining three corrosion probes.
- Remove the sensor elements from the center probe (in service for 3 months) and perform precision metrology. Reinsert the probe with new sensor elements.
- Upgrade computer links for better remote access
- Gather operating data from unit for corrosion correlation developments
- Complete precision metrology
- Initiate data reduction and correlation development on test results

Catalyst size and packing methods will be explored further in order to obtain more consistent data in the CCR. Catalysts particle diameters or coating thickness will be carefully controlled to minimize pressure drop without operating in mass-transfer and pore-diffusion limiting regimes. Once reliable methods of catalyst packing, appropriate catalyst sizes, and pretreatments have been selected, a new set of catalysts will be prepared. Based on a carefully considered statistical design, first-order rate constants for the reaction will be determined as a function of poison concentration and temperature in subsequent poisoning studies for the poisons under investigation (Na, K, and Ca). Early in the next quarter, BYU will begin to analyze surface area and pore size distributions of commercial monoliths. By the end of February they expect to have a good idea of what sample size to use in the monolith test reactor and how it should be operated.

SCR slipstream activity for the next quarter will focus on the following:

- Resume testing at Rockport Unit 1 after rectifying slipstream reactor problems developed during the outage.
- Continue discussions with Southern Company and Alabama Power about hosting a demonstration.

References

Chen, J. P., M. A. Buzanowski, et al. (1990). "Deactivation of the Vanadia Catalyst in the Selective Catalytic Reduction Process." Journal of the Air & Waste Management Association **40**(10): 1403-1409.

Chen, J. P. and R. T. Yang (1990). "Mechanism of Poisoning of the V_2O_5 TiO_2 Catalyst for the Reduction of NO by NH_3." Journal of Catalysis **125**(2): 411-420.

Chen, J.P. and Yang, R.T. (1993). "Selective Catalytic Reduction of NO with NH_3 on SO_4-2/TiO_2 Superacid Catalyst." J. Catal. **139**: 277-288.

Appendix A

Statistical Analysis of Poisoning Experiments

For the calcium poisoning experiments, pooled variance, standard deviation, effect and t-value were calculated, and sample size and curvature were checked. Table A.1 shows the results of a t-test conducted on the two factors and their interaction. At 95% confidence as a cutoff (where t_{crit} = 2.447), only poisoning level is significant (t = 11.84) (although SO_2 pretreatment is close at t = 2.26).

The number of replicates necessary to detect the significance of X2's effect, n_F, was calculated and found to be 1.37 (2), as illustrated in Table A.1. This shows that the present experiment was sufficient for the desired precision, despite the considerable spread in the data.

Curvature was checked (Table A.2). Since t_C of 3.948 is larger than the t-critical (2.447), curvature is significant. Thus, activity (conversion) goes through a maximum as the Ca/V ratio is increased from zero to one.

Complementing the curvature test, an ANOVA contrast analysis was performed on X2 (Ca/V) to identify the most appropriate model (linear or quadratic) for the effect of X2. The results are shown in Table A.3. Only the t-value for the quadratic model is larger than the critical t-value, indicating that a quadratic model is most appropriate for this data set.

ANOVA analyses were conducted for two reasons: first, to find out whether there is a significant difference between the effects of the two factors (Table A.4) and second, to see if the reactors had any observable effect on conversion since 4 separate reactors were used to collect data (Table A.5).

The ANOVA results (Table A.4) show that X2 (Ca/V) is significant (p-value < 0.05), in accord with the t-test analysis.

Table A.1. t-test summary.

S^2_p =	106.173	S_p =	10.304		
Runs =	6	Reps =	2		
S_E =	5.949	nf =	12		
Run	**Mean**	**X_1**	**X_2**	**X_1X_2**	**Y_{Ave}**
1	1	-1	0	0	67.50
2	1	-1	0.5	-0.5	91.85
3	1	-1	1	-1	67.75
4	1	1	0	0	49.50
5	1	1	0.5	0.5	79.35
6	1	1	1	1	58.00
SP	413.95	-40.25	211.35	-16.00	
Effect =		13.42	70.45	5.33	n_F = 1.369
t_E =		2.26	11.84	0.90	$t_{Critical}$ = 2.447
p =		0.0650	0.0000	0.4045	
H_O:	Effects = 0		α =	0.05	

Table A.2. Check of curvature.

X1	**X2**	**Y1**	**Y2**	**Y_{ave}**	
-1	0	62.000	73.000	67.5000	
-1	1	72.000	63.500	67.7500	
1	0	61.000	38.000	49.5000	
1	1	65.100	50.900	58.0000	60.688
-1	0.5	92.200	91.500	91.8500	
1	0.5	70.000	88.700	79.3500	85.600
				C =	24.913
				S_c =	6.309888
				t_c =	3.948168

Table A.3. Contrast calculation for factor X2 (Ca/V).

Ca/V	**Rep1**	**Rep2**	**Rep3**	**Rep4**	**Mean**	**Variance**	**linear**	**Quadratic**
0	62.00	73.00	61.0	38.0	58.5	216.33	-1	1
0.5	92.20	91.50	70.0	88.7	85.6	110.45	0	-2
1	72.00	63.50	65.1	50.9	62.88	77.34	1	1
SS							2	6
C							4.375	-49.825
S_c							7.2860	12.6120
t							0.6005	-3.9482
t critical							2.2622	

Table A.4. ANOVA analysis of pretreatment and Ca/V.

X1	X2		
	0	0.500	1.000
with SO2	62	92.2	72
	73	91.5	63.5
without SO2	61	70	65.1
	38	88.7	50.9

Anova: Two-Factor With Replication

SUMMARY	0	0.5	1	Total
with SO2				
Count	2	2	2	6
Sum	135	183.7	135.5	454.2
Average	67.5	91.85	67.75	75.7
Variance	60.5	0.245	36.125	175.88
without SO2				
Count	2	2	2	6
Sum	99	158.7	116	373.7
Average	49.5	79.35	58	62.2833
Variance	264.5	174.845	100.82	297.2457
Total				
Count	4	4	4	
Sum	234	342.4	251.5	
Average	58.5	85.6	62.875	
Variance	216.3333	110.4467	77.3358	

ANOVA

Source of Variation	*SS*	*Df*	*MS*	*F*	*P-value*	*F crit*
Sample	540.0208	1	540.0208	5.0863	0.0650	5.9874
Columns	1693.3017	2	846.6508	7.9743	0.0204	5.1432
Interaction	35.2917	2	17.6458	0.1662	0.8506	5.1432
Within	637.035	6	106.1725			
Total	2905.6492	11				

Analysis of variance on the effects of the reactor used and the effect of run-to-run differences was calculated. The data are shown in Table A.6 and the results are displayed in Table A.7. The first group (4 groups) is calculated for each row in Table A.5, the second group (6 groups) is calculated for each column in Table A.5. Since p values are greater than 0.05, there is no evidence of a significant difference among reactors in this data set, nor is there evidence of a significant run-to-run difference.

Table A.5. Conversion data vs. reactor number.

	Run					
Reactor	**1**	**2**	**3**	**4**	**5**	**6**
1			72		88.7	65.1
2	73	91.5			70	
3		92.2	63.5	61		
4	62			38		50.9

Table A.6. ANOVA analysis for reactors

	Group			
	1	**2**	**3**	**4**
Sample Size	3	3	3	3
Mean	75.27	78.17	72.23	50.30
Variance	147.24	135.58	300.56	144.27

Source	**Df**	**SS**	**MS**	**F**	**p**
Between Groups	3	1,450.33	483.44	2.66	0.1196
Within Groups	8	1,455.32	181.92		
Total	11	2,905.65			**H_o: No Difference**

	Group					
	1	**2**	**3**	**4**	**5**	**6**
Sample Size	2	2	2	2	2	2
Mean	67.50	91.85	67.75	49.50	79.35	58.00
Variance	60.50	0.25	36.13	264.50	174.85	100.82

Source	**Df**	**SS**	**MS**	**F**	**p**
Between Groups	5	2,268.61	453.72	4.27	0.0529
Within Groups	6	637.04	106.17		
Total	11	2,905.65			**H_o: No Difference**

Appendix B

Catalyst NO_x Data from Slipstream Reactor

The NO_x concentration at the inlet is calculated at 5% O_2. The inlet concentration has been interpolated based on measurements of the inlet concentration made before and after the measurement of the NO_x concentration at the outlet of each chamber. The ammonia concentration was calculated at 5% O_2, based on the total flow measured in the slipstream reactor and the set point to the ammonia mass flow controller. The NH_3/NO ratio is calculated from the ammonia concentration divided by the estimated inlet NO_x concentration. The average catalyst chamber temperature is calculated from the average of the temperature before the catalyst and at the exit of the catalyst chamber. The space velocity is calculated at 32 F (0 C).

Table B.1. NO_x data for catalyst C1 (blank monolith).

Chamber	Date	Inlet NO_x ppm (est)	NO_x reduc.	T before cat, F	NH_3/NO	Avg T catal, F	SV, hr^{-1}
one	3/26/03	329	6.1%	655	1.40	625	6,279
one	3/27/03	318	3.1%	662	1.35	634	6,283
one	8/11/03	334.5	6.1%	617	1.02	555	2,745
one	8/12/03	332.7	-0.3%	678	1.05	602	1,406
one	8/13/03	318.9	3.1%	617	0.94	553	1,803
one	8/21/03	392.5	-4.8%	696	0.88	654	4,050
one	8/21/03	383.3	1.8%	698	1.00	655	4,126
one	8/21/03	370.7	5.7%	691	1.23	647	4,225
one	8/21/03	373.4	12.8%	691	1.25	646	4,242

Table B.2. NO_x data for catalyst C2 (monolith).

Chamber	Date	Inlet NO_x ppm (est)	NO_x reduc.	T before cat, F	NH_3/NO	Avg T catal, F	SV, hr^{-1}
two	3/26/03	329.4	83.2%	657	1.43	627	7064
two	3/27/03	323.8	83.8%	662	1.43	628	7,087
two	3/27/03	335.9	85.4%	662	1.32	629	7,080
two	3/27/03	311.8	85.7%	655	1.32	623	7,073
two	3/27/03	308.5	83.5%	660	1.40	630	7,119
two	3/27/03	328.6	85.1%	658	1.29	628	7,076
two	3/27/03	239.6	78.4%	668	1.62	649	7,099
two	3/27/03	317.0	83.6%	667	1.26	648	7,093
two	4/5/03	301.4	83.8%	685	1.27	648	8510
two	4/5/03	301.4	83.7%	685	1.27	646	8501
two	8/11/03	334.5	71.4%	617	1.02	554	5,687
two	8/12/03	331.7	76.7%	644	1.20	570	3,568
two	8/13/03	318.9	62.2%	611	0.93	553	4,841
two	8/15/03	331.4	70.7%	612	1.23	543	5,125
two	8/21/03	383.6	74.8%	694	0.94	658	8,682
two	8/21/03	391.2	75.4%	698	0.94	661	8,654
two	8/21/03	382.7	75.4%	698	1.14	661	8,641
two	8/21/03	378.1	74.5%	692	1.16	656	8,696
two	8/21/03	371.1	73.5%	691	1.29	654	8,756
two	8/21/03	373.4	73.6%	691	1.27	654	8,751
two	8/22/03	361.6	72.2%	674	0.94	636	8,656
two	8/22/03	350.5	70.9%	678	0.92	641	8,800
two	8/22/03	337.5	69.2%	676	0.89	640	8,859
two	8/22/03	344.9	70.1%	683	0.92	645	8,967
two	8/22/03	365.7	72.0%	690	0.97	653	8,963
two	8/22/03	364.2	71.5%	690	0.96	654	8,973
two	8/22/03	345.5	70.6%	689	1.00	653	8,940
two	8/22/03	362.3	72.5%	690	0.98	654	8,837
two	8/22/03	351.9	71.2%	688	0.96	652	8,878

Table B.3. NO_x data for catalyst C3 (plate).

Chamber	Date	Inlet NO_x ppm (est)	NO_x reduc.	T before cat, F	NH_3/NO	Avg T catal, F	SV, hr^{-1}
three	3/26/03	311.3	93.0%	658	1.48	646	3113
three	3/27/03	324.0	92.8%	661	1.41	648	3,092
three	3/27/03	329.9	91.4%	665	1.21	652	3,105
three	3/27/03	309.4	91.2%	653	1.34	641	3,103
three	3/27/03	319.1	90.7%	659	1.34	649	3,092
three	3/27/03	327.4	92.0%	656	1.29	646	3,127
three	3/27/03	319.2	92.0%	661	1.52	651	3,101
three	3/27/03	318.7	89.3%	667	1.27	662	3,085
three	3/27/03	316.7	88.4%	668	1.27	663	3,103
three	4/5/03	301.4	97.2%	685	1.27	666	3120
three	8/16/03	349.1	56.8%	599	3.44	573	1,115
three	8/12/03	331.7	71.5%	678	0.97	652	2,583
three	8/13/03	318.9	64.7%	610	0.92	591	2,587
three	8/11/03	334.5	74.5%	619	1.01	600	2,599
three	8/16/03	349.1	84.2%	645	1.06	631	3,715
three	8/22/03	351.4	78.7%	688	0.97	673	5,251
three	8/22/03	363.3	79.9%	689	0.98	674	5,267
three	8/21/03	390.0	81.6%	700	1.02	683	5,293
three	8/21/03	382.0	81.5%	698	1.17	682	5,298
three	8/21/03	384.1	81.0%	695	0.95	679	5,322
three	8/21/03	377.0	80.3%	693	1.19	677	5,325
three	8/22/03	343.9	78.3%	690	1.01	674	5,330
three	8/21/03	371.4	80.0%	692	1.28	675	5,339
three	8/21/03	373.4	79.7%	692	1.24	675	5,345
three	8/22/03	365.9	79.3%	690	0.96	673	5,373
three	8/22/03	336.2	76.7%	678	0.90	659	5,409
three	8/22/03	366.2	79.5%	690	0.97	673	5,421
three	8/22/03	351.6	78.2%	679	0.92	661	5,438
three	8/22/03	342.9	77.1%	685	0.92	667	5,446
three	8/22/03	363.0	78.6%	677	0.93	658	5,464
three	8/21/03	407.5	82.5%	695	0.27	679	5,334

Table B.4. NO_x data for catalyst C4 (plate).

Chamber	Date	Inlet NO_x ppm (est)	NO_x reduc.	T before cat, F	NH_3/NO	Avg T catal, F	SV, hr^{-1}
four	3/26/03	312.0	92.1%	663	1.31	650	2154
four	3/27/03	324.4	94.5%	660	1.37	647	2,148
four	3/27/03	322.4	94.6%	661	1.32	648	2,158
four	3/27/03	307.7	94.3%	658	1.45	644	2,147
four	3/27/03	336.4	94.8%	659	1.26	647	2,154
four	3/27/03	326.4	94.8%	656	1.36	645	2,152
four	3/27/03	328.3	94.1%	663	1.46	654	2,984
four	3/27/03	325.0	87.0%	669	1.28	665	3,064
four	4/5/03	301.4	88.8%	685	1.27	676	6007
four	4/5/03	301.4	61.3%	489	1.26	456	6001
four	8/12/03	331.7	75.1%	617	1.19	605	2,541
four	8/13/03	318.9	64.0%	626	0.91	615	2,669
four	8/22/03	350.8	86.9%	686	0.97	673	3,196
four	8/22/03	364.3	87.4%	690	0.98	677	3,220
four	8/22/03	342.3	86.2%	691	1.02	677	3,224
four	8/22/03	366.7	86.3%	689	0.97	676	3,325
four	8/22/03	367.5	87.2%	690	0.95	677	3,421
four	8/22/03	352.7	84.9%	680	0.93	666	3,917
four	8/22/03	340.8	84.4%	686	0.93	671	4,012
four	8/22/03	364.4	84.9%	678	0.93	663	4,031
four	8/22/03	335.0	83.3%	676	0.92	663	4,059
four	8/11/03	334.5	79.8%	617	1.02	603	4,169
four	8/21/03	376.0	87.2%	693	1.32	679	4,170
four	8/21/03	371.7	86.7%	692	1.27	678	4,216
four	8/21/03	389.0	87.8%	701	1.04	685	4,235
four	8/21/03	381.3	87.4%	697	0.85	683	4,250
four	8/21/03	384.5	87.4%	695	0.94	680	4,250
four	8/21/03	373.4	86.5%	691	1.18	676	4,323
four	8/21/03	405.1	88.3%	696	0.53	681	4,308

Table B.5. NO_x data for catalyst C5 (monolith).

Chamber	Date	Inlet NO_x ppm (est)	NO_x reduc.	T before cat, F	NH_3/NO	Avg T catal, F	SV, hr^{-1}
five	3/26/03	330.9	88.3%	663	1.39	638	6988
five	3/27/03	320.0	90.4%	663	1.32	637	6,997
five	3/27/03	321.6	88.9%	660	1.25	635	7,026
five	3/27/03	303.5	89.2%	659	1.44	633	7,068
five	3/27/03	334.6	89.1%	658	1.29	635	7,016
five	3/27/03	326.9	88.5%	656	1.40	633	6,977
five	3/27/03	333.1	98.4%	663	1.36	641	7,021
five	3/27/03	328.7	79.7%	663	1.23	649	6,993
five	3/27/03	313.8	85.7%	668	1.31	656	7,047
five	4/5/03	301.4	83.2%	684	1.27	646	10772
five	4/5/03	301.4	67.2%	528	1.27	457	10924
five	8/12/03	331.7	72.4%	607	1.19	543	3,635
five	8/13/03	318.9	66.1%	608	0.92	547	4,564
five	8/16/03	349.1	68.0%	645	1.18	604	6,973
five	8/21/03	385.0	90.7%	695	0.94	665	9,742
five	8/21/03	402.9	90.7%	697	0.79	667	9,742
five	8/21/03	387.9	90.6%	698	1.06	669	9,743
five	8/21/03	380.6	90.7%	696	1.01	667	9,741
five	8/21/03	375.3	90.6%	694	1.23	663	9,740
five	8/21/03	371.9	90.3%	692	1.28	662	9,741
five	8/21/03	373.4	90.9%	691	1.15	660	9,743
five	8/22/03	365.9	89.6%	677	0.94	646	9,740
five	8/22/03	353.9	89.3%	680	0.93	649	9,738
five	8/22/03	333.7	88.3%	677	0.91	646	9,743
five	8/22/03	338.7	88.5%	686	0.94	654	9,741
five	8/22/03	367.2	89.6%	689	0.96	658	9,744
five	8/22/03	369.2	89.5%	689	0.95	658	9,742
five	8/22/03	340.7	89.3%	691	1.02	660	9,743
five	8/22/03	365.2	90.3%	691	0.98	660	9,739
five	8/22/03	350.3	89.4%	685	0.98	656	9,740
five	8/16/03	349.1	58.7%	608	3.75	544	2,593

Table B.6. NO_x data for catalyst C6 (monolith).

Chamber	Date	Inlet NO_x ppm (est)	NO_x reduc.	T before cat, F	NH_3/NO	Avg T catal, F	SV, hr^{-1}
six	3/26/03	324.0	81.6%	660	1.41	632	7198
six	3/27/03	313.1	79.9%	663	1.31	633	7,174
six	3/27/03	320.2	81.3%	663	1.34	632	7,191
six	3/27/03	309.7	79.2%	658	1.40	629	7,208
six	3/27/03	325.9	79.3%	655	1.35	628	7,213
six	3/27/03	334.3	81.5%	667	1.45	641	7,170
six	4/5/03	301.4	70.4%	684	1.27	649	10745
six	4/5/03	301.4	67.7%	554	1.28	494	10737
six	8/12/03	331.7	64.4%	603	1.22	555	2,219
six	8/13/03	318.9	58.2%	613	0.93	566	2,314
six	8/21/03	387.9	86.2%	695	0.94	673	9,619
six	8/21/03	400.9	86.2%	696	0.79	674	9,632
six	8/21/03	386.9	85.8%	697	1.04	675	9,606
six	8/21/03	379.9	85.9%	694	1.19	673	9,611
six	8/21/03	374.7	86.2%	693	1.30	671	9,615
six	8/21/03	372.1	86.0%	693	1.27	671	9,631
six	8/22/03	367.3	88.2%	676	0.92	655	9,614
six	8/22/03	355.0	87.1%	679	0.92	657	9,631
six	8/22/03	332.5	83.9%	679	0.92	657	9,660
six	8/22/03	336.5	85.7%	687	0.98	665	9,618
six	8/22/03	367.7	87.6%	689	0.97	668	9,623
six	8/22/03	370.9	88.3%	687	0.94	667	9,639
six	8/22/03	339.1	87.0%	691	1.03	670	9,630
six	8/22/03	366.2	88.9%	691	0.98	670	9,640
six	8/22/03	349.7	88.3%	685	0.98	664	9,603
six	8/22/03	357.7	80.6%	685	0.98	662	9,626
six	8/22/03	364.5	79.1%	691	0.98	669	9,634

Appendix C

MECHANISMS OF AMMONIA / FLY ASH INTERACTIONS

Final Report on the Brown University Task
within the Project:

"NOx Control Options and Integration for US Coal Fired Boilers,"

led by
Reaction Engineering International, Prime Contractor

funded by the
National Energy Technology Laboratory of the U.S. Department of Energy

report completed

November 13, 2003

report prepared by

Professors Robert Hurt and Eric Suuberg, Principle Investigators

Xu Chen, Indrek Kulaots, Graduate Students

Yuming Gao, Senior Research Engineer

Abstract

This report describes the results of an experimental project at Brown University on the fundamentals of ammonia / fly ash interactions with relevance to the operation of advanced NO_x control technologies such as selective catalytic reduction. The project focused on the measurement of ammonia adsorption isotherms on commercial fly ash samples subjected to a variety of treatments and on the chemistry of dry and semi-dry ammonia removal processes. This project was carried out at Brown University under subcontract to Reaction Engineering International. The following report contains a detailed description of the samples, experimental procedures, and results. The material in most sections is divided into two parts corresponding to the two tasks in the Brown project:

Task 5.1 Fundamentals of Ammonia Adsorption on Fly Ash

Task 5.2 Ammonia Removal by Dry and Semi-Dry Processes

Introduction

Ammonia vapor comes into contact with fly ash during pulverized solid fuel combustion if the unit is configured for NO_x control by selective catalytic reduction (SCR) or selective non-catalytic reduction (SNCR), or if it employs ammonia addition for electrostatic precipitator conditioning [Castle, 1980, Golden, 2001]. Typically some portion of the vapor phase ammonia adsorbs or deposits on fly ash, where it has the potential to cause problems in ash utilization, handling, and disposal [Larrimore,2000]. Of particular concern for disposal is the possibility for high ammonia contents in surface and groundwater near ash ponds [Golden, 2001] and at landfill sites in runoff, leachate and surrounding atmosphere [Golden, 2001, Lowe et al., 1989]. Problems with ash utilization in concrete arise not from degradation of concrete properties [Golden, 2001, Novak and Rych, 1989], but rather from worker exposure to odor, especially during enclosed pours. Current OSHA standards specify the threshold limit value for 8-hr exposure to ammonia vapor as 50 ppm. Ammonia odors are commonly perceived as a sufficiently serious nuisance when the ammonia content of ash reaches 300 ppm — these or higher levels can effectively destroy the ash utilization market. Acceptable ammonia levels to fully avoid problems in utilization and disposal have been cited by different sources as less than 50, 60, or 100 ppm [Novak and Rych, 1989, Necker, 1989].

There are few publications in the archival scientific literature on ash / ammonia interactions, exceptions being the work of Janssen et al. [Janssen et al., 1986], which focused on catalysis of the NO/NH_3 reaction and most notably the work of Turner et al. [Turner et al., 1994], which focused on the mechanism of *adsorption* and its potential impact on the operation of flue gas treatment technologies. Recently, however, there has been a flurry of applied studies reported in the conference literature, patent literature, and in industry reports, motivated by current projections of widespread SCR unit installation in the U.S. in the coming years [Golden, 2001, Larrimore, 2000, Muzio et al., 1995, Hinton, 1999, Brendel et al., 2001, Levy et al., 2001, Rubel et al., 2001, Ramme and Fisher, 2001, Bittner et al., 2001]. These sources discuss many aspects of the ammonia / ash problem and present a number of new ideas for remediation processes. The factors governing the extent of ammonia contamination are not fully understood, but are believed to depend on the concentration of unreacted ammonia leaving the SCR unit (the "ammonia slip"), duct temperatures/time history, ash composition [Muzio et al., 1995], and SO_3 concentration in the flue gas [Larrimore, 2000, Turner, 1994, Muzio et al., 1995]. Ammonia associated with fly ash can be in the form of ammonium sulfate or more commonly bisulfate

particles [Golden, 2001, Rubel et al., 2001], or ammonia species adsorbed on carbon sites [Rubel et al., 2001], likely on carbon surface oxides, or mineral surfaces[Turner, 1994]. Ammonia is well known to chemisorb on acidic surface sites [Sahu et al., 1998], and indeed is extensively used as a titrant to characterize the acidity of surfaces [Gedeon et al., 2001].

There is almost no information in the archival scientific literature on methods of ammonia *removal* from fly ash, despite great commercial interest in a variety of competing techniques [Golden, 2001, Larrimore, 2000], including thermal methods[Levy et al.,2001], combustion-based methods[Giampa, 2001], and water-based methods[Gasioroski and Hrach, 2000, Katsuya et al., 1996, Hwang, 1999].

The objectives of the present study are: (1) to measure complete adsorption isotherms of ammonia on carbon and fly ash surfaces for a more fundamental understanding of the adsorption process, and (2) to investigate the chemistry of room temperature methods for ammonia removal from fly ash using moisture and oxidizing agents, alone or in combination. These two objectives form the basis for the two tasks described below:

Task 5.1 Fundamentals of Ammonia Adsorption on Fly Ash

Task 5.2 Ammonia Removal by Dry and Semi-Dry Processes

In Task 5.2 on ammonia removal, special emphasis was placed on controlled addition of small amounts of moisture to avoid wet ash handling, so-called "semi-dry processing", which is the basis for several industrial patents [Gasioroski and Hrach, 2000, Katsuya et al., 1996], and on the use of ozone, which has recently been found to passivate unburned carbon surfaces in fly ash and thus improve air entrainment properties of problem ash streams[Gao et al., 2001].

Experimental Methods

Task 5.1 Fundamentals of Ammonia Adsorption on Fly Ash

This task deals with fundamental adsorption isotherms for ammonia on carbon-containing fly ash samples. First the surface area and porosity of fly ash samples were thoroughly characterized using standard volumetric gas adsorption experiments. These experiments were performed using an Autosorb-1 system from Quantachrome Corp. The fly ash sample was placed into the appropriately sized sample holder and, prior to the analysis, was outgassed for several hours at constant temperature (573 K) in vacuum.

In the adsorption experiments involving N_2, the customary temperature of 77 K was maintained using a liquid nitrogen bath. In the adsorption experiments involving CO_2 and NH_3, a bath temperature of 273 K was maintained using ice and water. At a temperature of 273 K, the generally accepted [Bridgeman, 1927] saturation pressure for liquid CO_2 is 26144.1 torr (3484.8 kPa). There remains some controversy in the literature regarding the phase of the sorbed CO_2, especially as regards the density of the sorbed layer. This manifests itself in an enormous range of values being reported for its sorption cross-section [Garrido et al., 1987]. Meanwhile, the very high value of saturation pressure, taken together with the operating limits of the available device (760 torr maximum pressure) suggests that CO_2 will only be useful for exploring microporosity. The experiments were, however, conducted below the critical temperature for CO_2, which is 304.14 K. While the saturation pressure is high and P/Psat is therefore always low (and thus one probes the smaller pores), at least we were below the critical temperature with this sorbate at ice bath temperatures. Therefore one can get reasonable isotherm information with a simple ice bath.

The saturation pressure for ammonia at 273.15 K is 429.62 kPa (3223 torr) [Haar and Gallagher, 1978]. Again, the critical temperature for ammonia is 405.5 K, so these experiments were conducted well below the critical point for this gas. The Brunauer, Emmet and Teller (BET) theory [Gregg and Sing, 1982] was used for calculating surface areas and Dubinin-Radushkevich (DR) theory [Gregg and Sing, 1982] was used for determining the microporosity of the fly ash samples. It should be recalled that the earlier reported work established that the main source of micropores in fly ashes is unburned carbon.

As is standard in the literature, the convention used here involves calling any pores smaller than 20Å in width "micropores", any pores between 20 and 500 Å "mesopores" and pores larger than 500 Å "macropores". The term "supermicropores" has recently come into use to describe the micropores between about 8 and 20Å. This terminology has been adopted by some workers in recognition of what is thought to be an upper limit of micropores that can be filled in a "standard" micropore filling process, in which the enhancement of gas-solid interactions plays a significant role. The 8 Å size roughly reflects twice the molecular diameter of typically employed molecular probes such as nitrogen and carbon dioxide. It may also be crudely estimated that the "primary" micropore filling process takes place at relative pressures between 10^{-5} and 10^{-2} and secondary micropore filling in the supermicropores takes place between 10^{-2} and 0.3. In this range of pore filling, some adsorbate-adsorbate interactions are also likely to play a role [Sing, 1995]. This means that mesopore filling is also possible.

Task 5.2 Ammonia Removal by Dry and Semi-Dry Processes

Samples

Four commercial ash samples were selected for this study from among the 80 ash samples in the Brown University ash sample bank [Kulaots, 2001]. Properties of the selected samples are shown in Tables C.1 and C.2. FA1 and FA2 are ammoniated ash samples, one with high and one with low pH, from two power stations in the New England region operating SNCR units and burning bituminous coals. FA3 and FA4 are typical non-ammoniated ashes from eastern and western U.S. coals respectively, and are used in experiments in which ammonia is loaded on the ash under a variety of laboratory conditions. Note that both the carbon content and the ammonia content of FA1 are unusually high. At 1060 ppm this ash has more than ten times the amount of ammonia than is commonly cited as the desired amount to avoid ash utilization problems [Larrimore, 2000]. The basic nature of FA1 is unusual for a class F ash whose alkaline and alkaline earth components sum to only 10.0 wt-% on a carbon-free basis (see Table C.2). It can be shown by simple equilibrium calculations for the reaction $NH_3 + H_2O \rightarrow NH_4^+ + OH^-$ that this basicity is in part due to its very high ammonia content¶.

¶ Consider 1 gm of ash in 30 ml of water, as used in our pH measurement procedure. If the 1060 ppm of ammonia is completely desorbed from the surfaces into solution in the aqueous phase, a pH of 10.3 would be observed before significant volatilization occurred if the remainder of the ash constituents (mineral phases and carbon surfaces) were neutral. Thus part of the basicity of the ash can be attributed to the ammonia itself.

Table C.1 Fly Ash Sample Properties

Designation[a]	Class	LOI[b]	as-received ammonia ppm,w	pH
FA1 (A22)	F	33.6%	1060	11.2
FA2 (A74)	F	10.0%	240	7.9
FA3 (A21)	F	6.1%	~ 0	7.1
FA4 (A73)	C	0.5%	~ 0	11.4

[a] in parentheses are given the codes in the Brown University sample bank, allowing cross-reference to other documents.
[b] "Loss on ignition," an approximate measure of unburned carbon content (see text).

Table C.2
Inorganic Elemental Composition
of Commercial Ammoniated Ash Samples

Element	FA1, bulk[a] wt-%	FA1, XPS[a] wt-%[b]	FA2, bulk[a] wt-%
Aluminum as Al_2O_3	19.6	20.6	28.8
Calcium as CaO	4.0	12.6	1.3
Iron as Fe_2O_3	7.2	4.3	4.7
Magnesium as MgO	3.2	1.5	0.97
Manganese, as MnO	0.06	--	0.02
Phosphorus as P_2O_5	0.05	--	0.2
Potassium as K_2O	2.1	--	2.4
Silicon as SiO_2	60.0	44.6	58.4
Sodium as Na_2O	0.56	0.84	0.91
Sulfur as SO_3	2.3	14.1	0.44
Titanium as TiO_2	0.92	1.0	1.8

[a] carbon-free, oxide basis
[b] near-surface composition, converted from atom-%

Experimental Procedures

Loss-on-ignition values were determined by weighing samples before and after air oxidation at 750 °C. Inorganic elemental compositions were determined for the ammonia-containing field

ashes at Huffman Analytical Labs (Golden, CO) and near-surface elemental compositions were determined by XPS at Evans East Laboratory (East Windsor, NJ). The XPS results are similar to the bulk analysis, with the exception of calcium and sulfur, which show signs of significant surface enrichment. XPS also detected nitrogen, and the high resolution N1s XPS spectrum suggested multiple peak behavior. This spectrum may contain information on nitrogen/ammonia forms, but low signal-to-noise ratio made the peak assignments and quantification uncertain.

The ammonia content of a test fly ash sample was determined by mixing two grams of ash with 3 ml of 2 v/v-% H_2SO_4 and 37 ml distilled water. The suspension was dispersed in an ultrasonic bath for 5 minutes, and the solid ash was separated from the solution by a 10-minute centrifugation. The supernatant solution was then filtered and 30 ml used to measure ammonium ion concentration by specific ammonium electrode and Corning pH/ion analyzer model 455 as well as by Corning's Ammonia Combination Electrode, which measures dissolved ammonia and pH. Potassium ion is known to interfere with the accurate measurement of ammonium, but the potassium levels in Table 2 are too low for the interference to be significant for these samples and the separate determinations of total ammonia based on ammonium ion detection and dissolved ammonia detection were in good agreement.

The acid/base character of the test fly ash samples was measured by mixing 1 gm of ash with 30 ml distilled water and dispersing the particles in an ultrasonic bath for 5 minutes. After centrifugation and filtration as above, the pH of the solution was measured by a Corning pH/ion analyzer 455. For some ash samples, pH values continued to change slowly for up to 30-45 minutes, presumably due to slow dissolution of basic mineral species. The pH values presented here are those existing after 5 minutes of ultrasonic dispersion and should not be interpreted necessarily as equilibrium values. The thermal desorption results were obtained with an Autosorb vapor adsorption apparatus used in outgassing mode to desorb NH_3 from 3-5 gm ash samples as a function of temperature and time under vacuum.

For experiments in static humid air, ash samples were enclosed in a laboratory dessicator that also contained calibrated aqueous solutions designed to provide gas environments of known H_20 and/or ammonia partial pressure. In the first type of experiment, 5 gms of an ammonia-containing fly ash was placed in a 50 x 9 mm dish and loaded into a 150 mm dessicator. A separate 90 x 50 mm dish was prepared with 40 ml of standard salt solutions designed to provide fixed relative humidity according to the procedure of Wexler and Seinfeld [1991]. Using 20 gm salt in 40 ml of water at 25 C the relative humidity (RH) values are 75% (NaCl), 84% (KCl),

92% (KNO_3). Both the ammonia content and the moisture content of the ash samples were measured before and after exposure.

The second type of experiment was identical to the first, except that calibrated solutions of ammonium salts were used instead of KCl, NaCl, or KNO_3. Dilute ammonium hydroxide solutions were prepared at various concentrations and the ammonia vapor concentration was measured in the dessicator for calibration [Fujisaki, 2000]. These experiments created vapor environments with both H_2O and NH_3 and, although designed to load NH_3 onto ash, in fact were capable of producing a net adsorption or net desorption of ammonia on/from ash, depending on ash type and conditions.

For experiments in flowing humid air, a fixed/fluidized bed reactor was used to contact ash with a continuous stream of air at a fixed relative humidity. Ten grams of ash were placed in a 25 mm diameter glass tube fitted with a porous glass distributor disc at the bottom with 0.15-0.18 mm pores and subjected to continuous mechanical vibration. The air flow to the reactor bottom was set at either 0.3 lit/min or 0.8 lit/min and was pre-humidified in a series of two water-filled tubes, while the humidity was measured at the reactor inlet using a digital hygrometer with an accuracy of 2% RH. Ash moisture and ammonia contents were measured before and after treatment by ion electrodes as described above.

Experiments with flowing fog were similar to those in humid air, but an ultrasonic nebulizer was used to introduce ultrafine water droplets to the humidified air upstream of the contact vessel, and some mechanical stirring was carried out manually or with a magnetic stir bar. Here, 10 gm of ash were placed in a 40 mm diameter reactor fitted with the same porous distributor (0.15-0.18 mm pore size) and exposed to a fog-containing upward airflow of 0.7 lit/min. After water addition, the sample was removed and the ammonia content measured. Half of the sample (5 gm) was returned to the glass reactor and dried in flowing air without water mist at a flow rate of 0.3 lit/min. The time between the end of the fog treatment and the beginning of the drying stage was always 1 minute. All experiments were at ambient temperature.

Additional experiments were conducted for acidic ashes in which basic additives, NaOH or $Ca(OH)_2$, were introduced into the liquid feed for fog generation, or in the case of $Ca(OH)_2$ were added as dry powder to the ash prior to treatment. In another variant on the basic experiment, ozone-containing air or oxygen was used in place of pure air as the drying gas or fog carrier gas, and/or a 30 wt-% H_2O_2 was employed as the liquid feed for fog generation in place of water. Joint treatment with ozone and H_2O_2 is the "peroxone" route to aqueous ammonia oxidation

[Kuo et al., 1997]. Experiments were also carried out in which dry ozone-containing air or oxygen was passed through the fixed bed of ash without moisture addition.

Results and Discussion

Task 5.1 Fundamentals of Ammonia Adsorption on Fly Ash

The comparative study of the adsorption behavior of different gases on fly ash was carried out using a representative fly ash sample. Fly ash sample 21 was selected from our sample bank for this purpose. This sample is typical of a class F type of ash, and has an LOI of 6.1%. The sample is typical of ashes produced by pulverized combustion of bituminous coals at the Brayton Point Power Station in Fall River, Massachusetts. This fly ash sample had been previously analyzed using the earlier reported flow microcalorimetric technique, and it was determined that the sample has a very small fraction (9%) of its surface in the form of polar functional groups. Its foam index behavior is consistent with this value, as this sample shows itself to be very active towards Air Entrainment Additive (AEA) adsorption.

This section begins with a thorough characterization of this ash sample using standard adsorbates (nitrogen, carbon dioxide) and methods, and then proceeds to the special case of ammonia adsorption. The nitrogen adsorption isotherm for this sample is shown in Figure C.1. The isotherm is shown in a typical form. The ordinate is given as volume of gas (cm^3 at STP) adsorbed per gram of solid and the abscissa as relative pressure P/P_0, where P_0 is the saturation vapor pressure of the adsorbate at the temperature of the experiment (in this case, 760 torr for liquid nitrogen). This type of isotherm is characteristic of microporous samples. The fact that the isotherm is seen to rise very steeply at very low relative pressure is indicative of sample microporosity. A very good linear BET plot is obtained, and a nominal surface area for the whole fly ash is 3.7 m^2/g. Earlier we reported on similarly obtained nitrogen isotherms on this ash. From the earlier data obtained after complete carbon removal by combustion, it was possible to back-calculate the surface area contribution from the carbon alone. The value that was obtained, 49 m^2/g-carbon, is very typical of the values seen for a great number of carbons from class F ashes.

The DR plot for the isotherm results of Figure C.1 is shown in Figure C.2. This plot is seen to be very linear in the micropore region, and it appears that a good estimate of micropore volume is therefore available. It will, however, be seen below that this estimate represents only an upper bound on the microporosity. There is evidence of a well-known problem [Rodrigeus-Reinoso and Linares-Solano, 1989] associated with inability to distinguish mesopore and supermicropore contributions to this estimate. The DR plot provides a micropore volume estimate of $1.5 \cdot 10^{-3}$ cc/g, which is attributable almost entirely to the carbon in the ash.

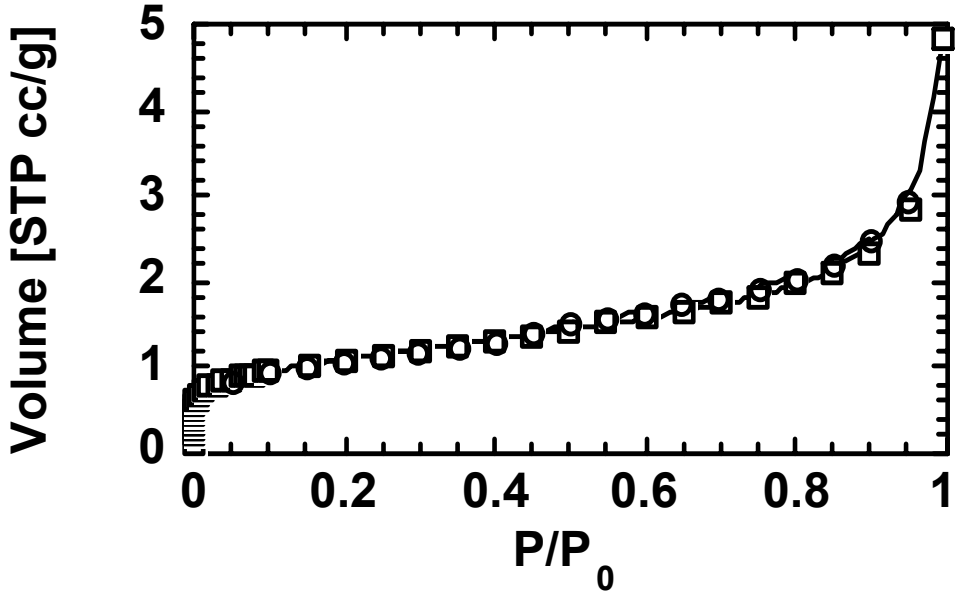

Figure C.1. Nitrogen isotherm (77 K) for "standard" fly ash 21 from the Brown University sample bank.

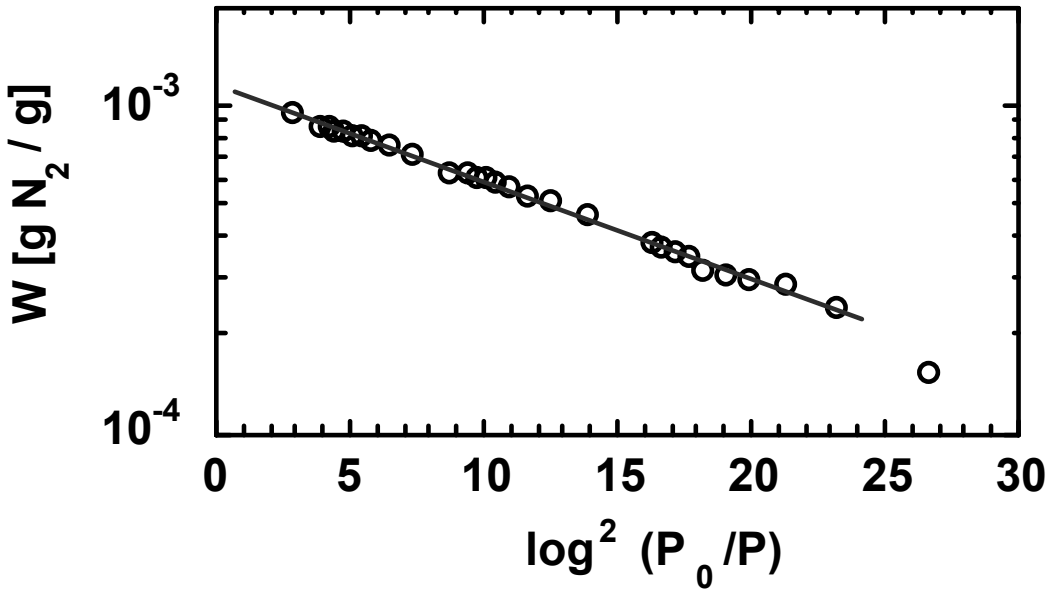

Figure C.2. Dubinin-Radushkevich plot for nitrogen on fly ash 21.

An alternative method for estimating microporosity involves construction of the so-called alpha plot[Gregg and Sing, 1982, Rodriguez-Reinoso and Linares-Solano, 1989]. In this procedure, it is assumed that an entire class of adsorbate-adsorbent interactions must follow the same general rules, dictated by the nature of the particular adsorbate-adsorbent interactions. All isotherms are normalized relative to a "standard" isotherm for the adsorbate-adsorbent pair (in this case, nitrogen on carbon). The result of the procedure is shown in Figure C.3, again for the data of Figure C.1. Quantachrome Corporation provided the nitrogen-carbon normalization isotherm. The alpha plot shows a form that is typical for microporous samples. A long linear region is seen at high alpha values, and there is a marked curvature of the data towards the origin at low alpha values. The latter behavior indicates a microporous sample, consistent with expectations. The extrapolation of the linear portion of the alpha plot to $\alpha=0$ provides an estimate of the micropore volume which in this case gives $2.2 \cdot 10^{-4}$ cc/g.

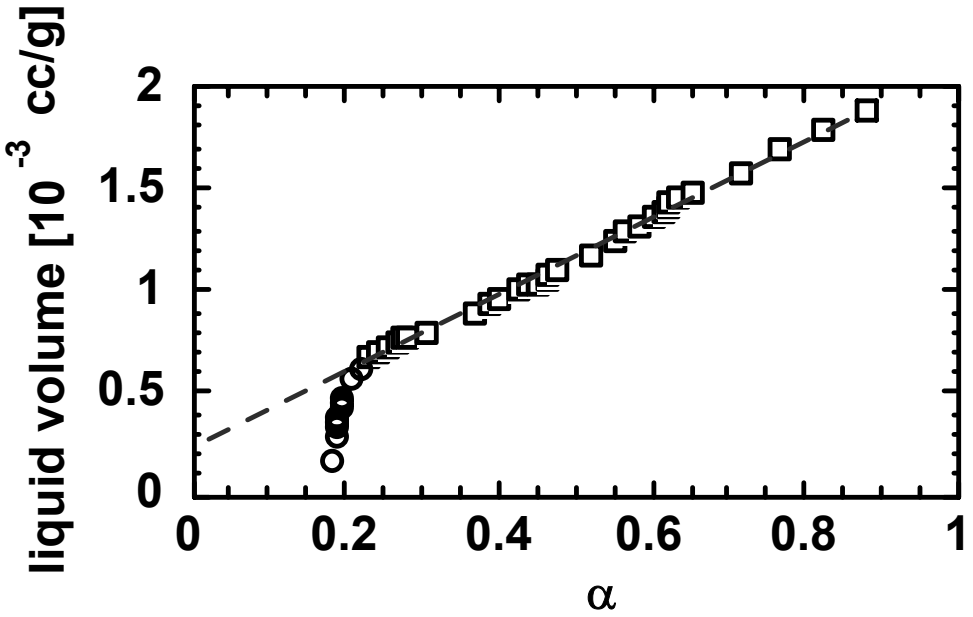

Figure C.3. Alpha plot for nitrogen on "standard" fly ash 21 from the Brown University sample bank.

It can be seen that the alpha plot procedure yields a considerably lower estimate of porosity than does the DR method. Nitrogen DR analysis will sometimes miss wider microporosity [Rodriguez-Reinoso, 1997], but as noted above, it might also sometimes erroneously include mesoporosity. Given the discrepancy noted here, it appears that the inclusion of mesoporosity is plausible. Nevertheless, it must be remembered that both analyses are being applied to a highly

heterogeneous material, including both ash and carbon components. There is a high degree of uncertainty in the estimates. The alpha plot procedure will be strongly influenced by external surface area of non-porous ash material at high relative pressures. This will necessarily have an influence on the slope of the alpha plot, and this might well invalidate the extrapolation procedure.

In order to understand better the nature of the microporosity in this sample, CO_2 was also employed as an adsorbate. Figure C.4 shows the adsorption isotherm obtained at 273 K. It should be noted that the results do not extend to very high relative pressures. This is because the saturation pressure of CO_2 at 273 K is 3484 kPa, and the instrument can probe no higher than 101 kPa. Nevertheless, this is an important range of relative pressures for examining microporosity.

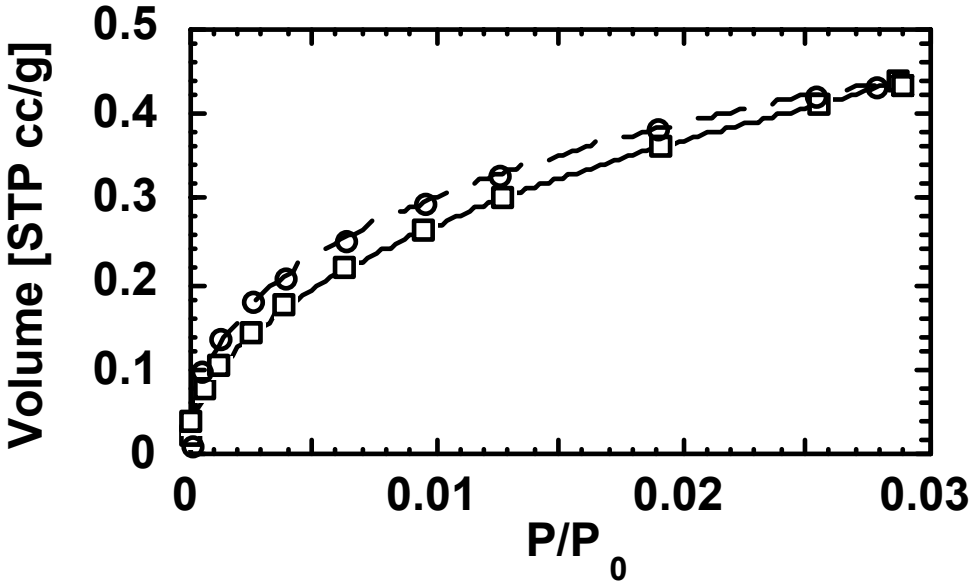

Figure C.4. Carbon dioxide isotherm (273 K) on "standard" fly ash 21 from the Brown University sample bank. Adsorption - solid line; desoprtion - dashed line.

The narrow relative pressure range of Figure C.4 should be noted. Were this figure plotted on the same scale as was Figure C.1, the isotherm would be steeply compressed near the ordinate. The isotherm shows a modest degree of hysteresis even in the very low pressure range involved. It is not possible to reliably determine a BET surface area from the data at such low relative pressures. A Dubinin-Radushkevich plot of the same data is shown in Figure C.5.

This DR plot displays a well-known deviation from linearity at high relative pressures (or low values of $\log^2 [P_0/P]$). Such deviations are not uncommon in carbons that have been activated (burned off) to a high degree [Rodriguez-Reinoso, F., Linares-Solano, 1989]. By extrapolation of the linear portion of the plot to the ordinate, as illustrated, another estimate of microporosity is obtained. In the present case, a micropore volume of $6.2 \cdot 10^{-5}$ cc/g is obtained (assuming as typical a CO_2 density of 1.04 g/cc, consistent with CO_2 in between a solid and liquid phase). Using a density of 0.91 g/cc, which is more representative of liquid CO_2, the micropore volume would be only slightly higher, $7.0 \cdot 10^{-5}$ cc/g. In either case, it appears that the earlier estimate from the nitrogen DR plot might well have included supermicropores and/or mesopores, as that estimate was about an order of magnitude larger. The present value is much closer to the estimate of microporosity from the alpha plot for nitrogen.

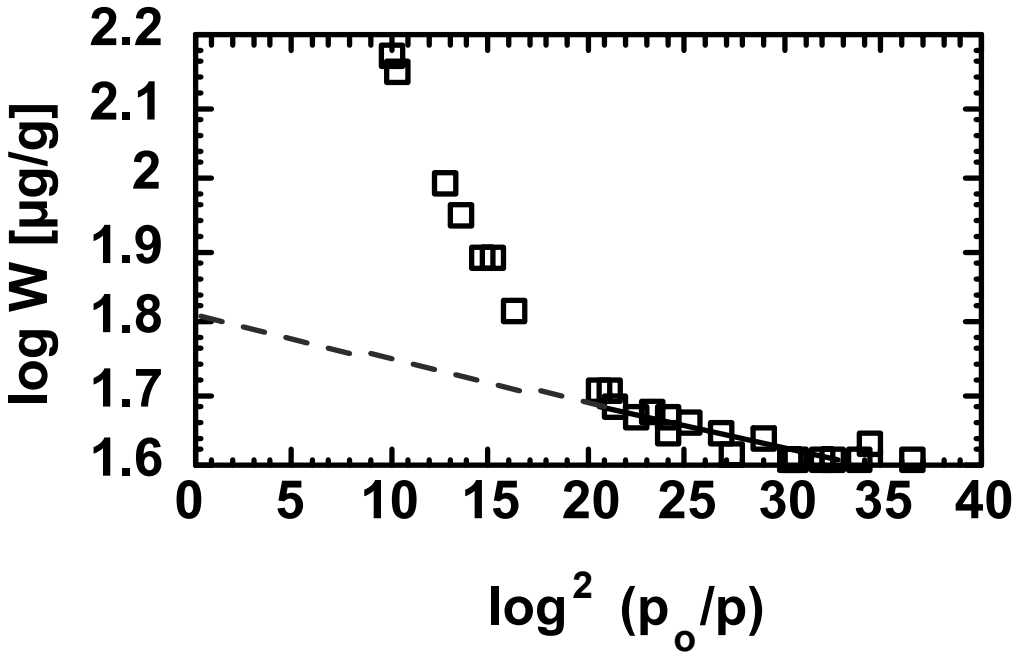

Figure C.5 Carbon dioxide DR plot (273 K) on "standard" fly ash 21 from the Brown University sample bank.

The implication of the above results is that this class F fly ash contains a significant amount of microporosity, probably characterized by a wide distribution of sizes. The question of size distribution in the porosity will be addressed again below.

Ammonia adsorption

Ammonia is not a common choice as a standard adsorbate. It is a polar molecule, which means that it would be expected to have a significant polarity mismatch with normally non-polar carbon surfaces. It was therefore anticipated that the isotherms of ammonia on fly ash would show relatively low uptake. Three replicate experiments were performed with ammonia on fly ash sample 21. All gave quite reproducible results. A typical isotherm is shown in Figure C.6.

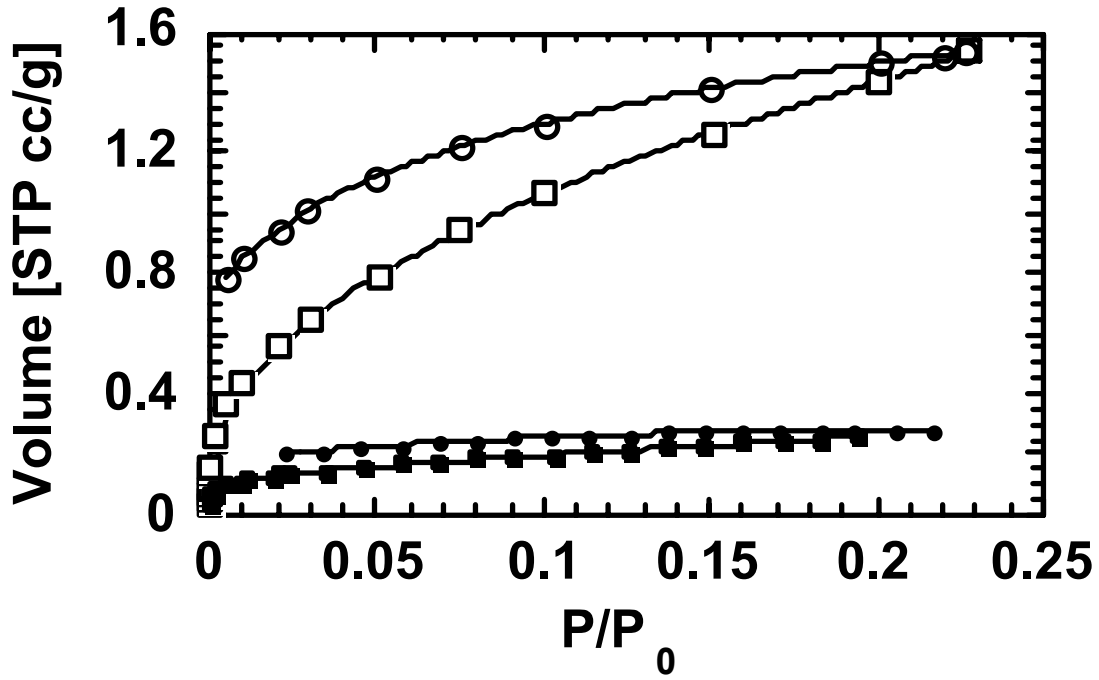

Figure C.6 Ammonia isotherms on "standard" fly ash 21 from the Brown University sample bank. Open points - whole fly ash, closed points - fly ash with carbon removed by oxidation. Squares - adsorption, circles, desorption.

Note that again because the saturation pressure of ammonia at 273 K exceeds 760 torr, the experiments were only performed up to a relative pressure of approximately 0.25. The ammonia isotherms showed a significant degree of hysteresis, as is evident from Figure C.6. In addition to the hysteresis, it was noted that desorption times became extremely long, during the low pressure desorption experiments. These results are suggestive of an irreversible sorption process. This would not be surprising, given that the earlier cited literature suggested this as a possible result of reactions with functional groups on the carbon.

The ammonia isotherms permitted calculation of a BET surface area, as there were enough points in the appropriate relative pressure range. The value obtained was approximately 5.4 m^2/g. This is a bit higher than the surface area calculated from the nitrogen results. There were, however, a significant number of assumptions that went into the calculation. First, the coverage area of the ammonia molecule had to be estimated from liquid ammonia densities; the value that was obtained was 14.0 $Å^2$. Also, despite the knowledge that the isotherm showed evidence of hysteresis probably due to irreversible reaction, it was assumed that the simple BET physisorption model applied to the adsorption results. Taking these factors into account, the surface area obtained here was in surprisingly good agreement with the nitrogen BET value. Use of the desorption branches of the isotherms gave an area of 4.7 m^2/g, in better agreement with the nitrogen values. It should also be recalled that heats of adsorption of ammonia on carbons have suggested that the behavior might be intermediate between that of solid and liquid[Spencer et al., 1958, Holmes and Beebe, 1957]. Just as in the case of CO_2, it is not clear what the appropriate condensed phase density might be, and therefore, whether the 14.0 $Å^2$ estimate might be too high. A values of 12.9 $Å^2$ has been used by others [Turner, 1993, Young and Crowell, 1962, Ashmore, 1963]. Use of this value with the desorption branch of the isotherm gives an area of 4.3 m^2/g.

The information of most interest with respect to the ammonia slip issue is contained in the region of the isotherm closest to the zero relative pressure axis. To show the behavior at low pressures more clearly, the isotherms can be plotted on a logarithmic scale. The results are shown in Figure C.7. A very notable feature of Figure C.7 is the sudden increase in adsorption volume near a relative pressure of 10^{-4}. This feature was reproducible in all of the experiments with the as-received sample of fly ash 21. A similar feature was not visible, at either the same relative pressure or at the same absolute pressure, in the results from nitrogen and carbon dioxide. A comparison of the isotherms for all three of these adsorbates is shown in Figure C.8.

In the very low relative pressure range associated with filling the smallest micropores, ammonia, carbon dioxide and nitrogen all show somewhat comparable behavior and adsorption amounts. There are, of course, significant differences as well. The ammonia shows the abrupt change in slope of the isotherm already described. The absolute amounts of adsorption differ by a factor of three or more, for the three gases. Ammonia shows behavior intermediate between that of carbon dioxide and that of nitrogen.

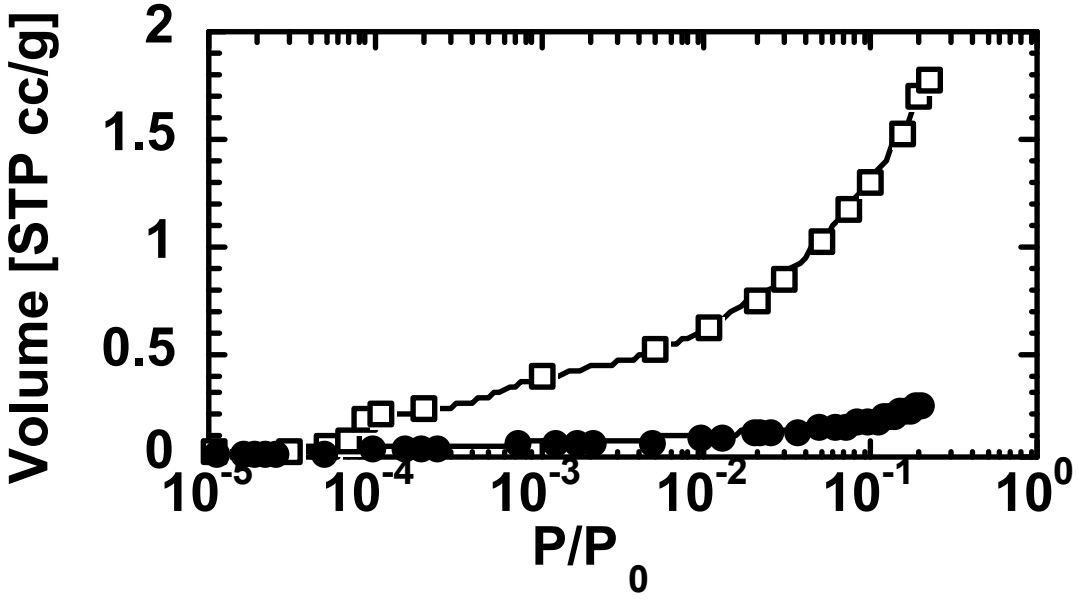

Figure C.7 Ammonia adsorption isotherms of Fig. C.6 on logarithmic pressure scale. Open points - whole fly ash, closed points - fly ash with carbon removed by oxidation.

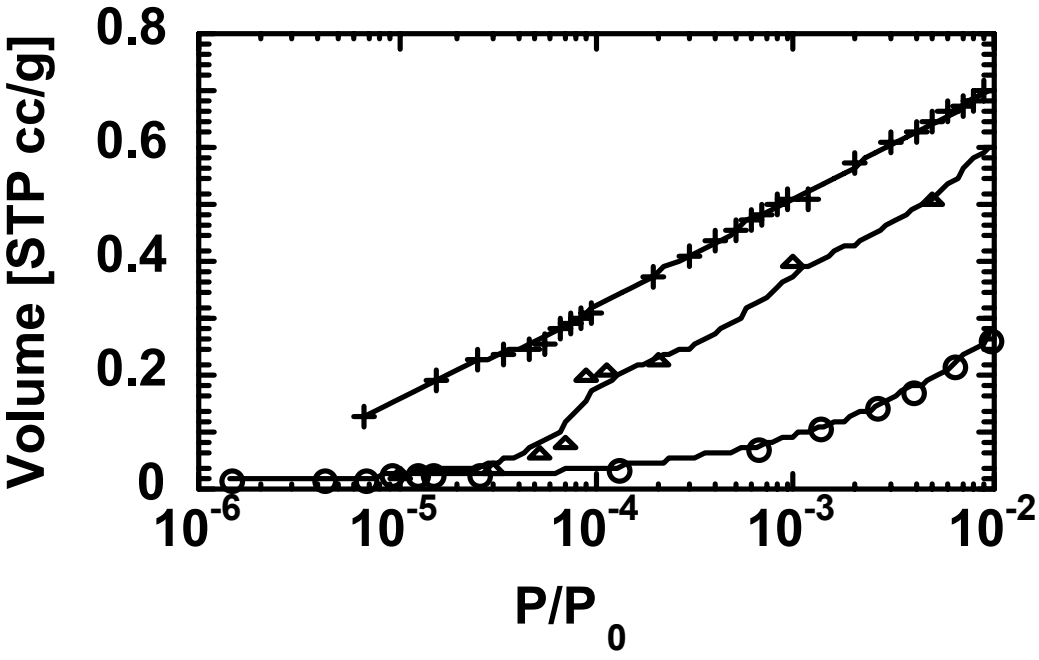

Figure C.8 Comparison of nitrogen (crosses), ammonia (triangles), and carbon dioxide (circles) isotherms.

The adsorption behavior of ammonia on this fly ash sample is dominated by the adsorption on carbon. This is consistent with an earlier conclusion regarding the relative roles of carbon and mineral components in nitrogen adsorption. The relative contributions of the two components may be judged from Figure C.6, which shows a comparison of the whole ash isotherm (already discussed) with the isotherm for the ash with the carbon completely removed. It is clear that most of the adsorption takes place on the carbon. Bearing in mind that the carbon represents about 6 % by mass of the whole ash, the importance of the carbon in the adsorption process is put into very clear perspective.

The ammonia-BET surface area of the carbon-free ash is 0.7 m^2/g, which is in excellent agreement with the values earlier obtained from nitrogen isotherms. The fact that there is good agreement between nitrogen and ammonia BET values for the carbon-free ash is not necessarily inconsistent with the less good agreement between these values for the carbon-containing ash. This is because most of the surface area in the mineral portion of the ash is external surface area. For illustration, a spherical particle of 10 μm diameter and 1 g/cc density would have an external surface area of 0.6 m^2/g, in reasonable order of magnitude agreement with the above estimate.

Figure C.7 shows the ammonia isotherm for the carbon-free ash, plotted on the logarithmic relative pressure scale. Here the comparison emphasizes the low relative pressure results. The contribution of the mineral portion is again seen to be very small in comparison with the contributions of the carbon, particularly after the sudden jump at a relative pressure of about 10^{-4}. Figure C.9 replots this data with the Y-axis converted to ppm,w on the ash and includes data for ozonated samples. Ozonation of the carbon surfaces is seen to enhance the 'jump" feature, while the rest of the isotherm is not significantly altered, suggesting that this feature is related to surface oxides on carbon. There have been a significant number of studies concerned with the adsorption of ammonia on carbons (e.g. Boehm et al., [1964] and Hofman et al. [1950]). These studies have also shown that oxide groups on the surface of a carbon enhance the adsorption of ammonia. It is often hypothesized that the acidic functional groups associated with the surface oxides act as Bronstead acids towards ammonia, which is a strong base [Zawadski, 1989]. These acid functionalities donate a proton to the ammonia in an acid-base interaction, yielding an ammonium ion, NH_4^+. There is also evidence of formation of groups that cannot be hydrolyzed in acid solution. · The suggestion has been made that the ammonia reacts with surface acid groups, probably yielding amides, or possibly even imides. As the temperature of the complexes is raised, the irreversibly formed amide groups can decompose, eventually giving rise to cyano

groups on the carbon surface. Hence, the adsorption process involving reaction of ammonia with acid groups to form amides may be observed to be irreversible, even at high temperatures.

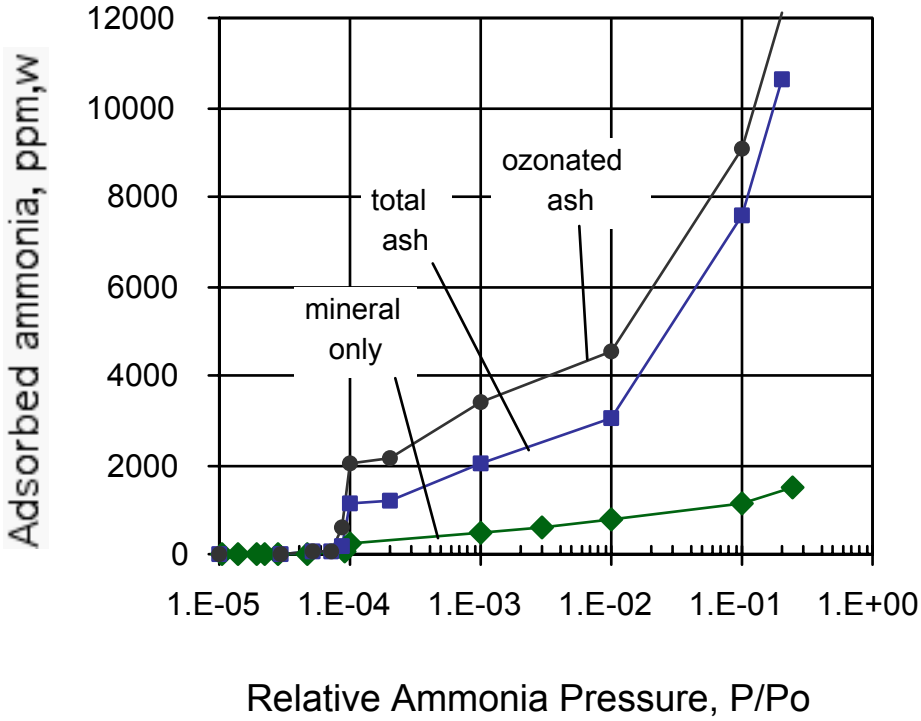

Figure C.9 Full ammonia adsorption isotherms on A21 fly ash (6.2% LOI from Brayton Pt.) at 273 K before and after carbon removal by air oxidation plotted as ppm,w on ash. Also shown is the ammonia isotherm on fly ash subjected to ozonation.

The information of most interest with respect to the ammonia slip issue is contained in the region of the isotherm most near the zero relative pressure axis (1-20 ppm). To show the behavior at low pressures more clearly, the isotherms can be expanded on the X-axis and the partial pressure units converted to an equivalent ppm by volume in a 1 atm gas (e.g. flue gas). The results are shown in Figure C.10. A low-concentration asymptotic value in Figure C.10 appears to be about 20 ppm and independent of the carbon content. This is comparable to the theoretical amount of ammonia corresponding to one monolayer on the geometric external surface of the mineral grains. In fact, analysis of this isotherm yields an ammonia-BET surface area of 0.7 m^2/g, which is in excellent agreement with the values earlier obtained from nitrogen isotherms for the carbon-free ash. It appears that this monolayer coverage of the mineral grains occurs at very low vapor concentrations, while at higher ammonia concentrations carbon begins to dominant the adsorption process.

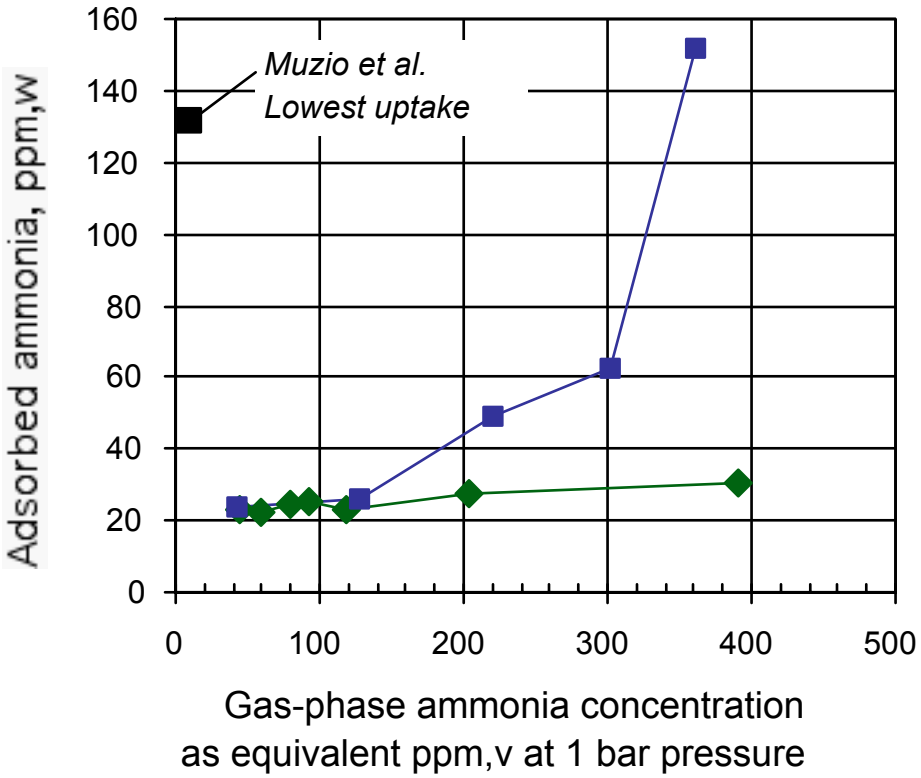

Figure C.10 Ammonia isotherms with the low partial pressure region expanded and the X-axis units converted to those commonly used to express ammonia slip concentrations.

Of particular interest in Fig. C.10 is the comparison between the present results and the experiments of Muzio et al. [1995] in simulated flue gas. Muzio et al. measured 132-347 ppm,w of ammonia adsorbed on a range of ash samples exposed to 10 ppm ammonia slip at 150 ^{o}C. The lowest of these data points is shown on Fig. C.10 for comparison. The low uptake in the present experiments cannot be explained by the low temperature (273 K vs. 423 K in Muzio et al.), as we have observed decreases in uptake with increasing temperature above 273 at constant partial pressure.

The reason for the discrepancy between the values observed in the field and the present isotherm is not fully understood. It might be that the present sample does not have as high an ammonia capacity as some other samples, due to its low surface polarity. On the other hand, the influence of processing conditions also cannot be overlooked. It is possible that SCR and SNCR processes somehow create greater ammonia capacity in ashes. This might involve a change in the carbon surface oxide population, or a creation of a sorbed water

layer on the carbon. A third possibility may be inferred from the literature on carbon blacks. A very slight increase in ammonia adsorption capacity with temperature has been reported in carbon blacks [Holmes and Beebe, 1957, Bomchil et al., 1979]. This is contrary to the temperature trends observed in the earlier work on ashes, however, and is therefore less likely as an explanation.

The micropore capacity of the ash towards ammonia may be examined with the aid of a DR plot. This plot is shown as Figure C.11. Extrapolation of the fit to the somewhat scattered low pressure data gives a micropore volume estimate of $1.5 \cdot 10^{-3}$ cc/g. This value is in very good agreement with the micropore estimate provided by nitrogen, using the DR analysis. Again, there may be some contribution of small mesopores to this value. The fact that both the ammonia and nitrogen provided values that were an order of magnitude higher than those given by carbon dioxide is not necessarily troubling. It is well known that carbon dioxide can only fill the smallest micropores [Garrido et al., 1987; Rodriguez-Reinoso and Linares-Solano, 1989].

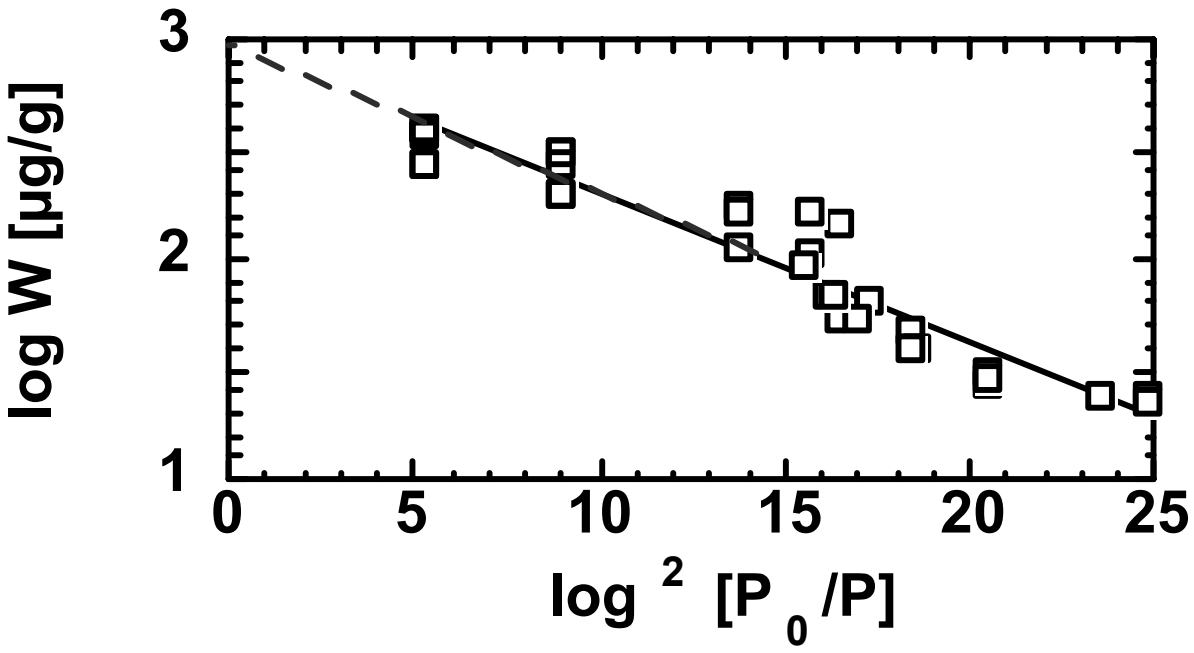

Figure C.11 D-R plot for ammonia on fly ash 21.

The implication of the above suite of results is that ammonia, like nitrogen, can be adsorbed into micropores in comparable amounts at very low relative pressures. The present results are entirely consistent with the observation by Turner [1993] that ammonia on outgassed ("pretreated") fly

ash is held to an extent that is comparable to that revealed by ordinary surface area probing techniques. Our samples were outgassed at 300°C, so they should be comparable to his "pretreated" samples. Moreover, Turner's experiments were performed in dry flowing gas, so the adsorption conditions were also quite comparable to ours. This dry ammonia adsorption process explained about two-thirds of the capacity of the as-received ash for ammonia in Turner's work. The remaining capacity was hypothesized by Turner to be due to moisture and oxides on the ash surfaces, which are lost on heating. We believe that our work has made it clear that it is the carbon in the ash that is mainly responsible for this dry adsorption capacity.

The present results appear to be inconsistent with the results obtained by Muzio et al.[1995]. They obtained adsorption capacities that were considerably higher than what would be predicted from our experiments. One possible reason is that not all of the fly ash samples are comparable. The Huntley sample of Muzio et al. had a higher LOI (10.81%) and a higher surface area (8.1 m^2/g) than the sample used in this work It is the surface area that is really the more important factor. Assuming for their sample a typical mineral surface area of 0.7 m^2/g, the carbon surface area of the sample would be 7.5 m^2/g-ash (about 69 m^2/g-carbon). This makes the available surface for adsorption of ammonia in the Huntley sample 2.5 times higher than the surface area of carbon on our sample (which is 0.061• 49 = 3.0 m^2/g). Similar calculations for their other samples yield 0.5 m^2/g for the Russel ash, 15 m^2/g for the Salem Harbor ash and 12 m^2/g for the Arapahoe ash. The available adsorption surface cannot, however, be used to explain the observed differences. The Russel ash exhibited an ammonia capacity of 132 ppm, the Salem Harbor 344 ppm, the Arapahoe nearly 347 ppm and the Huntley sample 190 ppm, all for 300°F (149 °C), 10 ppm concentrations and 60 minutes equilibration. Again, at such low relative pressures, our work would suggest a capacity that would be no more than 20 ppm.

The experiments of Muzio et al. differed from ours in one important respect. Their experiments were conducted with the ammonia in humidified air containing an acid gas (SO_2). The absorption of ammonia by water or acid sites could have played some role in yielding the high capacities that they observed. In the absence of the acid component in the gas, the ash itself would have very little moisture content at the temperature of their experiments. Data are available on solutions of ammonia and SO_2 in water[Emmert and Pigford, 1963]. The partial pressures of ammonia and SO_2 above such solutions are given by:

$$p_{NH_3}(\text{torr}) = F_2(T)\,\frac{C\,(C\text{-}S)}{(2\,S\text{ - }C)}$$

and

$$p_{SO_2}(\text{torr}) = F_1(T)\,\frac{(2\,S - C)^2}{C - S}$$

where

$$\log_{10} F_1\,(T) = 5.865 - [2368 / T\,(K)]$$

$$\log_{10} F_2\,(T) = 13.680 - [4987 / T(K)]$$

The parameter C represents the concentration of NH_3, in mols/100 mols of water, and the parameter S, the concentration of SO_2 in mols/100 mols of water. The actual correlations were developed for the temperature range from 308 K < T < 363 K, and ammonia concentrations in the range 5.8 < C < 22.4 mols/100 mols water. Clearly these correlations are intended for conditions somewhat out of the current range of interest, but it is instructive to examine the implications of an extrapolation.

A small extrapolation is possible at the lower end of the temperature range examined by Muzio et al. (T = 120 °C = 393 K). At this condition, $F_1 = 0.691$ and $F_2 = 9.78$. It may be shown that:

$$P_{NH3}P_{SO2} = F_1F_2\,(2\,y+C)\,C$$

and that

$$P_{NH3} = F_2\,C\,y/(-2y + C)$$

where y = (C – S). It can also be shown that the solutions to this pair of equations will normally yield values of y <<C, for the conditions of present interest. In this case,

$$P_{NH3} \approx F_2\,y$$

and

$$P_{NH3}P_{SO2} \approx F_1F_2\,C^2$$

For P_{NH3} = 20 ppm = 20 • 10^{-6} • 760 = 1.52 • 10^{-2} torr and P_{SO2} = 1500 ppm = 1500 • 10^{-6} • 760 = 1.14 torr, y = 1.55 • 10^{-3}, C = 0.051 and S = 0.049. These values are excellent approximations to the actual exact solutions. To the extent that the extrapolations involved reflect the real situation in an ash particle, it is possible to estimate the moisture content on the particle surface. If *f* represents the fraction by mass ammonia on the particle, then this quantity must be given by:

f = C • m • (100 mol.water / 1800 g-water) • 17 g NH_3/mol NH_3

where m is the g-moisture/g-ash. Assuming a typical f value of 200 ppm, the moisture content in this case would be 0.4%, assuming that all of the ammonia is held in the water phase.

The above calculation illustrates only that a small water film, assuming that it exists and that it can be modeled using bulk phase behavior, can explain a significant enhancement of ammonia capacity. At 120°C, the vapor pressure of water above an SO_2 solution with S = 0.49 would be around1480 torr, in the absence of the ammonia [Emmert and Pigford, 1963]. This is sufficiently high that it is not clear that a water film is even possible under the conditions used by Muzio et al. Still, it appears that the most plausible explanation for the considerably higher ammonia capacity observed in that study compared with ours is that there is some interaction of ammonia with SO_2 in the condensed phase. Again, assuming the present model reflects to some degree the real situation, it is also clear that if the partial pressure of SO_2 is somewhat lower than that used by Muzio et al. the ammonia capacity is also greatly diminished. Assuming, for example, that P_{SO2} = 100 ppm = 10^{-4} • 760 = 7.6 • 10^{-2} torr, keeping all other values constant, then C decreases to 0.013, implying roughly a factor of four decrease in the ammonia capacity at the same moisture content. At such levels, the dry adsorption capacity becomes significant in comparison. The above discussion points out the importance of studies on co-operative adsorption in these systems.

Task 5.2 Ammonia Removal by Dry and Semi-Dry Processes

Figures C.12-C.15, C.17-C.22 and Table C.3 summarize the experimental results on the ammonia removal task. Figure C.12 on thermal treatment shows that 200 ^oC is insufficient to remove significant ammonia, but that a majority of the ammonia in these ash samples can be removed by thermal treatment alone at 300 ^oC. Figure C.12 shows that the required desorption times are long at 300 ^oC, either due to desorption/decomposition kinetics or to slow diffusion through the deep sample beds. This simple thermal desorption experiment does not provide sufficient information to positively identify the ammonia form or forms, but significant evolution does occur at temperatures characteristic of ammonium bisulfate compositions (decomposition onset 214 C in inert [Rubel, Rathbone and Stencel, 2001]).

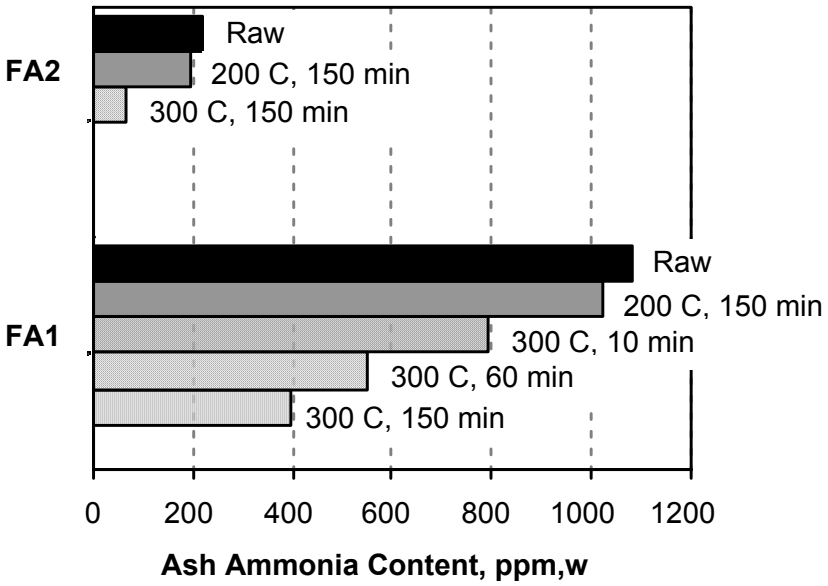

Figure C.12 Vacuum thermal desorption behavior of two ammonia-containing ash samples from the field.

Figures C.13-C.19, C.21,C.22 and Table C.3 summarize a large set of ammonia-removal experiments using controlled amounts of moisture at ambient temperature. Figure C.13 presents results from the earliest set of experiments, those using static humid air in closed dessicators. The plot shows that ammonia can be completely removed from the high-pH ash, FA1, simply by placing it near a dish with an aqueous salt solution - i.e. under conditions where no liquid water is added directly to the ash sample. Exposure to static humid air is observed to increase ash moisture content from about 0.8% initially to values ranging form 1.3-1.9%. It is believed that slight condensation in and around the individual ash/carbon particles causes the ammonia species to desorb, enter solution, and be converted to the highly volatile NH_3 form according to:

$$NH_3\,(aq) + H_2O\,(liq) \Longleftrightarrow NH_4^+\,(aq) + OH^-\,(aq) \qquad (C.1a)$$

$$NH_3\,(aq) \Longleftrightarrow NH_3\,(vap) \qquad (C.1b)$$

$$H_2O\,(liq) \Longleftrightarrow H^+\,(aq) + OH^-\,(aq) \qquad (C.1c)$$

NH_3 is highly volatile so equilibrium C.1b favors partitioning to the vapor phase, while equilibrium C.1a is highly dependent on solution pH. At 20 ^oC, $pK_b = 4.767$, which gives upon rearrangement

$$\log\{[NH_4^+]/[NH_3]\} = 9.23 - pH \qquad (C.2)$$

This combined reaction system leads to NH_3 as the predominant species and thus to extensive ammonia volatilization whenever pH values are greater than about 10 in the condensed film. Water vapor is always below saturation in the Fig. C.13 experiments, so partial condensation occurs by adsorption on surfaces and by capillary condensation in pores and fine intraparticle spaces. It is notable that ammonia removal can occur with the addition of so little liquid water (1.3-1.9 wt-%) that ash handling characteristics are not greatly affected.

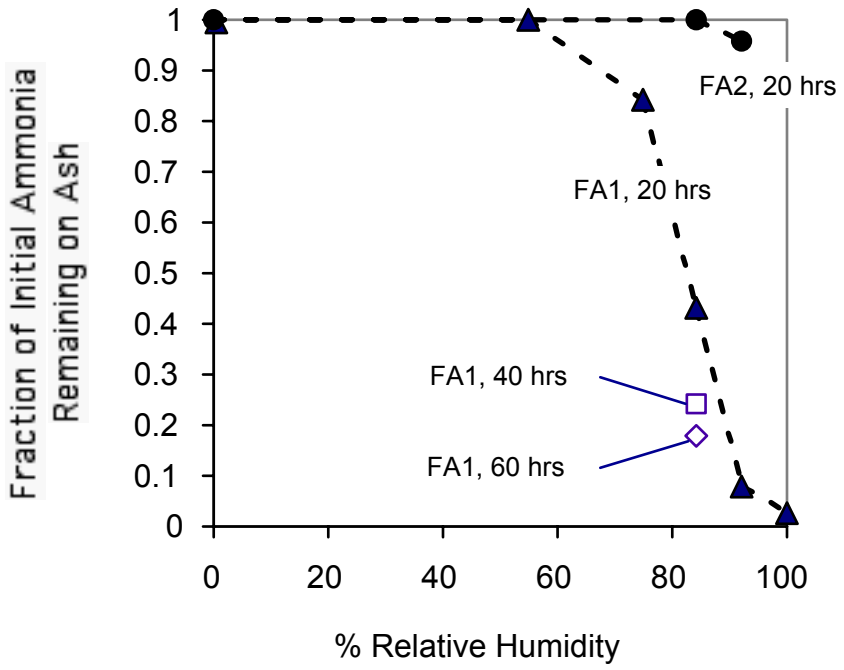

Figure C.13 Results of experiments on ammonia removal in static humid air. Initial ash moisture contents were 0.82 wt-% for FA1, and 0.80 wt-% for FA2. Moisture contents of selected treated ash samples shown on this figure were as follows: 1.3% for FA2 at RH84 (20 hrs); 1.6% for FA2 at RH94 (20 hrs); 1.6% for FA1 at RH84 (20-60 hrs); and 1.9% for FA1 at RH92 (20 hrs).

Figure C.13 also shows that the process is not effective for the low-pH ash, FA2. The critical role of solution pH is further illustrated in Fig. C.14, which presents results for two acidic and two basic ashes placed in proximity to aqueous ammonia solutions. The standard solutions were designed to create vapor environments with known partial pressures of ammonia. Although the original goal of these experiments was to load ammonia onto ash, it was found that this exposure can either increase or decrease ash ammonia content depending on ash type. Both acidic ashes

(FA2,3) adsorbed ammonia from the solutions, as expected (see Fig. C.14), but the basic ash, FA1, experienced a large ammonia loss. Further, adding a basic additive to the acidic ash, FA3, eliminated the uptake completely. Additional experiments on other ash samples show the same trends with pH[Fujisaki, 2000]. We conclude that in the presence of near-saturated humid air, we can remove but not add ammonia to basic ashes, and conversely we can add but not remove ammonia from acidic ashes.

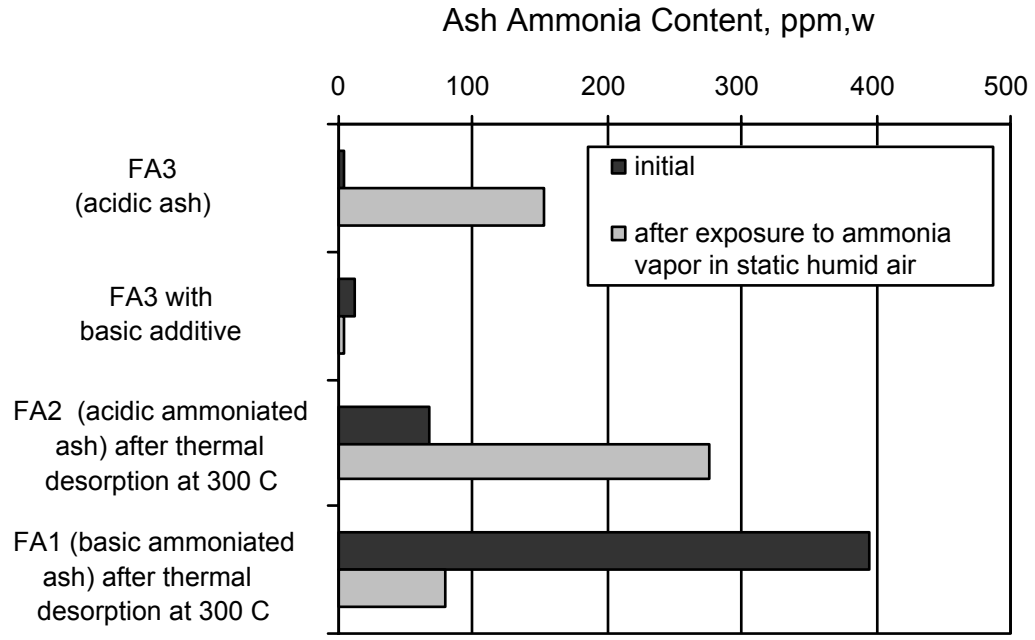

Figure C.14 Effect of pH on the removal or addition of ammonia in static mixtures of humid air and ammonia vapor (700 ppm) established with a calibrated ammonium hydroxide solution. The basic additive was CaO as a dry powder added to the ash. Similar results were obtained when CaO was added in solution, or using $Ca(OH)_2$ either as a dry powder or in solution.

These combined results show that the ammonia release is governed by solution chemistry as embodied by Eq. C.1, despite the very low moisture levels. It appears that above 1-2% moisture, a water film forms in and around individual particles and is sufficiently continuous to dissolve the adsorbed or deposited ammonia and to mediate its release in a way that is at least qualitatively similar to bulk solution behavior. This is not an obvious result considering the dry physical appearance of the ash and the lack of macroscopic evidence of a continuous water phase. The effectiveness of small amounts of water is claimed in several process patents [Gasiorowski and Hrach, 2000,Katsuya et al., 1996], where the authors quote the advantages of

rapid ammonia release and quasi-dry ash handling. We demonstrate here that even exposure to static humid air can bring about these effects. Indeed, using small amounts of water minimizes the inventory of ammonia in solution and thus favors its partitioning to the vapor phase. As pointed out by Gasiorowski et al.[2000], smaller amounts of moisture also produce higher pH values (provided the ash is intrinsically basic or made basic by solid additives), since any water in excess of that required to activate the aqueous solution chemistry serves only as a diluent, bringing the solution closer to pH neutrality and inhibiting ammonia release.

A contacting scheme using a continuous stream of humidified air passed through a fixed bed of ash in upflow configuration is more effective than one using static humid air. Figure C.15 illustrates that this contacting method is effective at removing ammonia from the basic ash at moisture levels of less than 3 wt-%. The rate of removal increases with increasing moisture content, but the total contact times are still long. The long times are believed to be the result of

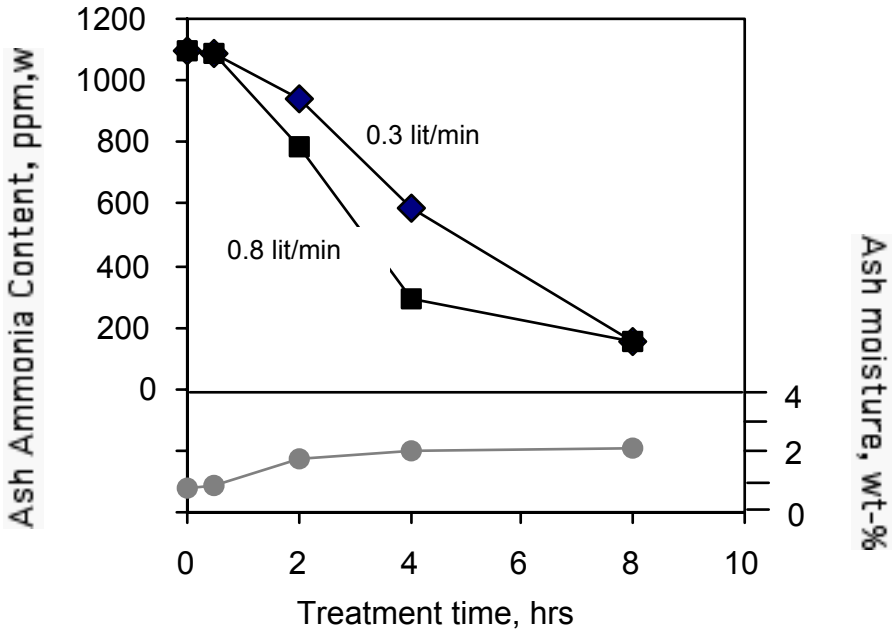

Figure C.15 Results of ammonia removal experiments in flowing humid air (RH 93%) passed upward through 10 gm fixed beds of ash at one of two different flowrates. Sample: basic fly ash, FA1.

(1) the slow rate of water addition due to the limited carrying capacity for water vapor in room temperature air (0.023 mole fraction); (2) the low driving force for water addition to the solid phase, which at these subsaturated conditions is driven by adsorption and capillary condensation, and; (3) slow diffusion of dissolved species within the microscopic water film.

The structure and properties of the water film can be appreciated by several simple calculations. Figure C.16 shows the geometric relationship between moisture content and water film thickness for a ideal ensemble of monodisperse, non-contacting spheres of density 2.2 gm/cm3, similar to the density of mineral phases in fly ash. The small amounts of water employed here give rise to a nominal film thickness well below 1 μm. For the humid air experiments, we further expect the water film to be highly non-uniform, consisting of very thin mono- or multi-layer adsorbed films on external particle surfaces or large pore surfaces in carbon, coexisting with bulk moisture in fine pores and fine neck regions lying at points of particle contact. The

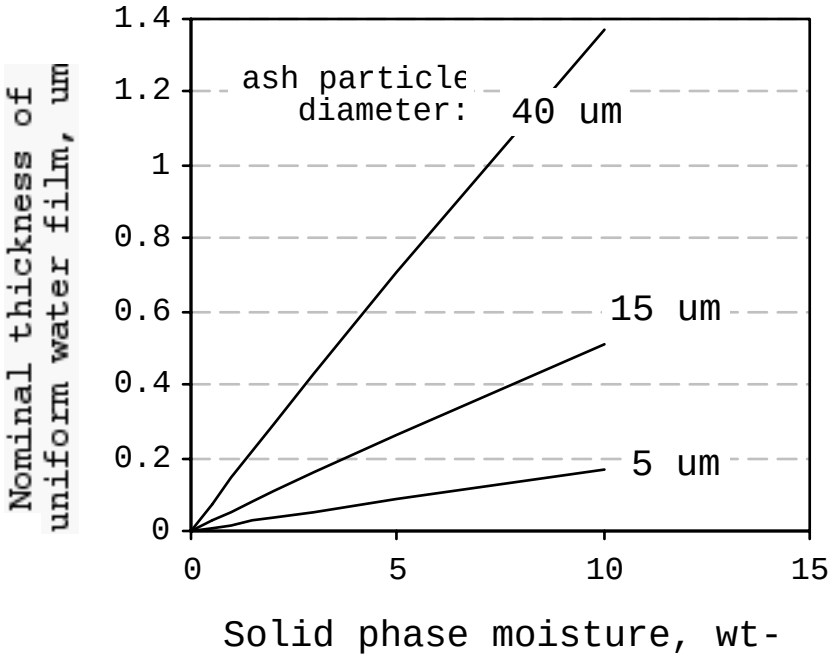

Figure C.16 Thickness of uniform water film on collection of ideal, nonporous, monodisperse spherical particles of typical mineral density, 2.2 g/cm-3. This calculation demonstrates that the water film produced by most humid air and flowing fog experiments (moisture contents 1-5%) have sub-micron mean dimensions.

Kelvin equation describes this sub-saturation condensation, and for the simple case of spherical geometry yields a maximum size of filled pores (or filled particle interstitial regions) of 1.5 nm at 50% RH, 5 nm at 80% RH, and 21 nm at 95% RH under these conditions. We therefore expect bulk water only in nanometric (meso) pores and nanometric interstitial regions. We expect much of the ash surface to be covered only by a multi-layer adsorbed film, making the water phase only semi-continuous and leading to slow diffusion of dissolved species. On the

other hand, desorption may be aided by the fact that ammonium salts and adsorbed ammonia species may serve as attractive sites for preferential water adsorption or condensation.

Flowing fog

In an attempt to reduce required contact times, experiments were performed in which 2-3 wt-% water was introduced quickly to the ash using an ultrasonic nebulizer to create a fine fog in the flowing humid air stream. The ultrafine water droplets remained in a quasi-stable aerosol as they passed through the porous distributor disk and entered the agitated ash bed. Figure C.17 shows the effect of the fog on ammonia removal under a variety of conditions. These experiments took place in two parts: a fog addition stage lasting 1.5 to 8 minutes followed by a 30-minute drying stage in air. The labeled data points give the ash moisture content at the end of the fog stage and prior to the onset of drying. As moisture levels rise above 2 wt-%, ammonia liberation becomes very rapid.

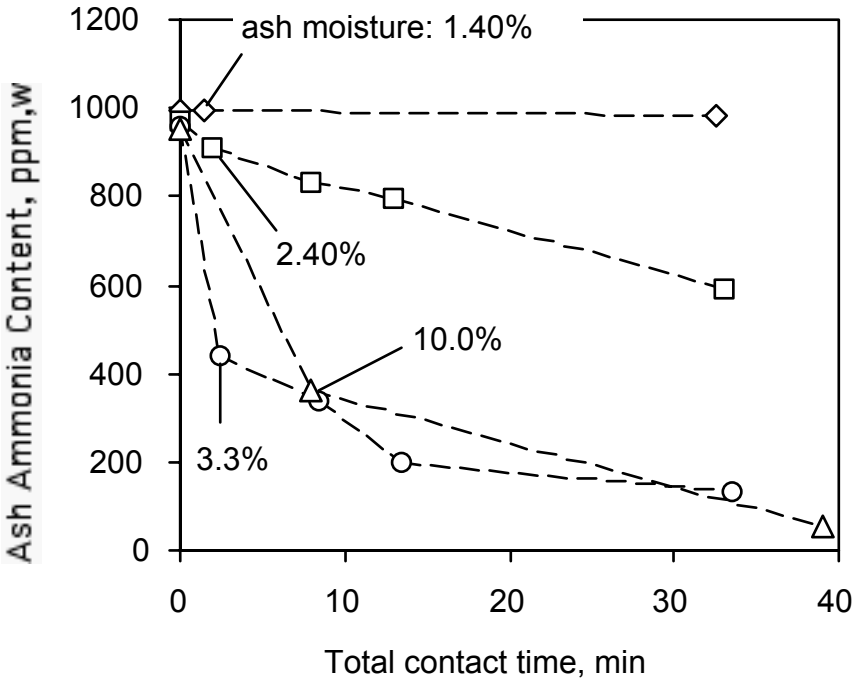

Fig. C.17 Results of four time-resolved experiments on ammonia removal with flowing fog. The first data point corresponds to the end of fog addition and the beginning of the air drying stage. Sample: basic ash, FA1. The extent of moisture addition is varied by varying the total fog generation time from 2-8 minutes. Moisture-in-ash measurements are shown on graph at the end of the fog addition prior to the start of air drying.

Adding 3.3 wt-% water in 2.5 minutes drives off half of the adsorbed ammonia with no drying time. Figure C.18 shows the time-resolved measurements of both ammonia and ash moisture in another flowing fog experiment. At moisture levels above 3 wt-%, ammonia removal is rapid, but the rate falls off quickly when moisture levels drop to about 2% during the subsequent drying stage. During the transfer of samples for measurement, a strong ammonia odor was noticed when moisture contents were 3% or greater. These combined results show promise for practical processes involving rapid uniform addition of small amounts of moisture followed by limited air drying to achieve high levels of ammonia removal.

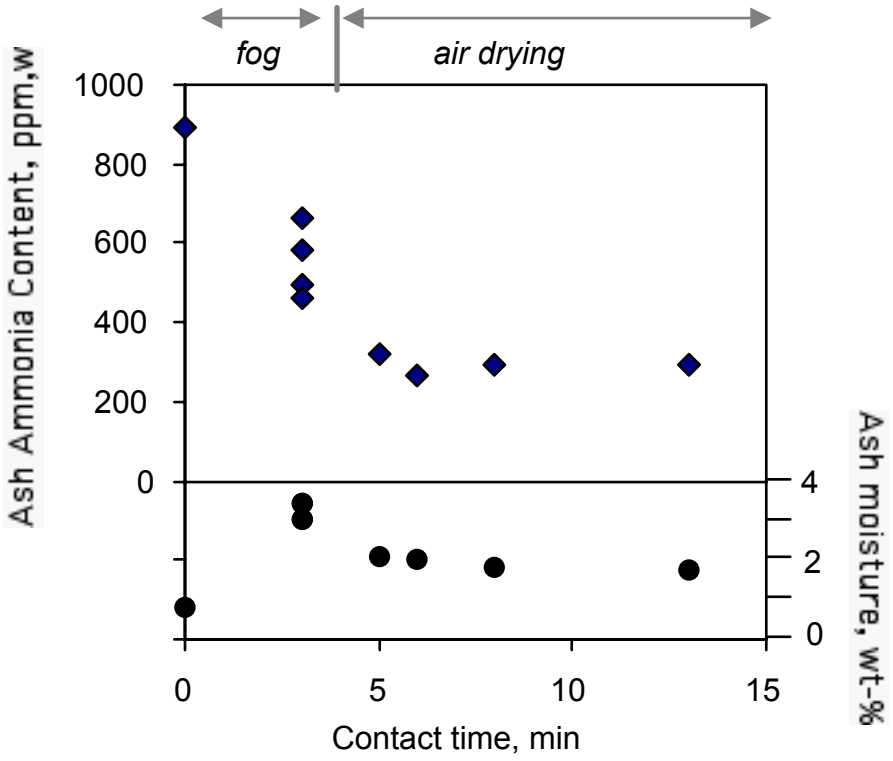

Figure C.18 Ammonia removal by flowing fog. Plot shows time-resolved values of both ash moisture and ammonia content during fog addition and air drying. Multiple points at 3 minutes represent duplicate experiments.

Flowing fog treatment produces rapid ammonia release, but was observed in separate experiments to be ineffective for acidic ashes, which represent a commercially important fly ash class. Several industrial patents [Gasiorowski and Hrach, 2000,Katsuya et al., 1996] and the results of Fig. C.13 in static humid air suggest that acidic ashes can be successfully treated after introduction of inexpensive basic additives. Figure C.19 and Table C.3 confirm this behavior for

the flowing fog treatment using NaOH solutions for fog generation (Table C.3) or $Ca(OH)_2$ added as a dry powder to the ash.

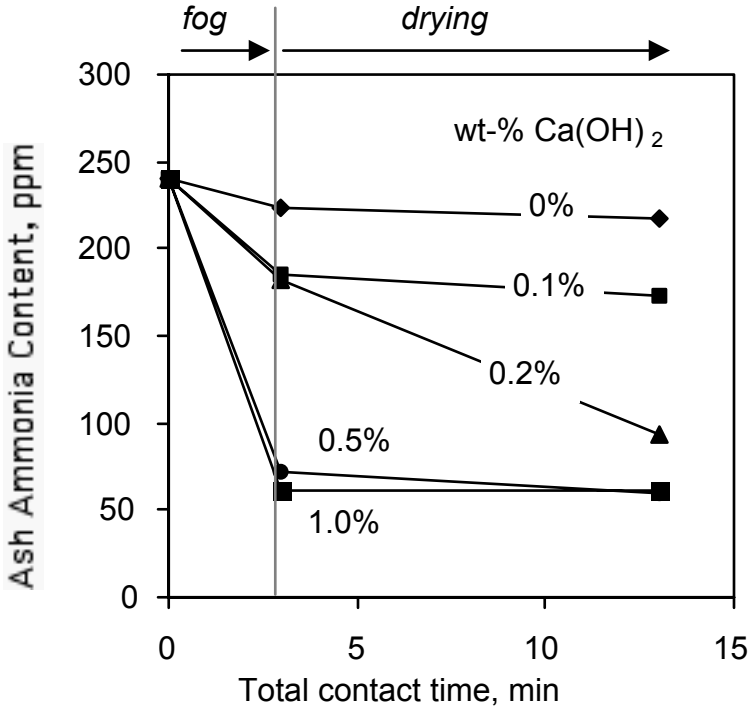

Figure C.19 Effect of dry $Ca(OH)_2$ as basic additive on ammonia removal from acidic ash (FA2) with flowing fog. Moisture levels in the ash were similar in the 5 experiments, ranging from 3.3% to 3.9% directly after fog addition, and ranging from 2.1% to 2.7% after drying.

Table C.3 Results of Ammonia Removal with High-pH Fog† from Acidic Ash, FA2 (initial ammonia content 240 ppm)

Processing conditions	Ash properties after fog stage		Ash properties after drying stage	
	moisture (wt-%)	*ammonia (ppm,w)*	*moisture (wt-%)*	*ammonia (ppm,w)*
3 min fog / 10 min dry	1.0	240	0.1	229
6 min fog / 10 min dry	2.6	94	1.5	62
10 min fog / 10 min dry	5.2	62	3.9	56

† 4 M NaOH solution

Experiments with ozone

Figure C.20 shows the effect of ozonation on ammonia under dry conditions as a function of ozone concentration and temperature. Ozone reduces ash ammonia content under all conditions, but the truly significant reductions are observed at elevated concentration (2 vol-%) and temperature (150 oC). The primary measurement in these experiments is residual ammonia on ash, and thus the data do not directly distinguish between removal and destruction, although direct oxidative attack leading to destruction of ammonia species is the most likely mechanism. The experiment in oxygen alone proves that gas stripping is not responsible for the loss of ammonia.

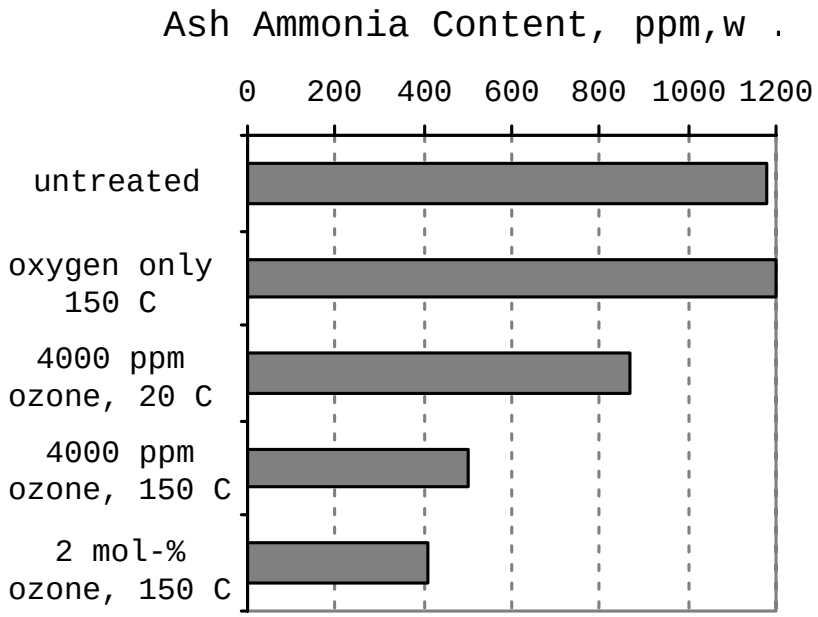

Figure C.20 Reduction in fly ash ammonia content by dry ozone treatment. Sample: 8 gm bed of basic fly ash, FA1. Flow rate: 2 lit/min ozone-containing oxygen; contact time: 30 minutes in each case, except the 2% case at 20 C for which the contact time was 60 min.

The cumulative amounts of ozone fed to the reactor in these experiments ranged from 51 to 251 gm-ozone/kg ash and were 4 to 21 time higher than the minimum theoretical stoichiometric requirement for complete NH_3 oxidation to nitrate and water. This high ozone usage is likely due to kinetic limitations of the ozone / ammonia reaction, which has been previously studied in aqueous solution where it exhibits reaction times on the order of minutes or greater[Kuo et al. 1997, Singer and Zilli, 1975], and to competition from the ozone/carbon chemisorption reaction, which is fast[Gao et al., 2001]. The ozone/carbon chemisorption reaction is known to improve the air entrainment behavior of these high carbon ashes by reducing hydrophobic surface

area[Gao et al., 2001], but here the reaction rapidly consumes ozone that would otherwise be available for ammonia destruction. The extent of ammonia removal/destruction by ozone increases with increasing temperature to 150 ^{o}C, further suggesting kinetic limitations for this reaction.

Several experiments were conducted to explore whether ozone has a beneficial effect during the drying stage of the wet ammonia removal processes, which could eliminate the need for off-gas treatment. Figure C.21 shows experiments in which 3 vol-% ozone was substituted for the drying air in the flowing fog experiment. This plot shows that the ammonia removal is sensitive to the moisture content directly after fog addition (as observed previously), and that ozone has no substantial enhancing effect on ammonia release. It is likely that the release of ammonia from the liquid phase is too fast under these conditions to allow significant aqueous-phase reaction with ozone, which exhibits finite kinetics[Kuo et al. 1997, Singer and Zilli, 1975].

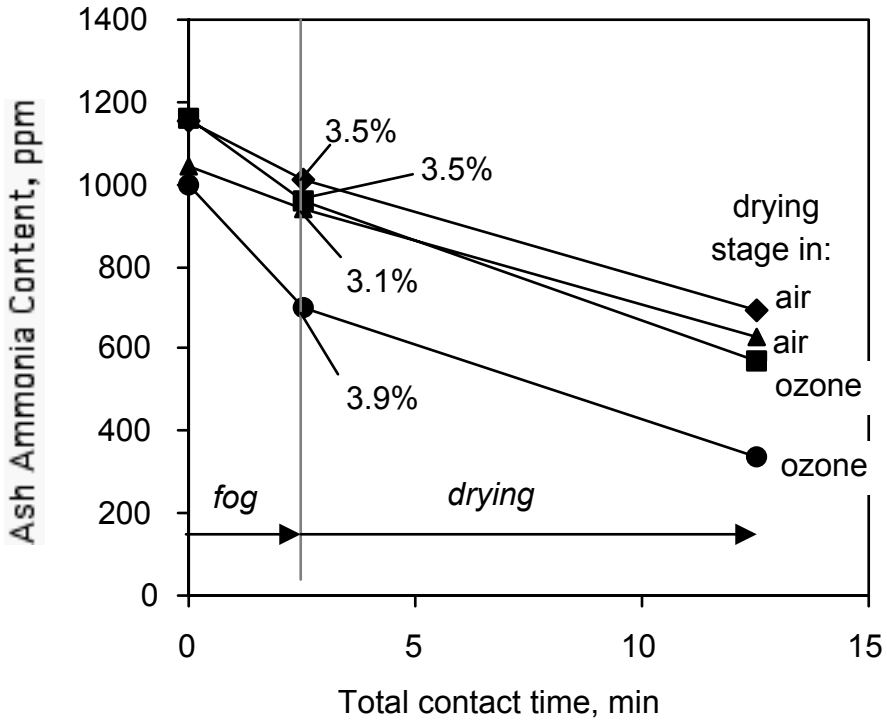

Figure C.21 Effect of ozone addition during the drying stage of ammonia removal. Sample: basic fly ash, FA1. The ozone containing stream was 3 vol-% ozone in air.

In acidic ashes, by contrast, the ammonia species remain in solution where they may be available for aqueous oxidative attack. Figure C.22 shows the effect of H_2O_2 and ozone as joint (peroxone) oxidizing agents during the semi-dry treatment of the acidic ash FA2 with flowing fog. Only modest reductions in ammonia are observed over a 60-minute treatment interval. Ammonia ozonation is heavily favored at equilibrium, so this result implies slow kinetics, again with likely competition from the ozone/carbon reaction. Peroxone oxidation is known to attack dissolved ammonia preferentially to ammonium ion, and the kinetics are thus sharply dependent on pH [Kuo et al., 1997]. Under these conditions the peroxone kinetics are too slow to achieve substantial ammonia reductions, likely due to low concentrations of dissolved ammonia at the prevailing low pH. Perversely, at high pH, ammonia is rapidly evolved as vapor, so effective peroxone destruction of ammonia would require careful control of pH at *intermediate* levels, if indeed it is possible at all in this system.

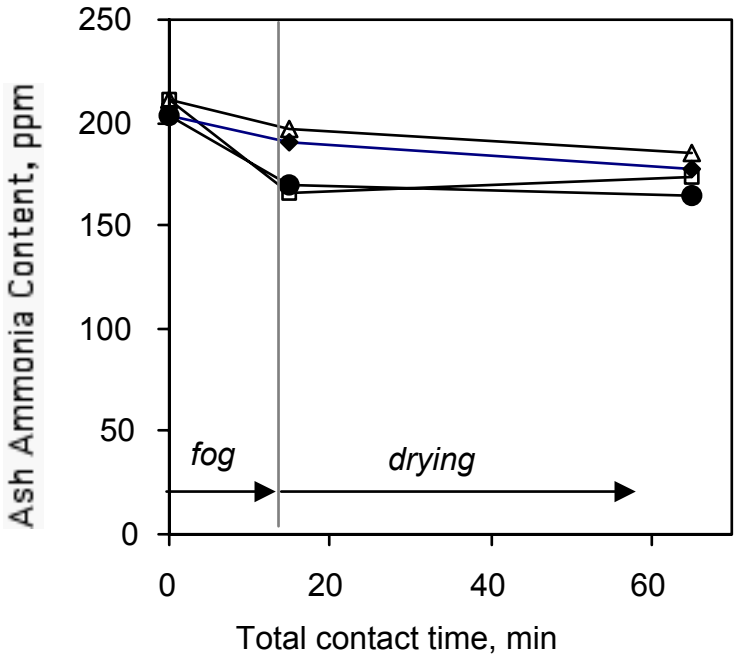

Figure C.22 Effect of H_2O_2 / O_3 fog on ammonia removal / destruction from acidic ash (FA2). Fog contained 30 wt-% H_2O_2 and was transported using 0.7 lit/min of 3% ozone in oxygen. The drying stage used 0.3 lit/min of 5% ozone in dry oxygen. Moisture levels in the ash were similar in the 2 experiments, ranging from 12.7% to 13.7% directly after fog addition, and from 6.1% to 7.2% after drying. Similar results were seen for 3-minute fog addition, in which the initial ash moisture contents were 2.8-3%.

Conclusions

This work presents the first fundamental ammonia isotherms on carbon-containing fly ash samples obtained after a custom retrofit of a commercial vapor adsorption apparatus for compatibility with ammonia. Ammonia adsorption near room temperature is shown to be dominated by adsorption on carbon with only of order 20 ppm adsorption on the mineral component. The adsorption on carbon is a combination of physisorption and chemisorption on acidic surface sites. Introduction of additional oxygen functional groups on carbon increases ammonia adsorption by increasing the number of these acidic sites. The absolute amounts of ammonia adsorbed on fly ash in this study are much less than those of concern in the utility sector and much less than those found by Muzio in a study using simulated flue gas. Secondary components of the flue gas, either water, SO_2, or SO_3 are likely responsible for most of the ammonia observed associated with ash in utility practice, with a lesser component attributed to true adsorption on carbon surfaces.

This work also demonstrates that ammonia species can be removed from fly ash at or near room temperature by a variety of dry and semi-dry techniques. The work confirms industrial reports that aqueous solution chemistry takes place upon the introduction of even very small amounts of water, while the ash remains in a semi-dry state for handling. Rapid ammonia removal occurs from a microscopic water film on surfaces, in fine pores, and in ash particle interstitial regions whenever the film pH is high — achieved either by dissolution of the natural basic components of the ash or by the separate introduction of soluble basic additives. Flowing humid air and flowing water aerosol (fog) are promising methods for the uniform addition of small amounts of water to fly ash for semi-dry ammonia removal. Ozone is capable of destroying ammonia on ash in the dry state, but is less effective under semi-dry conditions due to kinetic limitations on the aqueous phase reaction at the lower pH values needed to keep ammonia in solution.

Literature References

Ashmore, P.G. *Catalysis and Inhibition of Chemical Reactions*, Butterworths, London, 1963.

Bittner, J.; Gasiorowski, S.; Hrach, F. *14th International Symposium on Management and Use of Coal Combustion Products*, **2001,** San Antonio, Electric Power Research Institute, Palo Alto, CA.

Boehm, H.P., Diehl, E., Heck, W. and Sappok. *Angew Chem. 76*, 742 (1964).

Bomchil, G, Harris, N., Leslie, M., Tabony, J., White, J.W., Gamlen, P.H., Thomas, R.K. and Treweren, T.D., *J. Chem. Soc. Faraday I, 75*, 1535 (1979).

Brendel G.; Rathbone, R.; Frey, R. *14th International Symposium on Management and Use of Coal Combustion Products*, **2001** San Antonio, Electric Power Research Institute, Palo Alto, CA.

Bridgeman, O.C., *J. Am Chem . Soc., 49*, 1174 (1927).

Castle, G.S.P. *IEEE Trans. Ind. App.* **1980**, *1A-16* 297-302.

Emmert, R.E. and Pigford, R.L. in *Perry's Chemical Engineer's Handbook, 4th Edition*, chapter 14, McGraw-Hill, 1963. This article cites Johnstone *I&EC, 27*, 587 (1935) and *30*, 101 (1938) as the source of the data.

Fujisaki, G., Sc.B. Honors Thesis, 2000; Division of Engineering, Brown University, Providence, RI.

Gao, Y.; Külaots, I.; Chen, X.; Aggarwal, R.; Mehta, A.; Suuberg, E. M.; Hurt, R. H. *Fuel* **2001**, *80* 765-768.

Garrido, J., Linares-Solano, A., Martin-Martinez, J.M., Molina-Sabio, M., Rodriguez-Reinoso, F., and Torregrosa, R., *Langmuir, 3,* 76 (1987).

Gasiorowski; S. A.; Hrach, F. J. Jr.; Frank J. U.S. Patent US1999000256128, issued June 20, 2000.

Gedeon, A.; Lassoued, A.; Bonardet, J.L.; Fraissard, J.; *Microporous and Mesoporous Materials,* **2001**, *44*, 801-806.

Giampa,V.M.; *14th International Symposium on Management and Use of Coal Combustion Products*, **2001**, San Antonio, Electric Power Research Institute, Palo Alto, CA.

Golden, D.; *14th International Symposium on Management and Use of Coal Combustion Products*, **2001**, San Antonio, Electric Power Research Institute, Palo Alto, CA.

Gregg, S.J. and Sing, K.S.W., *Adsorption, Surface Area and Porosity*, Academic Press, 1982.

Haar, L. and Gallagher, J.S., *J. Phys. Chem. Ref. Data*, *7*, 635 (1978).

Hinton, S.; "Investigation of Ammonia Adsorption on Fly Ash and Potential Impacts of Ammoniated Ash," EPRI Report, Palo Alto, CA 1999: TR-113777.

Hofman, U. and Ohlerich, G. *Angew. Chem. 62*, 16 (1950).

Holmes, J.M. and . Beebe, R.A., *Can. J. Chem., 35*, 1542 (1957).

Hwang, J.-Y.; "Method for Removal of Ammonia from Fly Ash," International Patent WO9948563A1, issued Sept. 30, 1999.

Janssen, F.; Van der Kerkof, F.; Lefers, J.; Lodder, P.; Luierweert, L. *Anal. Chim. Acta* **1986**, *190* 245-254.

Katsuya, M., Taisuke, S., Yukio K., Tamotsu, N., Japanese Patent JP8187484A "Deammonification Treatment of Coal Ash and Apparatus Therefore," issued July 23, 1996.

Kulaots, I. Ph.D. Dissertation, Division of Engineering, Brown University, 2001.

Kuo, C.; Yuan, F.; Hill D. *Ind. Eng. Chem. Res.* **1997**, *36* 4106-4113.

Larrimore, L. *EPRI Conference on the Effects of Coal Quality on Power Plant Management*, The Electric Power Research Institute, May 2000.

Levy, E., Huang, d., Herrea, C., *14th International Symposium on Management and Use of Coal Combustion Products*, **2001** San Antonio, Electric Power Research Institute, Palo Alto, CA.

Lowe, P. A.; Ellison, W. A.; Makansi, J. *Power* **1989**, 130 53-56.

Muzio, L. J.; Kim, E. N.; McVickar, M.; Quartucy, G. C.; McElroy, M.; Winegar, P. *Joint EPRI/EPA Symposium on Stationary Combustion NOx Control*, **1995**, Kansas City.

Novak, M.; Rych, H. G. *1989 Symposium on Stationary Combustion Nitrogen Oxide Control*, Electric Power Research Institute, Volume 2 pp. 7A-1 to 7A-26.

Necker, P.; *1989 Symposium on Stationary Combustion Nitrogen Oxide Control*, Electric Power Research Institute, Volume 2 pp. 6A-19 to 6A-38.

Ramme, B.; Fisher, B. *14th International Symposium on Management and Use of Coal Combustion Products*, **2001**, San Antonio, Electric Power Research Institute, Palo Alto, CA.

Rodriguez-Reinoso, F., Linares-Solano, A., *Chem. and Phys. Carbon, 21,* p1, Dekker, New York (1989).

Rubel, A.; Rathbone, R.; Stencel, J. *14th International Symposium on Management and Use of Coal Combustion Products*, **2001**, San Antonio, Electric Power Research Institute, Palo Alto, CA.

Sahu N.; Arora, M. K.; Upadhyay, S. N.; Sinha, A. S. K. *Ind. Eng. Chem. Res.* **1998**, *37* 4682-4688.

Sing, K.S.W. in *Porosity in Carbons*, J. W. Patrick, Ed., p. 49 Halstead Press, New York, 1995.

Singer, P. C.; Zilli, W. B. *Water Research* **1975**, *9* 127-134.

Spencer, W.B., Amberg, C.H. and Beebe, R.A., *J. Phys. Chem. 62*, 719 (1958).

Turner, J. R. "*Studies in Reaction Engineering of Nitrogen Oxides Abatement*" Doctoral thesis, Washington University, St. Louis, December 1993.

Turner, J. R.; Chone, S.; Dudukovic, M. P.; *Chemical Engineering Science*, **1994**, *49 24A* 4315-4325.

Wexler, A. S.; Seinfeld, J. H. *Atmospheric Environment,* **1991**, *25A* 2731.

Young, D.M. and Crowell, A.D. *Physical Adsorption of Gases*, Butterworths, London, 1962.

Zawadzki, J. *Chem. and Phys. Carbon*. *21*, P. 147, Dekker, New York (1989).